UNIVERSITA' DEGLI STUDI DI MILANO

DEPARTMENT OF BIOMEDICAL, SURGICAL AND DENTAL SCIENCES

"Minimally invasive surgery to facilitate micro-implant supported maxillary skeletal expansion in adult patients"

A thesis submitted in satisfaction

of the requirements for the degree of

Philosophy Doctorate (PhD) in Clinical Research

by

PhD Candidate: **Daniele Cantarella**

(Matricule no: R12170)

Tutor: Professor Massimo Del Fabbro

Co-tutor: Professor Aldo Bruno Giannì

A.Y. 2020-2021

TABLE OF CONTENTS

Abstract.....2

List of acronyms……..6

List of tables…….8

Chapter 1: Introduction 9

Chapter 2: Materials and Methods 15

- Digital planning and manufacturing of MSE……..... 15
- Clinical trial……..... 27
- Study design……..... 27
- Surgical intervention……..... 28
- Appliance activation protocol……..... 34
- 3D analysis on CBCT……..... 35
- Two CBCT axial sections to evaluate changes in maxilla and pterygoid processes of the sphenoid (APS, UNS).....……..... 39
- Measurements on the axial palatal section (APS) ..…….. 43
- Measurements on the upper nasal section (UNS) .....……..... 50
- Measurements on the coronal zygomatic section (CZS) ……..... 52
- Measurements on the axial zygomatic section (AZS) …… 61
- Statistical analysis ..…… 66

Chapter 3: Results 69

Chapter 4: Discussion 86

Chapter 5: Conclusions and Future directions..... 118

Bibliography..... 120

ABSTRACT OF THE THESIS

Title

Minimally invasive surgery to facilitate micro-implant supported maxillary skeletal expansion in adult patients.

Introduction

The aim of the present study is to evaluate the skeletal modifications induced by maxillary expansion supported by palatal micro-implants and localized osteotomies produced with minimally invasive surgical technique in young-adult and adult patients.

In the present investigation, osteotomies had a lower extension than the ones used in conventional surgically assisted rapid palatal expansion (SARPE), to adopt a minimally invasive surgical technique that can be performed with greater comfort for the patient and less post-operative sequelae. More in detail, the localized osteotomies were executed only in the anterior part of the midpalatal suture and bilaterally at the basis of the zygomatic process of the maxilla without involvement of the piriform rim. These areas represent a great resistance to the lateral maxillary movement. Furthermore, they are of simple surgical access and don’t present important arterial plexuses.

Patients requiring micro-implant supported maxillary expansion and/or SARPE routinely undergo a pre-treatment cone-beam computed tomography (CBCT) of the skull, to plan the surgical operation and, one month after treatment a secondary CBCT for a surgical and orthodontic control.

CBCT is a low radiation tomography, extensively used in maxillofacial surgery and in dentistry. For the implementation of this study, that aims at evaluating the efficacy of micro-

implant-supported maxillary expansion in combination with localized osteotomies, only radiologic exams that are anyway needed for the planning and post-treatment evaluation were used.

Aim

The aim of the present study is to evaluate the advantages introduced in the treatment of maxillary constriction by the therapy with micro-implant supported Maxillary Skeletal Expander (MSE) and localized osteotomies in young-adult and adult patients.

The main objective is to evaluate the efficacy of the technique, by measuring the movement of skeletal landmarks in the midface, particularly on the maxillary and zygomatic bones, and on the lateral wall of the nose, by comparing the pre-treatment and post-treatment CBCT.

For this particular technique, a new methodology for digital planning of position of MSE and miniscrews on patient CBCT was developed. Furthermore, incorporation of 2 additional miniscrews to the original MSE design, which conventionally features only 4 miniscrews, was developed with the aid of computer aided design – computer aided manufactured (CAD-CAM) technology.

Methods

The study presented the following steps:

- Development of a digital planning methodology for positioning the miniscrews and MSE appliance on pre-treatment CBCT
- Development of a CAD-CAM methodology for incorporating 2 additional miniscrews to the original MSE design with 4 miniscrews
- Selection of patients with age above 17 years, without congenital craniofacial syndromes, who require intervention of maxillary skeletal expansion

- Acquisition of initial CBCT with 17 x 13.5 cm field of view (FOV)
- Intervention of maxillary expansion supported by palatal micro-implants and localized osteotomies executed with minimally invasive surgical technique
- One month after treatment, acquisition of post-treatment CBCT with 17 x 13.5 cm FOV
- Analysis of skeletal modifications in the midface (maxillary bone, sphenoid bone, zygomatic arch, nasal cavity, etc.), by comparing the pre- and post- treatment CBCT with a 3D software (OnDemand software by Cybermed)

Results

The new methodology allowed the digital planning of MSE and miniscrews positioning on patients' CBCTs, and the incorporation of two additional miniscrews to the original MSE design through CAD-CAM technology.

In the clinical trial, a total of four patients had an average age of 27.6 years (range 22.1 – 39.9 years).

MSE appliance was activated by an average of 6.0 mm and generated a parallel split of the midpalatal suture of 3.4 mm, 3.0 mm and 3.6 mm at anterior nasal spine (ANS), nasopalatine foramen (NPF) and posterior nasal spine (PNS), respectively.

Skeletal modifications were found in all CBCT sections evaluated in the study (axial palatal, upper nasal, coronal zygomatic, axial zygomatic), indicating that all midfacial bones are affected by maxillary expansion with MSE and localized osteotomies.

Particularly, skeletal changes were noticed also in CBCT sections above the lateral maxillary osteotomies (LMOs), in the maxilla, zygomatic bone, zygomatic arches, and nasal cavity. In the upper nasal section (UNS) the maxilla was laterally displaced by 2.4 mm and 0.9 mm, at its anterior and posterior extremities, respectively.

The frontozygomatic angle (FZA) increased by 1.9° (average of right and left side), while the lower interzygomatic distance increased by 2.9 mm, indicating a rotation of the zygomatic bone in a lateral direction.

The zygomatic arch was affected by bone bending phenomena and was deflected in an outward direction, with increase in the anterior intermaxillary distance by 1.7 mm and in the posterior inter-zygomatic distance by 1.6 mm.

The nasal width (NW) parameter increased by 2.9 mm with treatment: this anatomical finding is the basis for a potential improvement in nasal breathing for patients suffering from increased nasal airway resistance.

The cited modifications in skeletal structures above lateral maxillary osteotomies (LMOs) are most likely due to the fact that LMOs didn't involve the piriform rim of the maxilla, and this point needs further investigations.

Regarding dentoalveolar modifications, the inter-molar distance increased by 7.4 mm, and molars underwent a small dentoalveolar tipping in a buccal direction by 1.1° (average of right and left side), as evidenced by the change in molar basal bone angle (MBBA).

No intra-operatory hemorrhage nor post-operatory bleeding was reported in treated patients, probably due to the lack of pterygopalatine suture surgical disjunction.

A limitation of the study is its small sample size, represented by 4 patients. A larger number of patients is required to confirm the above results.

Keywords: maxillary expansion, adult patients, Maxillary Skeletal Expander (MSE), MARPE, surgically assisted rapid palatal expansion (SARPE), minimally invasive surgery, skeletal changes, orthopedic effects, midpalatal suture, circummaxillary sutures, midface, CBCT, digital orthodontics.

LIST OF ACRONYMS

- AIMD: anterior inter-maxillary distance (in the AZS)
- ANS: anterior nasal spine
- APP: axial palatal plane
- APS: axial palatal section
- AZS: axial zygomatic section
- BZL: bi-zygomatic line (line passing through ZR and ZL)
- CAD-CAM: computer aided design – computer aided manufacturing
- CA point: center of appliance point
- CMP: coronal maxillary plane
- CM point: center of maxilla point
- CZS: coronal zygomatic section
- DOME: distraction osteogenesis maxillary expansion
- FZA: frontozygomatic angle (in the CZS)
- FZS: frontozygomatic suture
- HPP: horizontal palatal plane
- IMD: inter-molar distance
- LID: lower inter-zygomatic distance
- Lt: left
- MAPE: miniscrew assisted palatal expansion
- MARPE: miniscrew assisted rapid palatal expansion

- MBBA: molar basal bone angle
- MISMARPE: minimally invasive surgical and miniscrew assisted rapid palatal expansion
- MS5: midpalatal suture 5 (at the level of second premolars)
- MS7: midpalatal suture 7 (at the level of second molars)
- MSE: maxillary skeletal expander
- MSP: maxillary sagittal plane
- Mx Incl: maxillary inclination (in the CZS)
- NW: nasal width
- NPF: nasopalatine foramen
- PITD: posterior inter-temporal distance (in the AZS)
- PIZD: posterior inter-zygomatic distance (in the AZS)
- PNS: posterior nasal spine
- Rt: right
- UID: upper inter-zygomatic distance (in the CZS)
- Up Ant Mx: most anterior point of maxillary bone (in the UNS)
- Up Post-med Mx: most posterior-medial point of maxillary bone (in the UNS)
- UNS: upper nasal section
- VAS: visual analog scale
- VP: vomer posterior (most posterior point of vomer)
- ZMA: zygomaticomaxillary angle (in the CZS)
- ZMS: zygomaticomaxillary suture

- ZR: most lateral point of zygomatic process of right maxilla
- ZL: most lateral point of zygomatic process of left maxilla
- ZPA: zygomatic process angle or angle of the zygomatic process of maxilla (in the AZS)
- ZTA: zygomaticotemporal angle (in the AZS)
- ZTS: zygomaticotemporal suture

LIST OF TABLES

Table 1. Parameters evaluated in the axial palatal section (APS) ……..…….... 45

Table 2. Parameters evaluated in the upper nasal section (UNS) ……..…….... 51

Table 3. Parameters evaluated in the coronal zygomatic section (CZS) ……..…... 54

Table 4. Parameters evaluated in the axial zygomatic section (AZS) ……..…… 62

Table 5. Results for axial palatal section (APS)……..……..…….... 69

Table 6. Statistical analysis of the frequency of openings in the lower part of the pterygopalatine suture: Fisher's exact test…….……. 70

Table 7. Results for upper nasal section (UNS)……. 72

Table 8. Results for coronal zygomatic section (CZS)……..…….. 74

Table 9. Results for axial zygomatic section (AZS)……..……..…….. 80

Table 10. Results for analysis of midface expansion symmetry……. 82

Table 11. Average treatment change for surgical and non-surgical MSE……. 84

Table 12. Midface expansion efficiency index (MEEI) for surgical and non-surgical MSE…85

CHAPTER 1: INTRODUCTION

Maxillary transverse deficiency is a common finding in orthodontics [1] which, if left untreated can result in masticatory disfunction, occlusal instability and breathing inefficacy. The advocated treatment approach is the rapid maxillary expansion (RME), proposed by Angell [2] and re-introduced by Haas [3,4]. RME is achieved by means of a tooth-borne appliance that usually consist of two bands around deciduous or permanent upper molars and a jackscrew at the level of palatal vault supported or not by an acrylic base [5]. Following the activation of the jackscrew the mid-palatal suture is separated leading to maxillary expansion. Despite being a safe and predictable treatment approach, RME is limited in terms of treatment timing. In growing patients there is a high probability of treatment success with a predominant orthopedic effect [6]. However, some dental side effects are present, including dental tipping that may lead to gingival dehiscence.

In skeletally mature patients, a higher resistance of mid-palatal suture due to the increased inter-digitation, significantly compromises the success rate of tooth borne RME treatment [6-7]. In such patients, orthopedic effects are neglectable and dental side effects become predominant [8,9].

To overcome the limitations of tooth borne appliances for RME especially in skeletally mature patients, and to avoid a surgical treatment approach for such cases, a miniscrew-assisted rapid palatal expansion (MARPE) procedure has been proposed [10]. It consists of the incorporation of miniscrews in the tradition RME appliance, directly inserted in the palatal bone. This way, a higher expansion force is directly transmitted at the palatal bone increasing the possibility of mid-palatal suture split [11]. Dental side effects are also minimized [12-19]. There is a variety of appliances for MARPE differing from the design, number and location of miniscrews [19-26]. Among them, the Maxillary Skeletal Expander

(MSE) has been thoroughly documented in the past decade [11,27-33]. The appliance has a central jackscrew fixed at the palatal bone with four miniscrews and stabilized by two ductile arms usually anchored on maxillary first molars. From a biomechanical viewpoint, MSE has some distinguishing characteristics. First, all miniscrews are positioned in the posterior palatal area between the two zygomatic buttresses. The mid-palatal suture is not the only area of resistance for the expansion. All peri-maxillary sutures and bony structures contribute in such resistance. Therefore, for a successful maxillary expansion, other peri-maxillary sutures must be disarticulated. By positioning the miniscrews posteriorly, the expansion force is applied closer to the area with higher resistance against the expansion, which increases the probability of producing a peri-maxillary suture disarticulation with parallel midpalatal suture split [34-36]. Second, all four miniscrews are bicortically engaged, through the palatal and nasal cortical bones. This way bending and tipping of miniscrews is minimized and a more effective movement of maxillary bone is secured [35-36,43-44]. Third, the extensive investigations in recent years have identified the rotation fulcrum of the zygomaticomaxillary complex during MSE expansion [34-43,44].

In the coronal plane, it has been found that the zygomaticomaxillary complex rotates with a fulcrum located near the frontozygomatic suture, and as a consequence of the rotation, the maxilla moves laterally and downwards [43-44] (Fig. 1.1).

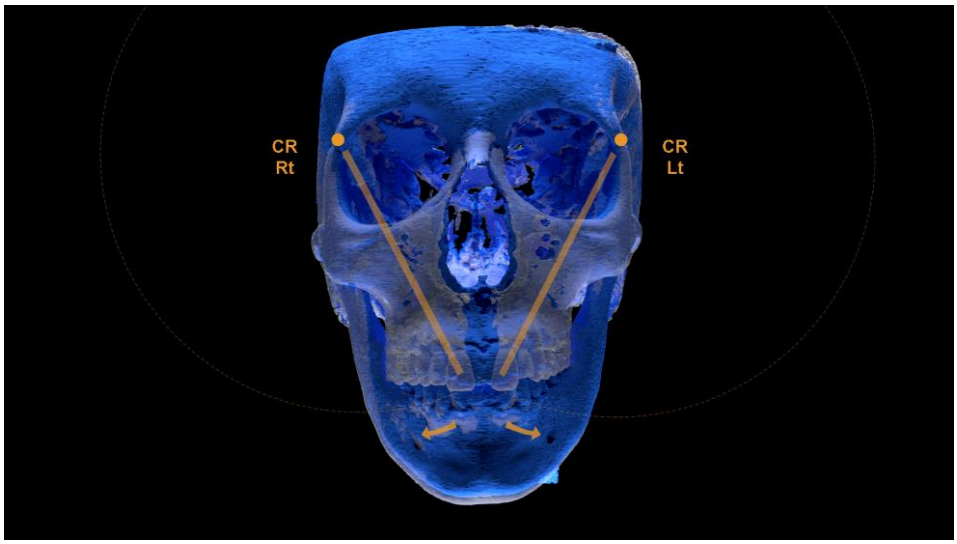

Fig. 1.1. A 3D rendering showing the rotation of the zygomaticomaxillary complex in the coronal plane with a fulcrum located near the frontozygomatic suture, during non-surgical maxillary expansion with MSE [43-44]. Blue: pre-expansion. White: post-expansion.

In the horizontal plane, the rotation fulcrum has been found to be located at the proximal portion of the zygomatic process of the temporal bone [34,44]. As a consequence of the rotation, the maxilla moves laterally and forward (Fig. 1.2).

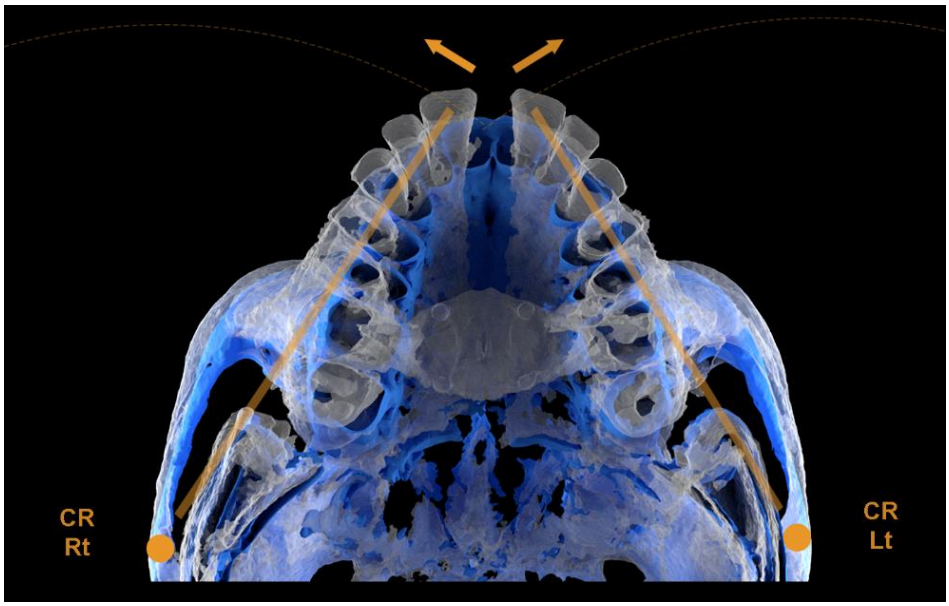

Fig. 1.2. A 3D rendering showing the rotation of the zygomaticomaxillary complex in the horizonal plane with a fulcrum located at the proximal portion of the zygomatic process of the temporal bone, during non-surgical maxillary expansion with MSE [34-44]. Blue: pre-expansion. White: post-expansion.

The rotation fulcrum at the proximal portion of the zygomatic process of the temporal bone has been explained by a bone bending phenomenon at the thinnest point of the zygomatic arch, which is positioned immediately anteriorly to the articular tubercle of the temporomandibular joint glenoid fossa [34].

Beyond moving laterally, maxilla relocates downward and forward as a consequence of rotational fulcrums, and this favors the disarticulation of the pyramidal process of the palatine bone from the pterygoid process of the sphenoid bone. The split of the pterygopalatine suture, in turn, allows the movement of the posterior part of the maxilla and the parallel pattern of midpalatal suture split [34,36,44].

The above biomechanical findings have been confirmed by following studies [37-39].

The MARPE approach has undoubtedly offered a valid treatment alternative for young adults or adults with maxillary transverse deficiency. However, this approach is not always successful. The causes of a failed maxillary expansion with MARPE are not clearly identified. Some investigators proposed an index of mid-palatal suture maturation to use as a guide for patient selection for MARPE [45]. However, other investigators have demonstrated that the mid-palatal suture is not the only one to consider for maxillary expansion and that the maturation stage of such suture is not a reliable tool for patient selection [46]. Others have emphasized age as a crucial factor for case selection. In a recent study, authors concluded that patients 25 years of age and older are less likely to have a successful maxillary expansion with MARPE [47]. Other influencing factors have also been considered such as bone density, patients' specific anatomy, the type of MARPE and the activation protocol [48]. A recent study found that above the age of 18 years, the risk of complications with miniscrew assisted palatal expansion (MAPE) increased by 10% per year, in a group of patients with age ranging from 18 years to 59 years [48].

In skeletally mature patients with significant transverse deficiency of the maxilla (usually more than 5mm of deficiency) for which an orthodontic approach alone is insufficient, and a MARPE approach has failed or is considered inappropriate, surgery remains the treatment of choice [49]. The main surgical approach advocated for such cases is the surgically assisted rapid palatal expansion (SARPE) [50]. It consists of selected osteotomies on maxilla aiming at resecting maxillary and peri-maxillary sutures and maxillary pillars. These structures represent areas of resistance for the expansion of the maxillary bone and are identified as: mid-palatal suture, piriform rim of the maxilla, zygomatic buttress and pterygomaxillary junction [51]. The SARPE approach has undergone continues modifications over time depending on patients' age or which suture/structure is considered of higher resistance. Some authors suggest a subtotal Le Fort I osteotomy involving all four areas of resistance which are considered as equally important for a successful expansion [52]. Others consider the zygomatic buttress the main resistance to expansion and therefore recommend a simplified SARPE technique with no mid-palatal suture surgical osteotomy [53].

Despite variations, SARPE is potentially associated with minor or major complications [54,55]. One of the most serious complications is bleeding mainly due to the interruption of terminal branches of internal maxillary artery during the pterygopalatine suture disjunction [56]. It can occur intra-operatively or post-operatively within two weeks after surgery and is usually manifested in the form of epistaxis [57]. Other serious complications include bone fracture, nerve injury or carotid cavernous fistula [58,59]. Moreover, a series of less invasive complications have been reported including asymmetric expansion [60], post operative pain, discoloration, fracture or loss of central incisors due to the mid-palatal suture split [54].

Until recently, there was no treatment alternative for skeletally mature patients who were considered unsuitable candidates for MARPE, or for which MARPE approach had failed and

a more invasive surgical approach like SARPE was not accepted by the patient. In 2017, Liu et al. published a paper describing the Distraction Osteogenesis Maxillary Expansion (DOME) technique performed in skeletally mature patients diagnosed with obstructive sleep apnea syndrome (OSAS) [61]. DOME consists of a modified and simplified SARPE combined with MSE. The following osteotomies are performed: the Le Fort I osteotomy, bilaterally, for addressing lateral resistance of the zygomatic buttresses with the involvement of the piriform rim of maxilla, and the osteotomy of the anterior part of mid-palatal suture. No pterygopalatine suture disjunction is performed, avoiding the above-mentioned risks associated with this procedure. The authors reported significant improvement of clinical obstructive sleep apnea (OSA) parameters probably due to two mechanisms: enlargement of nasal floor and internal nasal valve width and enlarged space for tongue positioning [62,63]. However, no midface skeletal effects of such procedure have been reported. Furthermore, because of the disintegration of the piriform rim associated with the lateral osteotomies, there is a V-shaped pattern of midpalatal suture split with predominant anterior expansion, and the modification in the upper part of the nasal cavity is not likely.

In the present study, we introduce an alternative approach for the treatment of skeletally mature patients with maxillary transverse deficiency. This simplified SARPE technique consists of localized lateral osteotomies without involving the piriform rim, combined with the osteotomy of anterior mid-palatal suture. MSE is used for delivering the expansion force.

CHAPTER 2: MATERIALS AND METHODS

The study received approval from the Milan Area 2 Ethics Committee on September 17th 2019, the acronym of the study is “OSTEOMSE-2019”, the approval number 740_2019.

The study involved the following steps:

- Development of a digital planning methodology for positioning the miniscrews and MSE appliance on pre-treatment CBCT, and a CAD-CAM methodology for incorporating 2 additional miniscrews to the original MSE design.
- Execution of a prospective clinical trial characterized by the intervention of maxillary skeletal expansion with MSE and localized osteotomies with a minimally invasive surgical technique on young adult and adult patients
- Analysis of skeletal modifications induced in the midface by the therapy, by comparing the pre- and post-expansion CBCTs of the treated patients

Digital planning and manufacturing of MSE

Maxillary Skeletal Expander (MSE) is a prefabricated appliance, with an expansion jackscrew, a body with 4 slots for the miniscrews and 4 arms that connect the body to the molar bands [11,34-44] (Fig. 2.1 and 2.2). Appliance arms are bent and welded to the molar bands. Appliance arms are made with a ductile material, so in case the miniscrews tip during appliance activation, the arms deform and prevent the expansion force loading the maxillary molars.

After appliance cementation, miniscrews are inserted through the appliance slots, into the maxillary bone. Miniscrews have a diameter of 1.8 mm and are available in 3 different lengths: 9 mm, 11 mm, 13mm; the miniscrew length is chosen based on the thickness of palatal mucosa and palatal bone. Miniscrews should penetrate the MSE appliance body, the palatal mucosa, the cortical bone layers of palatal vault and nasal floor, and 1 mm into the nasal cavity [11,34-44] (Fig. 2.3).

Activation of appliance is made with a hexagonal activation key; 1 activation turn produces an appliance expansion of 0.13 mm.

Fig. 2.1: Prefabricated MSE appliance, manufactured by Biomaterials Korea Inc. Company.

Fig. 2.2: MSE appliance cemented in the oral cavity, showing the MSE position in the posterior part of the palate.

Fig. 2.3: A 3D rendering of CBCT after expansion, showing MSE miniscrews penetrating the palatal bone and about 1 mm into the nasal cavity.

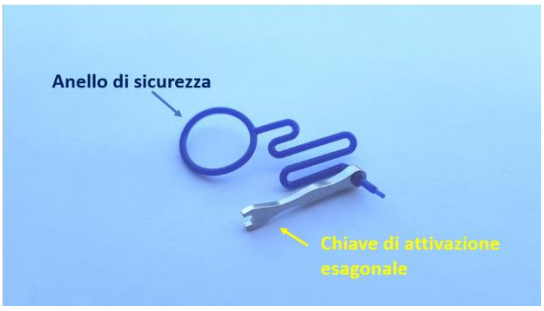

Fig. 2.4: MSE hexagonal activation key, with safety ring to be worn on operator finger.

MSE positioning is traditionally planned using dental stone models and 2D headfilms [11]. This approach presents some critical issues, such as the inability to identify the MSE position relatively to skeletal structures, and the potential risk of damaging anatomical structures.

To resolve the problem above, in the present study, a novel methodology has been developed to establish an optimal MSE position using the digital dental arches and cone-beam computed tomography (CBCT) images [64].

After patient's CBCT and digital dental arches are produced, they are merged with the Real Guide software (3Diemme, Figino Serenza, Italy) to generate the composite model, as shown in Fig. 2.5.

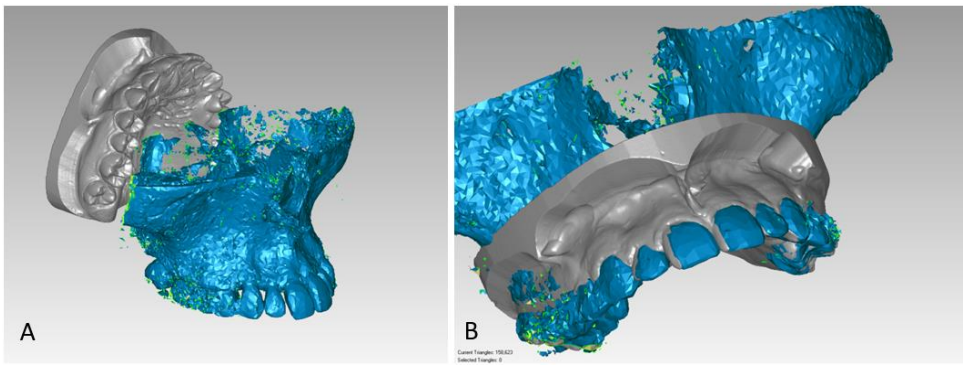

Fig. 2.5. Merging of CBCT and digital dental arch. A) Before and B) after merging [64].

The composite model of CBCT and digital dental arch is imported to Rhinoceros (v. 6) software (Robert McNeel & Associates, Seattle, Washington USA). Reference planes are identified in the bony structures of the patient's midface, to create the x, y, z coordinate system of the maxilla. The first plane is the Midsagittal Plane (MP), passing through the following points: Midpalatal Suture 5 (MS5), Midpalatal Suture 7 (MS7), and Vomer Posterior (VP) (Fig. 2.6 A-B).

The reference points are defined as follows: MS5 is the point placed on the oral side of the midpalatal suture at the level of second premolars; MS7 is the point placed on the oral side of the midpalatal suture at the level of second molars; VP is the most posterior point of the vomer.

The Horizontal Palatal Plane (HPP) is identified as the plane perpendicular to the Midsagittal Plane (MP) and passing through MS5 and MS7 (Fig. 2.6 C).

Then, the bi-zygomatic line (BZL) connecting the most lateral point of the zygomatic process of the maxilla on the right and left side (ZR and ZL, respectively) is drawn, and the line is orthogonally projected to the horizontal palatal plane (HPP). On this plane, the intersection

between the projection of the BZL and the midpalatal suture (MS4-MS7 line) is named the Center of Maxilla (CM) point (Fig. 2.6 D).

A coronal plane, called Coronal Maxillary Plane (CMP), which is perpendicular to the Midsagittal Plane (MP) and to the Horizontal Palatal Plane (HPP) and passing through the CM point represents the third plane of the maxillary x, y, z coordinate system (Fig. 2.6 E), and CM point represents the origin (0,0,0) of the system (Fig. 2.6 E).

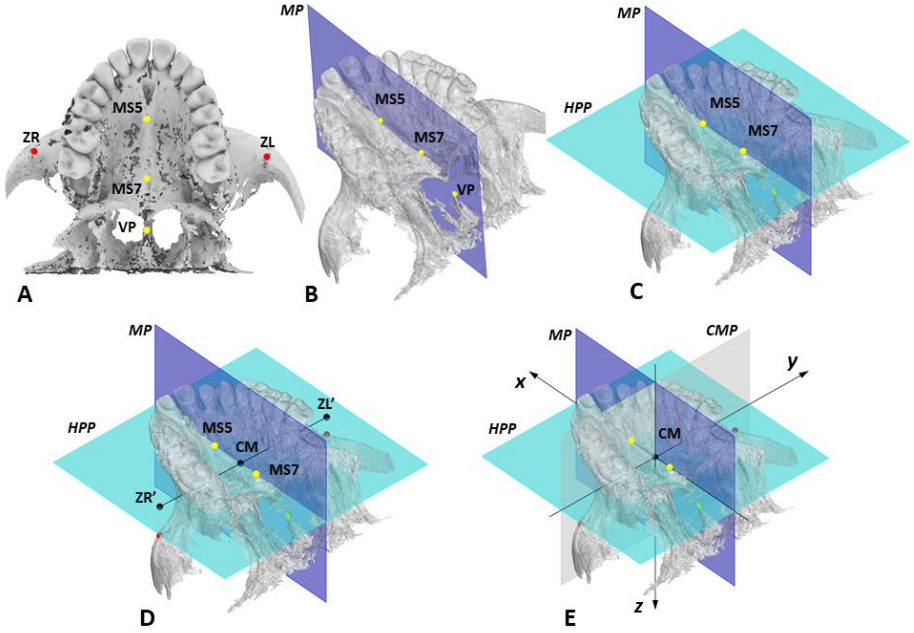

Fig. 2.6. Determination of reference planes and x,y,z coordinate system for the maxilla [64].

The virtual model of the MSE appliance was designed using Rhinoceros software (Fig. 2.7 A).

The MSE model is a single file that includes both the body of the expander and the four micro-implants, which are represented by four cylinders 13 mm long that have a notch at the level of 11 mm. The groove allows a visualization of the micro-implant length (11 mm versus 13 mm) during the MSE positioning procedure with the CBCT.

An x', y,' z' coordinate system is also generated for the MSE virtual model (Fig. 2.7 A), and the origin of the system is set at the Center of MSE Appliance (CA) point, which is designated at the center of 4 micro-implant slots in the mucosal face of the MSE.

The MSE model was then positioned in the maxilla at the initial default position so that the CA point is coincident with the CM point, and in which the x', y,' z' coordinate system of the MSE appliance is aligned with that of the maxilla (Fig. 2.7 B).

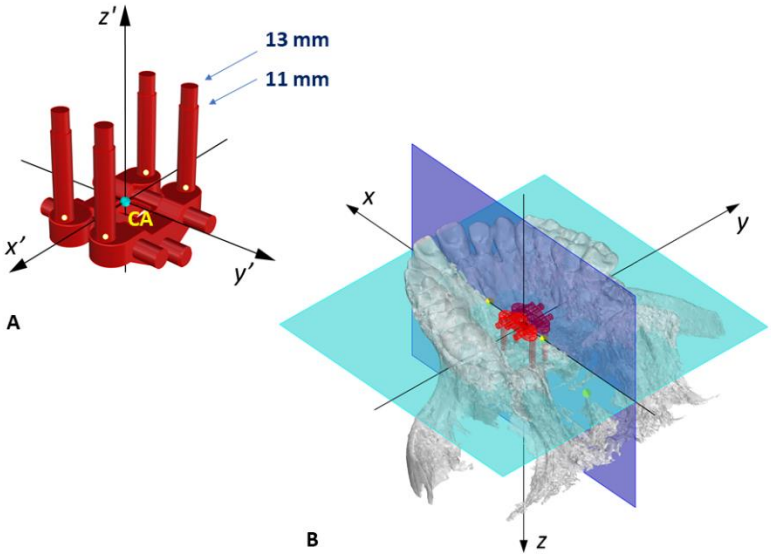

Fig. 2.7. Positioning of MSE appliance (A) in the maxilla at the initial default position, where x', y', z' coordinate system of MSE is aligned with x, y, z coordinate system of maxilla (B) [64].

A user interface has been developed (Fig. 2.8 A), with which the position and inclination of the MSE appliance can be changed from its initial default setting. The MSE position can be modified by moving the CA along the x, y, z axes of the maxilla (Fig. 2.6 E), while the MSE inclination can be modified by changing the Yaw, Pitch and Roll of the appliance (Fig. 2.7 B). The terminologies used for the appliance's inclination is derived from the conventional skull orientation terms [65]: Yaw is defined as the rotation around the vertical axis, Pitch as the rotation around the transverse axis, and Roll as the rotation around the sagittal axis.

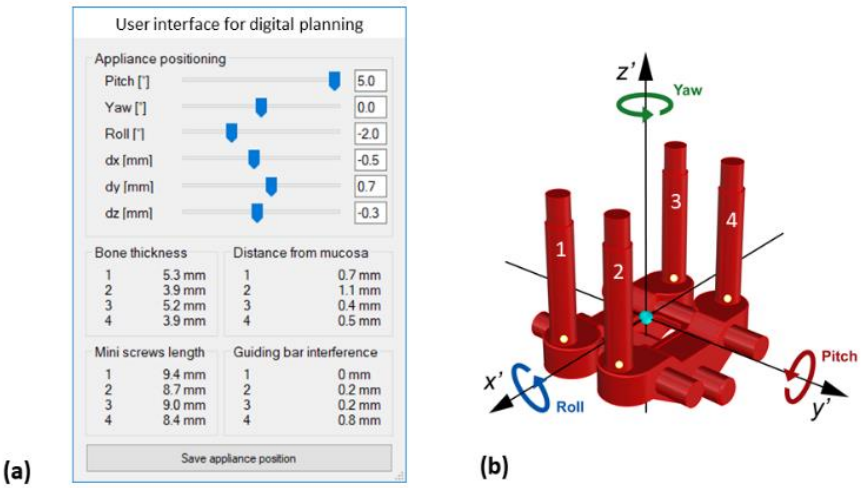

Fig. 2.8 User interface developed with Rhinoceros software, with which the inclination (Yaw, Pitch, and Roll) and position (dx, dy, dz) of MSE appliance can be changed to optimize the bone thickness (BT) at the level of the 4 micro-implants identified with numbers 1-4, the appliance distance from the palatal mucosa (DM), the micro-implant length required to obtain bicortical engagement (ML) and the guiding bar interference (GBI). (B) yaw, pitch, roll, and reference axes for MSE [64].

The position and inclination of MSE appliance was changed from the initial default setting, taking into consideration the following parameters: bone thickness at the level of the four micro-implants (BT), appliance distance from palatal mucosa (DM), minimum micro-implant length for bicortical engagement (ML) and guiding bar interference (GBI) with palatal mucosa, as shown in Fig. 2.9. As MSE appliance was moved or tilted, the user interface provided, in real-time, the measurements of the parameters to be evaluated.

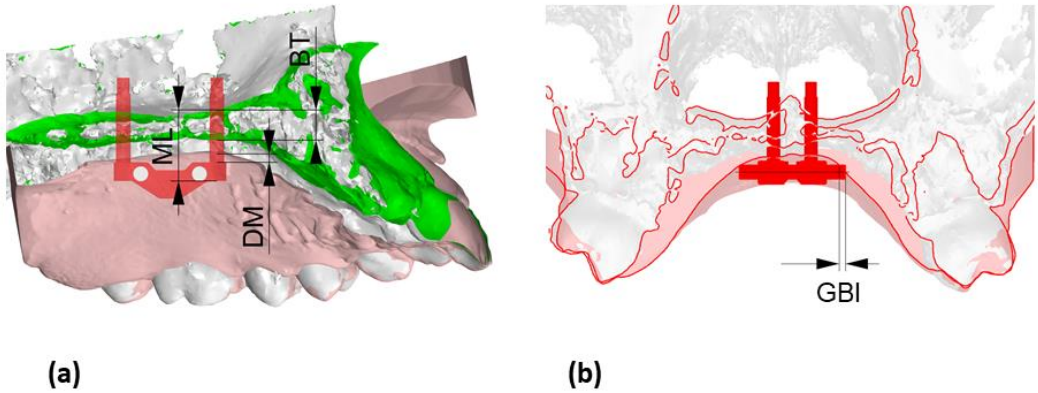

Fig. 2.9. Parameters analyzed during the digital planning of the MSE position and inclination: minimum micro-implant length required to obtain bicortical anchorage (ML), appliance distance from palatal mucosa (DM), bone thickness at the level of the micro-implant insertion sites (BT), guiding bar interference (GBI) with palatal mucosa. (A) sagittal section. (B) coronal section [64].

When a final position and inclination of MSE was identified for the patient (Fig. 2.10 A), a 3D positioning guide was designed on top of the virtual dental arches with the final MSE position (Fig. 2.10 B). Subsequently, the virtual guide was 3D printed with Grey resin (Formlabs, Somerville, USA), the MSE appliance was inserted into the resin positioning guide and secured with steel-ligature (Fig. 2.10 C), and the guide and the appliance were placed on the stone model for the bending and welding of the appliance arms to the molar bands (Fig. 2.10 D).

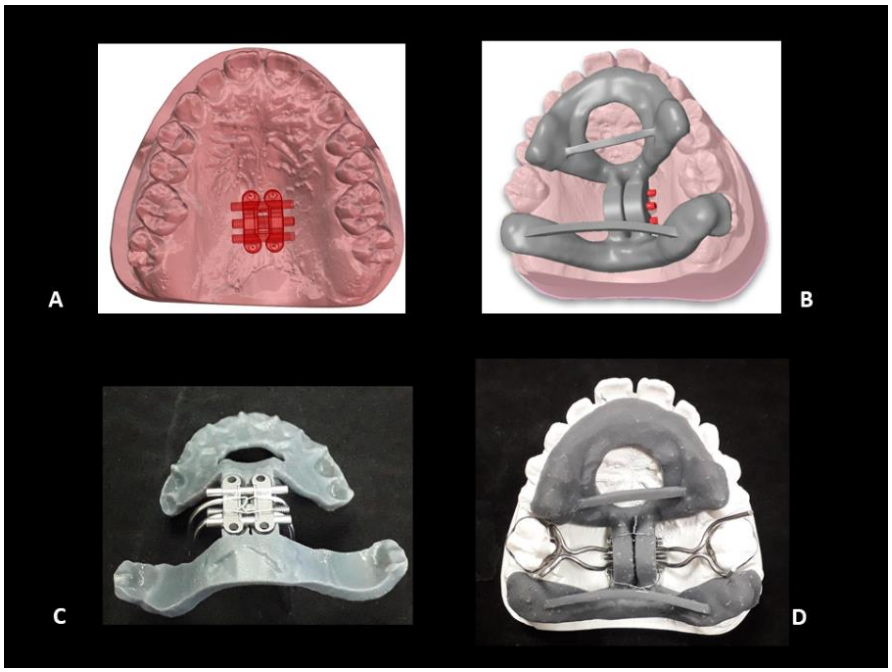

Fig. 2.10. Lab work for MSE. (A) Virtual model with the final position of MSE after digital planning. (B) Digital design of positioning guide. (C) Fixation of the MSE appliance in the positioning guide with steel ligatures. (D) Positioning of the MSE appliance on the dental stone model by means of the resin guide for bending and welding of MSE arms [64].

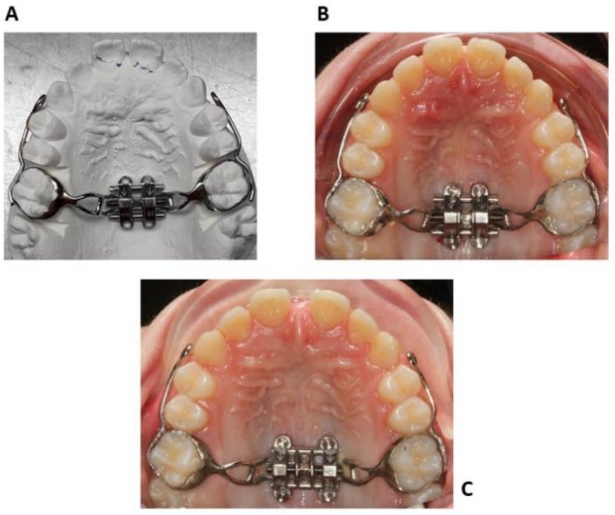

Fig. 2.11 (A) Finalized MSE appliance on the dental stone model. (B) MSE appliance after placement in the patient oral cavity. (C) Intraoral picture after maxillary expansion [64].

The finalized appliance (Fig. 2.11 A) is cemented in the patient oral cavity, and subsequently, 4 micro-implants are inserted through the appliance slots into the palatal bone (Fig. 2.11 B). The appliance itself acts as a surgical guide; hence the micro-implants are embedded in the palate in the same positions selected on the CBCT during the virtual planning.

The resin positioning guide (Fig. 2.11) is used solely by the dental lab technician to fabricate the MSE appliance and not by the orthodontist, since miniscrews are placed after the MSE cementation in the oral cavity, and the appliance itself acts as a surgical guide. The purpose of this methodology is to simplify the clinical appliance positioning in the oral cavity.

With the use of this protocol, a notable tipping of miniscrews was noticed after the first surgical intervention, especially in regions with a thin palatal bone. For this reason, the methodology was slightly modified, incorporating two additional miniscrews to the original MSE design.

After virtual positioning of MSE in the composite model of patient's CBCT and dental arch, palatal bone thickness is measured (Fig. 2.12); then two additional bushings and miniscrews were generated with Rhinoceros software (Fig. 2.13).

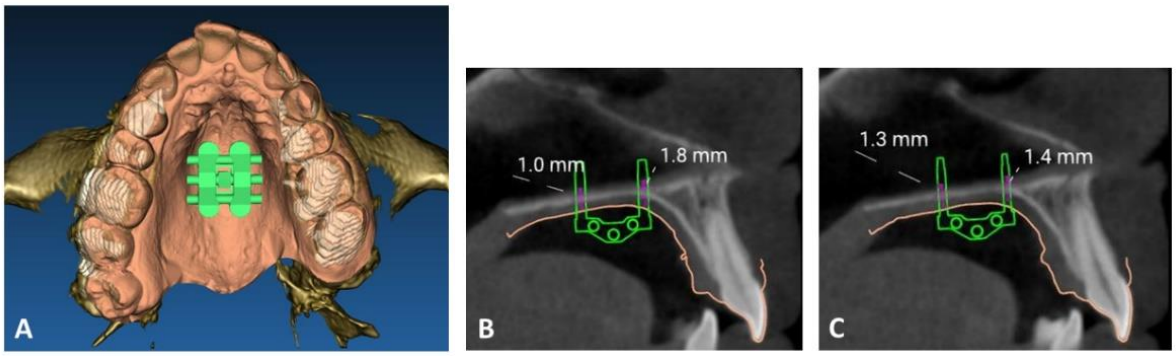

Fig. 2.12. Measurement of palatal bone thickness at the level of 4 miniscrews: bone thickness is less than 2 mm in all miniscrews insertion sites [66].

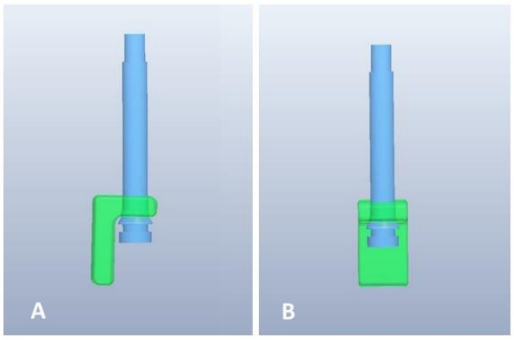

Fig. 2.13. Virtual model of additional bushing and miniscrew for positioning anteriorl to MSE body. A) Lateral view. B) Anterior view. The bushing (in green) represents the slot for the miniscrew insertion, and the cylinder (in light blue) represents the mini-screw itself [66].

Two additional virtual bushings and miniscrews are imported in the patient composite model and positioned anterior to the body of MSE (Fig. 2.14 A-D), where bone thickness is usually higher. The bushings are then produced with Selective Laser Melting (SLM) technique, with Mysint 100 machine (Sisma, Piovene Rocchette, Italy) and Medloy S-Co Cobalt-Chromium alloy (Bego, Bremen, Germany). Bushings are placed along with MSE in a positioning guide which is virtually designed and then 3D printed (Fig. 2.14 E). The positioning guide is utilized to bend and laser weld the MSE arms to the molar bands, and also to laser weld the two additional bushings to the MSE body. The finalized appliance (Fig. 2.14E) presents 6 slots:

the 4 original ones in the MSE body and the 2 additional ones that are generated with CAD-CAM technology and laser welded to the anterior aspect of the MSE. The rationale of this methodology is to dissipate the expansion force on 6 miniscrews, instead of 4, thus reducing the load on each singular miniscrew and surrounding bone, potentially increasing the stability of miniscrews during maxillary expansion.

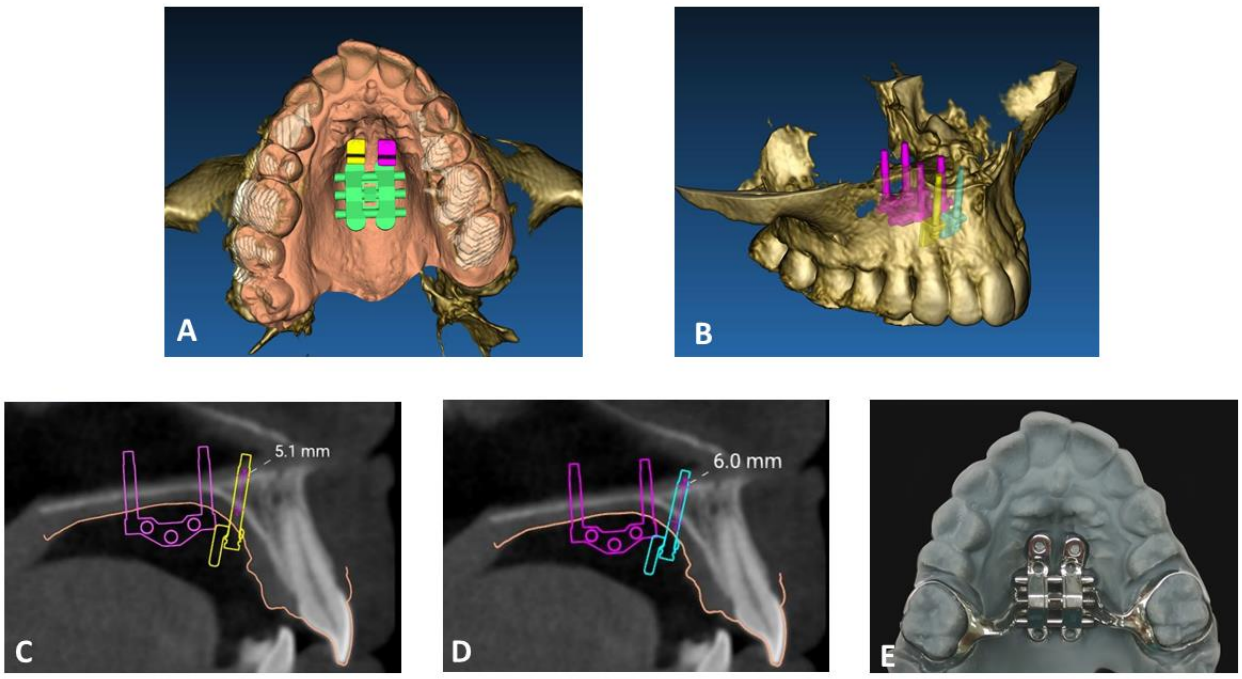

Fig. 2.14. Positioning of additional anterior bushings and miniscrews on the patient integrated virtual model. A) Occlusal view. B) ¾ view. C) Sagittal section, measurement of bone thickness at the level of additional anterior right miniscrew. D) Sagittal section, measurement of bone thickness at the level of additional anterior left miniscrew. E) Finalized MSE appliance [66].

Also, for MSE with 6 miniscrews, appliance is cemented first in the oral cavity, and miniscrews are inserted afterwards. The appliance acts as a positioning guide for the miniscrews, thus simplifying the clinical procedure of appliance delivery. Consequently, the miniscrews are inserted in the exact planned positions during the virtual planning. This

methodology of integrating two additional miniscrews to the original MSE design has been recently published [66].

Clinical trial

Study design

The clinical trial was prospective, spontaneous, and non-pharmacological; the intervention was combining a medical device with minimally invasive surgical technique. The clinical trial was approved by the Milan Area 2 Ethics Committee with approval number 740_2019. All performed procedures were in compliance with the Ethical principles for Medical Research Involving “Human Subjects”, adopted by the Helsinki Conference, June 1964, and an informed consent was obtained from all participants.

Patients were enrolled at the Departments of Orthodontics and Maxillofacial Surgery of Fondazione Ca’ Granda IRCCS Ospedale Maggiore Policlinico of the University of Milan.

Inclusion and exclusion criteria were as follows.

Inclusion criteria:

- Maxillary transverse deficiency, as defined below in this section
- Age of patients above 17 years
- Signature of informed consent

Exclusion criteria

- Presence of craniofacial syndromes

- Pregnancy or lactation
- Concurrent treatment with drugs that interfere with bone metabolism

Maxillary transverse deficiency was defined by analyzing the relationship between maxillary and mandibular width, as described in previous publications [36,43] (Fig. 2.15).

Maxillary width is defined as the distance between the right and left most concave point on maxillary vestibules at the level of maxillary first molars. Mandibular width is defined as the distance between the right and left mandibular WaLa ridge at the level of the mandibular first molars. WaLa ridge represents the most prominent portion of the buccal alveolar bone. In a normally developed maxilla, the maxillary width should be compatible to the mandibular width. Maxillary transverse deficiency is calculated as the difference between mandibular and maxillary width, and represents the amount of maxillary skeletal expansion required for the patient, as shown in Fig. 2.15.

Fig. 2.15. Measurement of maxillary (a) and mandibular width (b) on a stone model. The frontal view of maxillary (blue line) and mandibular width (red line) is shown in (c) [36,43].

Surgical intervention

Patients were treated with MSE appliance and localized osteotomies performed with a minimally invasive surgical technique.

Position of MSE and miniscrews was digitally planned on the composite model of patient's CBCT and digital dental arch, as previously described in this chapter (Pg. 19-23). After the first surgical intervention, a substantial tipping of miniscrews was noticed, for this reason, in all following interventions, MSE with 6 miniscrews was utilized. Additional bushings were added with CAD-CAM technology to the original MSE design, as previously described in this chapter (Pg. 25-26). Furthermore, MSE rigid arms, instead of soft arms were adopted, and additional arms connecting the palatal surface of maxillary first molar, second premolar and first premolar were added. The purpose of these modifications was to increase the rigidity of the appliance and the involvement of a larger number of teeth to reduce the load on miniscrews during intra-operatory appliance activations. The modified MSE appliance utilized in the study is shown in Fig. 2.16.

MSE and miniscrews position were digitally planned to satisfy the following criteria:

- Maximum thickness of palatal bone at the level of miniscrews insertion sites (Fig. 2.9 A)
- Proximity of MSE expansion force vector to maxillary center of resistance, represented by the bi-zygomatic line (Fig. 2.6 D)
- Proximity of MSE appliance to palatal mucosa (Fig. 2.9 A), to minimize the leverage effect on miniscrews during the activation of the appliance

During digital planning, the length of miniscrews was chosen to obtain a bicortical anchorage (Fig. 2.8 A): miniscrews should penetrate the MSE appliance body or additional bushings, the palatal mucosa, the cortical bone layers of palatal vault and nasal floor, and 1 mm into the nasal cavity (Fig. 2.3 and 2.8 A).

Fig. 2.16. MSE with 6 miniscrews utilized in the study. Intraoral view of a patient after treatment.

MSE was cemented in the oral cavity of the patients, and 4 or 6 miniscrews were inserted after appliance cementation, at the Orthodontic Department of the University of Milan. First operated patient had MSE with 4 miniscrews. All following patients had MSE with 6 miniscrews. Miniscrews were inserted after injection of local anesthesia (Carbocaine with 1:100.000 Adrenaline) in the palatal mucosa around MSE miniscrews slots.

Surgical interventions were performed at the Maxillofacial Surgery Department of the University of Milan, 1 to 7 days after appliance and miniscrews positioning.

Patients underwent sedation with Remifentanil and Midazolam, then local anesthesia (Carbocaine with 1:100.000 Adrenaline) was injected in the vestibule of maxilla from maxillary first molar to contralateral maxillary first molar.

A horizontal incision was performed on the alveolar mucosa in the region above upper central and lateral incisors (Fig. 2.17).

Fig. 2.17. Horizontal incision above upper central and lateral incisors

A first osteotomy was performed with a piezoelectric instrument (Piezosurgery, Mectron, Carasco, Italy) and a long blade (MT8-20 L, Mectron, Carasco, Italy) (Fig. 2.18), along the anterior portion of the midpalatal suture. The blade was inserted below the anterior nasal spine and progressed backwards, towards the posterior nasal spine, for its entire length of 2 cm. This osteotomy was named “midpalatal osteotomy” (MO).

Fig. 2.18. Blade of piezoelectric instrument utilized in the study.

Then, with submucosal tunneling technique, utilizing the same piezoelectric blade, two lateral osteotomies were performed (Fig. 2.19), one per each side of the skull, at the basis of the zygomatic process of the maxilla. The lateral osteotomies extended from the distal aspect of the zygomatic process of maxilla (usually at the level of mesial aspect of maxillary second molar) to an area above the canine root, and did not extend to the piriform rim of

maxilla. Lateral osteotomies were performed apically to dental root apices, to prevent dental lesions. Lateral osteotomies were named “lateral maxillary osteotomies” (LMOs).

Fig. 2.19. Lateral maxillary osteotomy (LMO) performed at the basis of zygomatic process of maxilla, extending from the distal aspect of the zygomatic process to an area above the canine root. Lateral osteotomy did not extend to the piriform rim of maxilla.

In total, 3 osteotomies were performed: one at the anterior portion of the midpalatal suture for a depth of 2 cm (midpalatal osteotomy), and one per side at the basis of the zygomatic process of the maxilla (lateral maxillary osteotomies), like shown in Fig. 2.20 – 2.21.

Fig. 2.20. Three osteotomies performed in the study: intraoral frontal view.

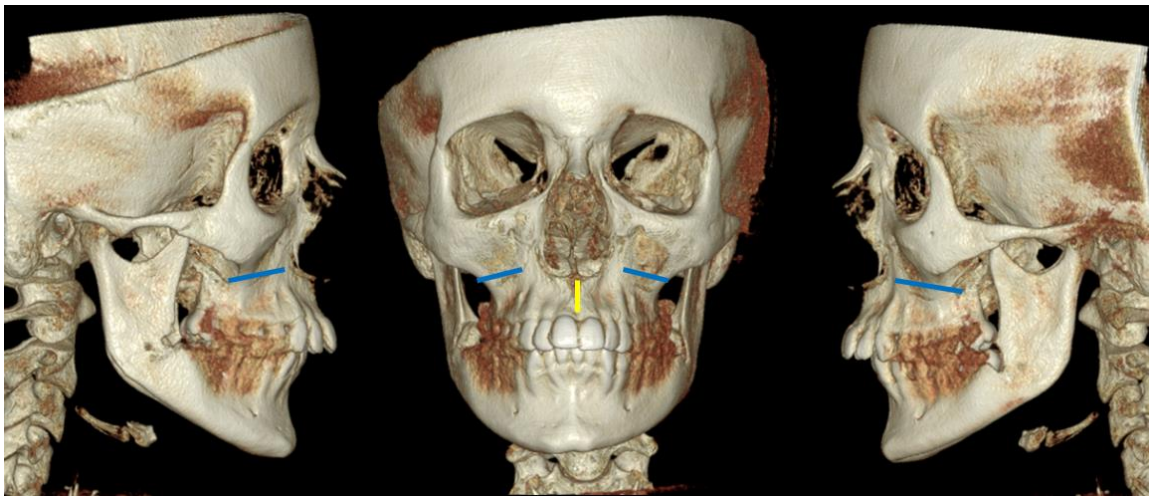

Fig. 2.21. Illustration with skull 3D renderings, showing the central “midpalatal osteotomy” (MO) at the midpalatal suture (in yellow) and the “lateral maxillary osteotomies” (LMOs) at the basis of the zygomatic process of maxilla (in blue).

As shown in Fig. 2.22, osteotomies did not extend to the:

- basis of nasal septum
- medial wall of maxillary sinus
- piriform rim of maxilla
- pterygopalatine suture

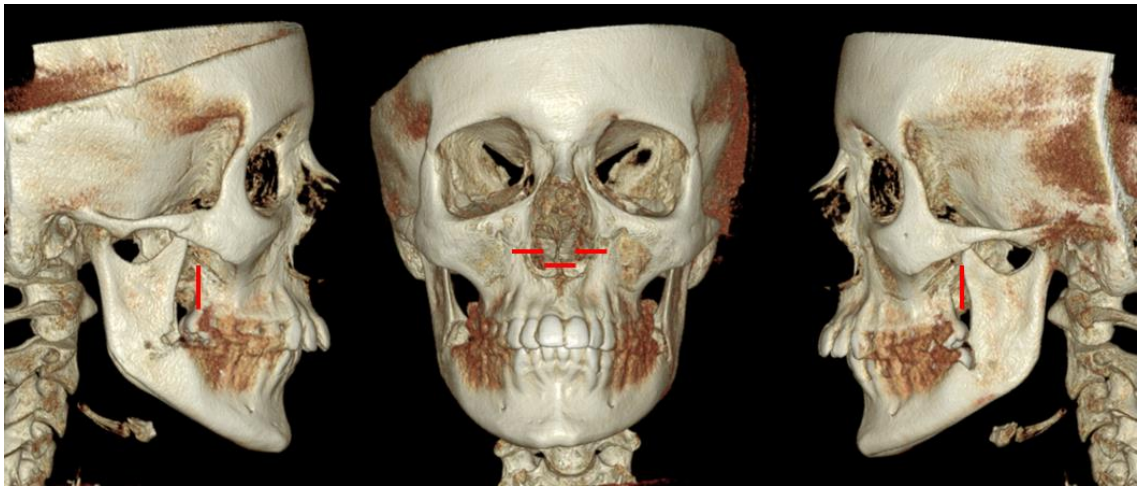

Fig. 2.22. Differently from conventional Surgical Assisted Rapid Palatal Expansion (SARPE), osteotomies were not performed at the basis of nasal septum, medial wall of maxillary sinus, piriform rim, pterygopalatine suture (in red).

Protocol for intra-operatory MSE activations is explained in the following section.

Mucosal incision was then sutured with Vicryl 3-0 resorbable suture.

Patient underwent therapy with antibiotics (Amoxicillin and Clavulanic Acid, 1 gr, twice a day) for 6 days, Dexamethasone 4mg the day of surgery, Ketorolac 30 gr every 12 hours for the first day and then only in case of pain.

Appliance activation protocol

MSE appliance was activated intra-operatively with 20 turns (1 turn = 0.13 mm expansion) immediately after the execution of osteotomies. A set of 5 consecutive activations per time was performed; after each cycle of 5 activations, mobility of maxillary halves was checked at the midpalatal osteotomy (MO) site. In case, after 20 activations, maxillary halves were not mobile, the osteotome was enhanced by a hammer to produce a fracture in the midpalatal suture that could propagate in an antero-posterior direction.

After surgical intervention, MSE was not activated for 7 days, to avoid discomfort to the patient.

After 7 days, MSE was activated with a rate of 2 turns per day until completion of maxillary expansion.

However, after the first operated patient, a noticeable tipping of miniscrews was noticed in the post-expansion CBCT. For this reason, the activation protocol was changed as follows:

- 20 activations during surgical intervention
- No activations for 7 days after the surgical intervention
- Afterwards, 1 activation per day until completion of maxillary expansion

This activation protocol was utilized for all operated patients, except for the first one.

During the MSE activations period, the patient was examined every 7 days. The activation of maxillary expansion was stopped when the maxillary width was equal to the mandibular width.

3D analysis

CBCT scans were taken both before and within 1 month after the completion of expansion on all patients. CBCT scans were taken by a Carestream 9000 3D machine in an 17x13.5 field of view (FOV). Scan times were 11.3 seconds, with 110 kV. Data from the CBCT was reconstructed to produce 0.4 mm slices.

Analysis of midface skeletal and dentoalveolar effects was performed utilizing a methodology adopted in the previous publications [34,36-39,43-44]. Using the OnDemand3D software by Cybermed Inc., the pre- and post-expansion CBCTs of the patients were superimposed using the grey level intensity of the voxels of the anatomical structures within the entire cranial base [67]. This superimposition method utilizes the voxel gray scale and is fully automated by the software through the "Automatic Registration" tool, to avoid errors by the operator. The accuracy of the method has been validated by Weissheimer et al. in 2015 [68].

After this superimposition, a plane, named "Maxillary Sagittal Plane" [36,43] (Fig. 2.23), passing through the anterior nasal spine (ANS), posterior nasal spine (PNS) and Nasion (N) was identified on the pre-expansion CBCT.

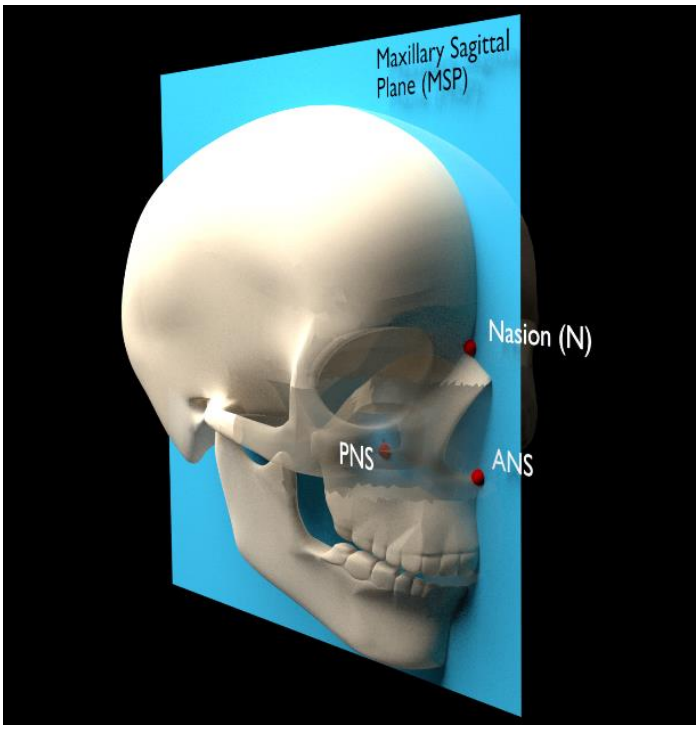

Fig. 2.23. Maxillary Sagittal Plane (MSP) [36,43,44], for evaluating skeletal movements of the midface induced by MSE and localized osteotomies [36-43].

The distance from the maxillary sagittal plane (MSP) to various landmarks on maxillary and circummaxillary bones are the parameters used for evaluating lateral skeletal displacements induced by the treatment.

The maxillary sagittal plane (MSP) passes through the center of maxilla and midface, and the lateral movements of maxillary and circummaxillary bones can be accurately described by tracking the landmarks moving away from this reference plane during the expansion. This reference plane was established from the pre-expansion CBCT and applied to the post-expansion CBCT, utilizing the automated superimposition on anterior cranial base by the software. The positions of the bony landmarks between pre- and post-expansion CBCT were analyzed relative to this reference plane.

Furthermore, the lateral movement of the two halves of maxilla can be quantified independently by measuring the relative displacement of ANS and nasopalatine foramen (NPF) against MSP during the expansion for each half. The extent of asymmetry during expansion can be quantified by tracking the relative displacements of ANS and NPF of the two halves, and its association with the circummaxillary structures can be explored [36,37,44].

The **maxillary sagittal plane (MSP)** passes through the anterior nasal spine (ANS), posterior nasal spine (PNS), and through Nasion (N) in the pre-expansion CBCT as shown in Fig. 2.23 and 2.24.

Another utilized reference plane was axial palatal plane (APP), which passes through PNS and ANS and is perpendicular to MSP (Fig. 2.24 and 2.25).

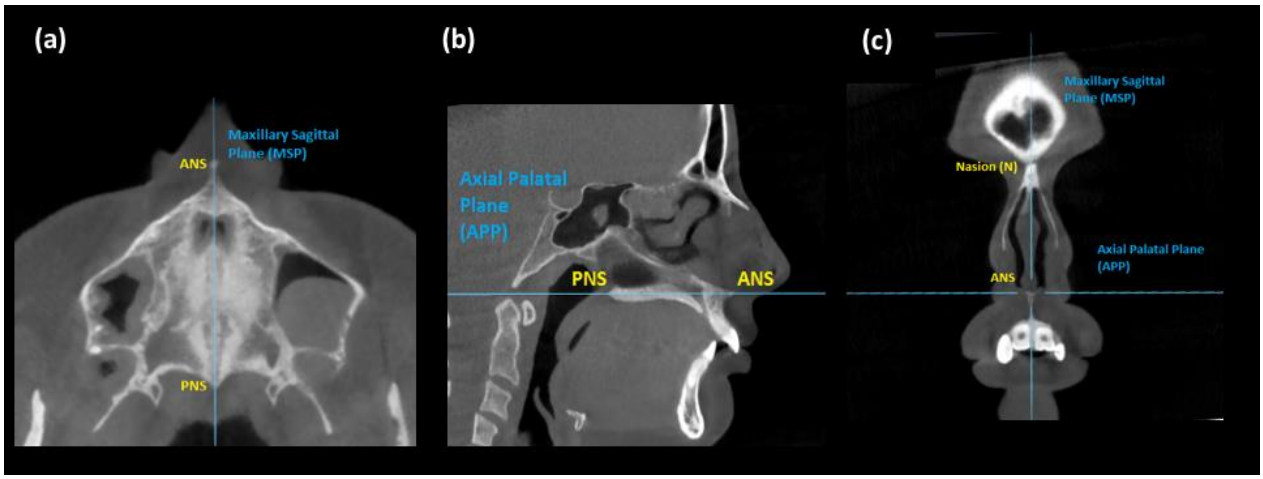

Fig. 2.24 Sections used to identify the Maxillary Sagittal Plane (MSP) and Axial Palatal Plane (APP). A) Axial section. B) Sagittal section. C) Coronal section [36,43,44].

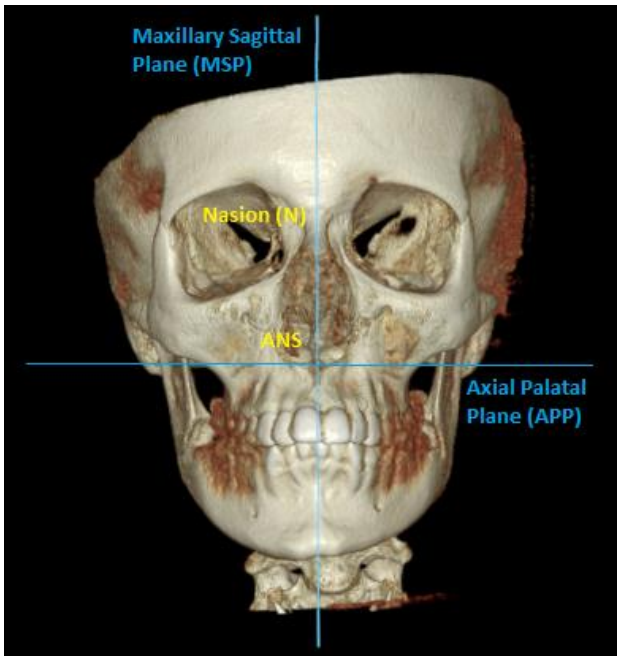

Fig 2.25. 3D rendering showing the axial palatal plane (APP) perpendicular to maxillary sagittal plane (MSP) [36,43,44].

An axial section, parallel to the axial palatal plane (APP) and passing through sella turcica was checked in every patient before taking the measurements, to verify the accuracy of the software automated superimposition on anterior cranial base (Fig. 2.26).

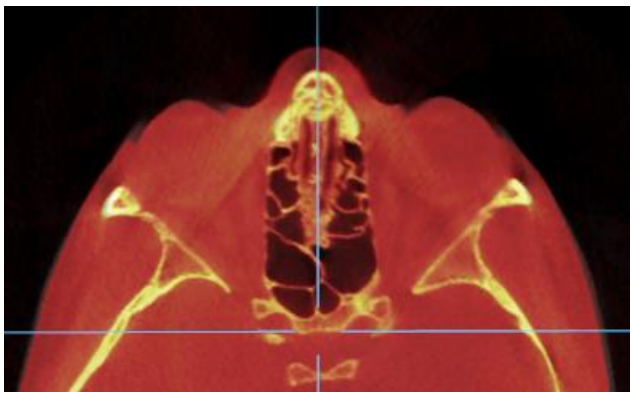

Fig. 2.26 Superimposed image of pre-expansion (grey) and post-expansion (yellow) CBCT: axial section through the anterior cranial base, showing the accurate superimposition of anatomical structures [36,43,44].

To analyze the skeletal modifications in the horizontal plane in the maxilla and sphenoid bone, two sections were selected in the pre- and post-expansion CBCT of the patients, the axial palatal section (APS) and the lower nasal section (LNS).

The axial palatal section (APS) is a slice passing through the axial palatal plane as defined above in this section (Fig. 2.24-2.25).

The upper nasal section (UNS) is parallel to the axial palatal plane (APP) and passes through the most posterior point of vomer (V point) (Fig. 2.27).

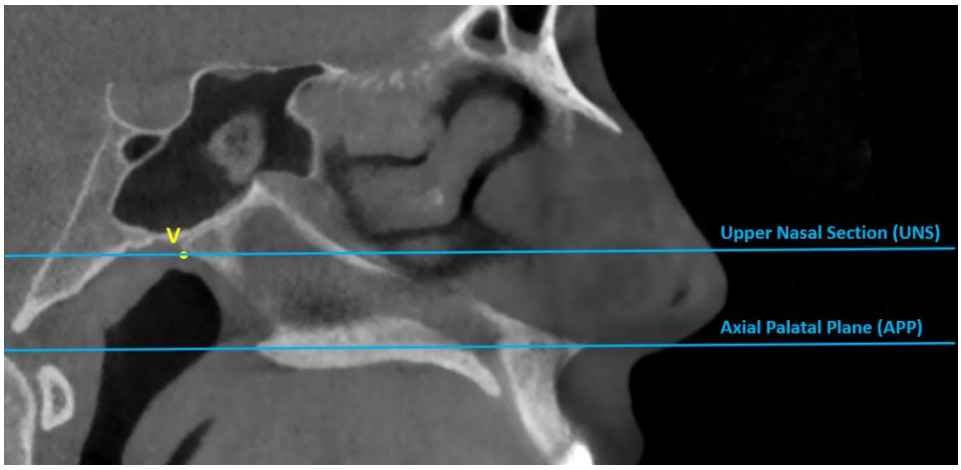

Fig 2.27. Upper Nasal Section (UNS), parallel to axial palatal plane and passing through the most posterior point of vomer (V) [36,44].

Fig. 2.28 shows the two axial sections utilized to evaluate the skeletal changes in the maxilla and in the pterygoid processes of the sphenoid bone: axial palatal section (APS), and upper nasal section (UNS).

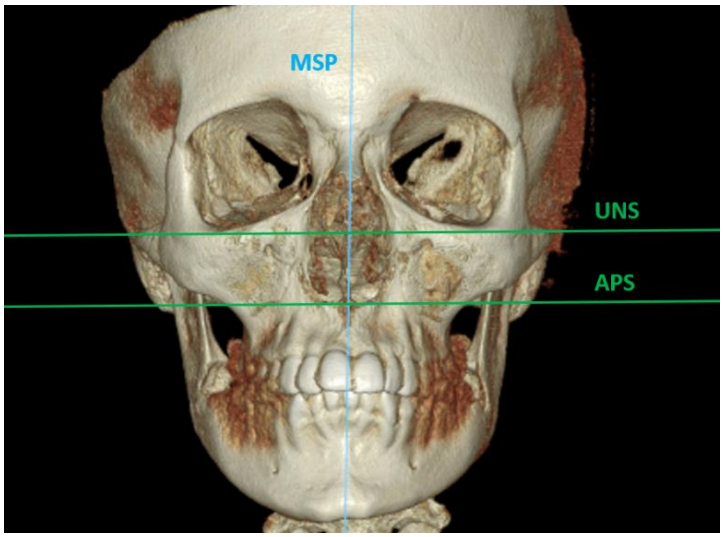

Fig 2.28. Skull 3D rendering with the two axial sections (APS, UNS) [36,44].

The two axial sections, APS and UNS, cut through the pterygopalatine suture in distinct areas [36,43] as shown in Fig. 2.29 and 2.30.

The axial palatal section (APS) cuts the pterygopalatine suture in an area where the "pyramidal process" of the palatine bone articulates with the "pterygoid notch" located between the lateral plate and the medial plate of the pterygoid process. The changes in this area due to the maxillary expansion will be described as "openings" between the lateral and medial pterygoid plates. The frequency of openings (i.e. the percentage of patients and the percentage of sutures with openings between these plates) and the width of the openings will be described as indicators for loosening of the suture in treated patients.

The upper nasal section (UNS) cuts through the pterygopalatine suture in an area where the perpendicular plate of the palatine bone forms the medial wall of the pterygopalatine fossa. The perpendicular plate of the palatine bone in its upper portion presents the "sphenopalatine notch" where nerves (posterior superior lateral nasal nerve and nasopalatine nerve) and vessels (sphenopalatine artery and vein) pass from the pterygopalatine fossa to the superior meatus of the nose. The upper portion of the

perpendicular plate of the palatine bone presents also the “sphenoidal process” that articulates with the medial surface of pterygoid process of the sphenoid and the “orbital process” that articulates with the maxilla (Fig. 2.29).

Furthermore, APS and UNS cut through maxilla and sphenoid bone in the lowest and highest points of choanae, respectively (Fig. 2.31).

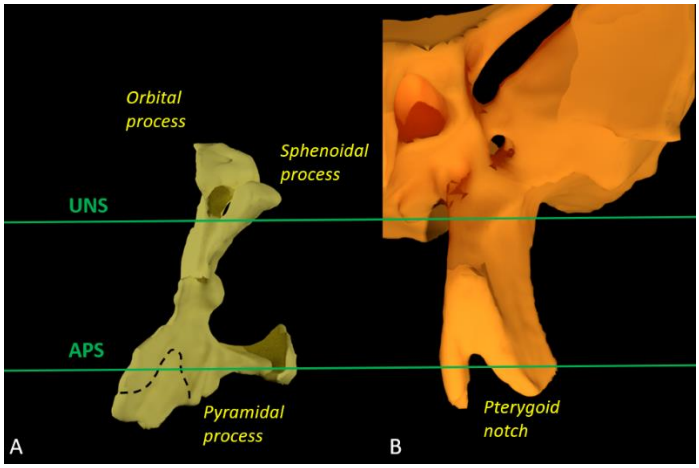

Fig. 2.29. Illustration showing axial palatal section (APS) and upper nasal section (UNS) crossing the left palatine bone (posterior view in A) and the left pterygoid process of the sphenoid bone (anterior view in B) [36,44].

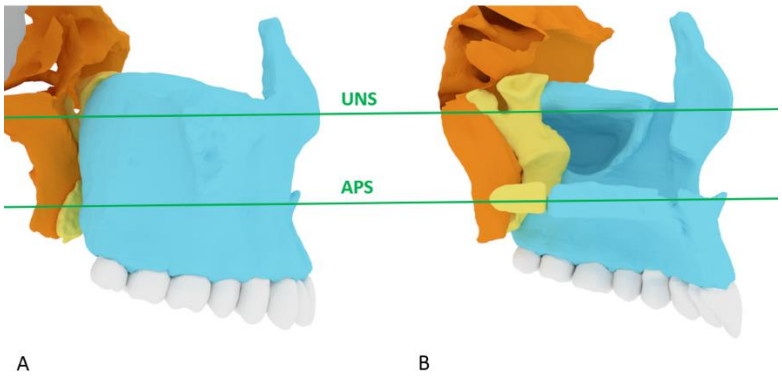

Fig. 2.30. Illustration showing the axial palatal section (APS) and upper nasal section (UNS) crossing the pterygomaxillary region. A: lateral view. B: medial view. Sphenoid bone in orange, palatine bone in yellow, maxillary bone in light blue [36,44].

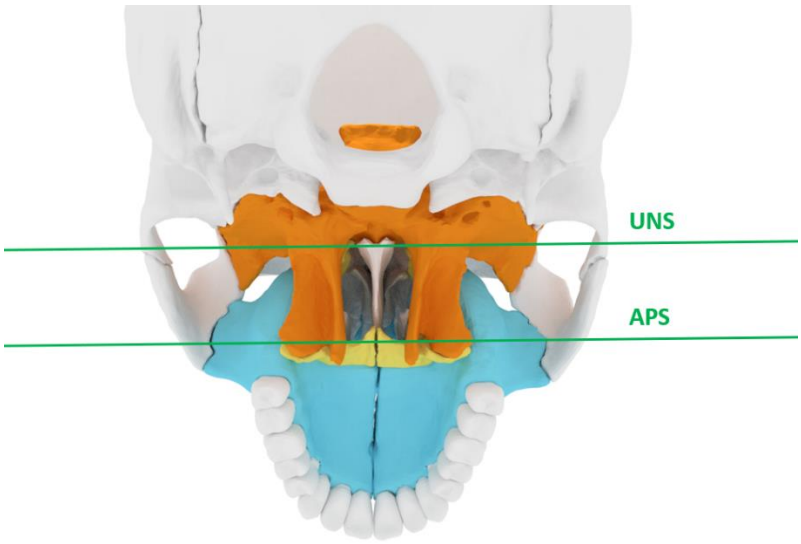

Fig. 2.31. Illustration showing the axial palatal section (APS) and upper nasal section (UNS) crossing the lowest and highest point of choanae, respectively. Posterior view. Sphenoid bone in orange, palatine bone in yellow, maxillary bone in light blue [36,44].

The procedure to assess the displacement of maxillary bones and pterygoid processes is explained in Fig. 2.32. The post-expansion CBCT is superimposed on the pre-expansion CBCT on the anterior cranial base (Fig. 2.32 A). The maxillary sagittal plane (MSP) and axial palatal plane (APP) are identified in the pre-expansion CBCT. Then the axial palatal section (Fig. 2.32 B) and upper nasal section (Fig. 2.32 D) are selected for the measurements. The slice through the anterior cranial base (Fig. 2.32 E) was checked in every patient before taking the measurements in order to verify the accuracy of automated superimposition by the software.

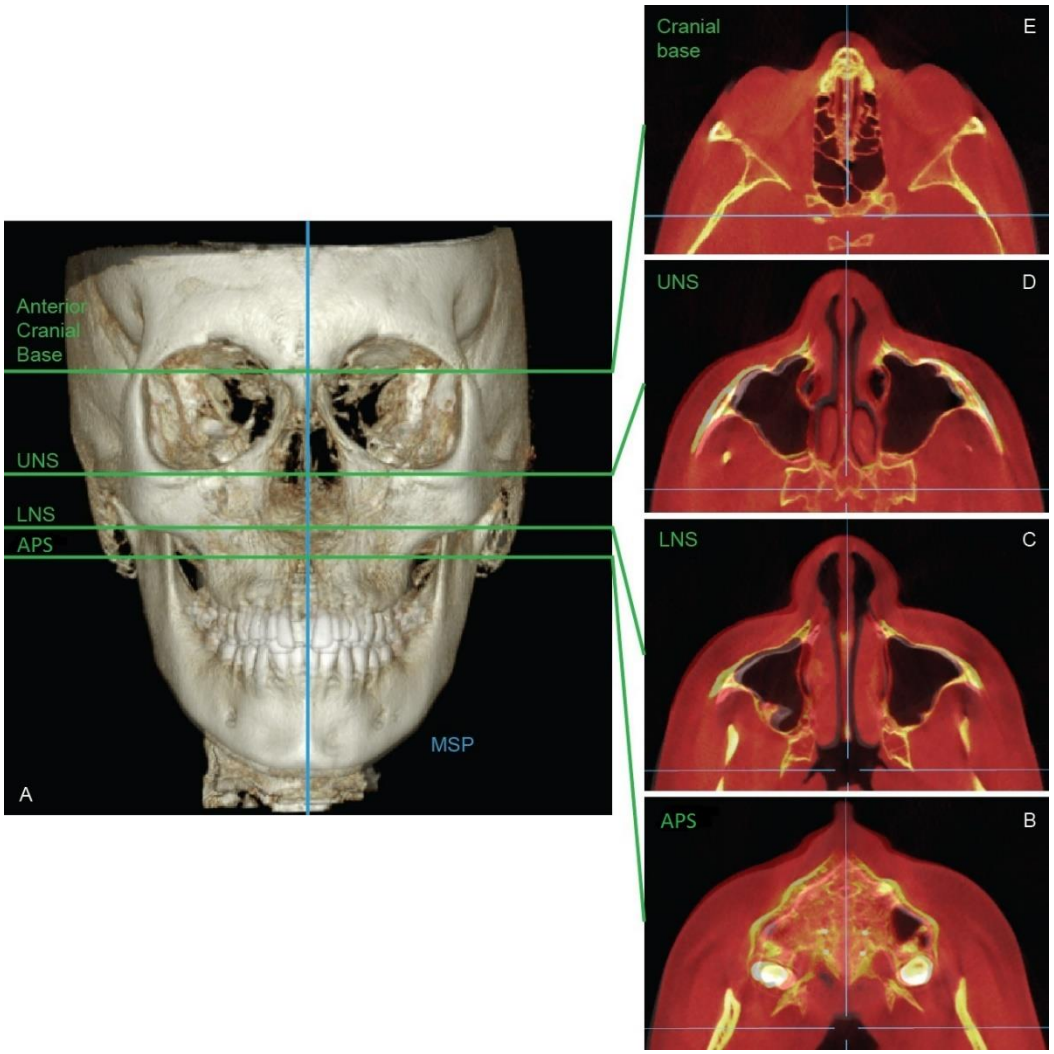

Fig 2.32. Illustration showing the procedure followed to assess the displacement of the maxilla and pterygoid processes of the sphenoid. A: a 3D superimposition rendering of the skull. B: axial palatal section (APS). C: lower nasal section (LNS). D: upper nasal section (UNS). E: section through the anterior cranial base [36,44].

Measurements on the axial palatal section (APS)

The axial palatal section (APS) was used to measure the lateral movement of ANS, NPF and PNS, and the openings between the lateral and medial plates of the pterygoid process. The landmarks identified in APS are shown in Fig. 2.33. With the exception of NPF, these landmarks could be detected only in the post-expansion CBCT. In the pre-expansion CBCT, ANS and PNS for right and left halves are in contact, and no gaps between the lateral and

medial plates of the pterygoid processes exist since the pterygoid notch is occupied by the pyramidal process of the palatine bone. A value equal to zero was assigned to these landmarks as distance measurement in the pre-expansion CBCT.

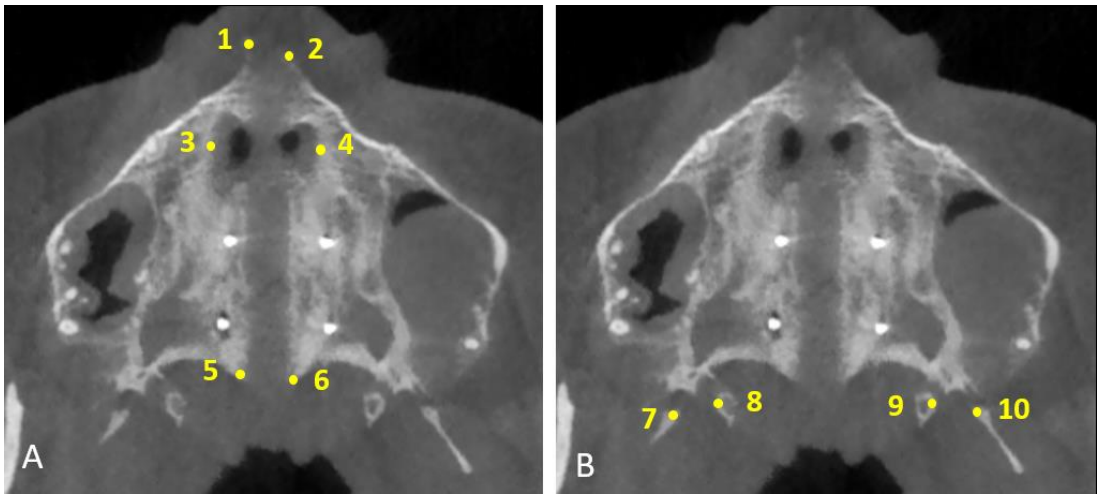

Fig. 2.33. Landmarks identified in the axial palatal section (APS) for the post-expansion CBCT. A: Landmarks in the midpalatal suture. B: Landmarks in the pterygoid processes of the sphenoid bone. 1: Right anterior nasal spine (Rt ANS); 2: Left anterior nasal spine (Lt ANS); 3: Most lateral point of nasopalatine foramen on right maxilla (Rt NPF); 4: Most lateral point of nasopalatine foramen on left maxilla (Lt NPF); 5: Right posterior nasal spine (Rt PNS); 6: Left posterior nasal spine (Lt PNS); 7: Most medial point of the lateral plate of the right pterygoid process (Rt Lat Pter); 8: Most lateral point of the medial plate of the right pterygoid process (Rt Med Pter); 9: Most lateral point of the medial plate of the left pterygoid process (Lt Med Pter); 10: Most medial point of the lateral plate of the left pterygoid process (Lt Lat Pter) [36,44].

The parameters evaluated in the axial palatal section (APS) are listed in Table I.

Table 1. Parameters evaluated in the axial palatal section (APS)
ANS: anterior nasal spine; PNS: posterior nasal spine;
NPF: nasopalatine formen

1	Distance of Rt ANS from maxillary sagittal plane
2	Distance of Lt ANS from maxillary sagittal plane
3	Distance of Rt NPF from maxillary sagittal plane
4	Distance of Lt NPF from maxillary sagittal plane
5	Distance of Rt PNS from maxillary sagittal plane
6	Distance of Lt PNS from maxillary sagittal plane
7	Lateral displacement of Rt ANS + Lt ANS (total split at ANS)
8	Lateral displacement of Rt NPF + Lt NPF (total increase of NPF width)
9	Lateral displacement of Rt PNS + Lt PNS (total split at PNS)
10	Width of opening in Rt pterygoid process
11	Width of opening in Lt pterygoid process
12	Pterygoid plates width (PPW)
13	Distance between the two halves of MSE appliance (measured in a CBCT section slightly below APS)

The post-expansion CBCT of the patient was superimposed on the pre-expansion CBCT at the stable anterior cranial base; MSP and APP and were identified in the pre-expansion CBCT; and then the axial palatal section (APS) was selected (Fig. 2.34).

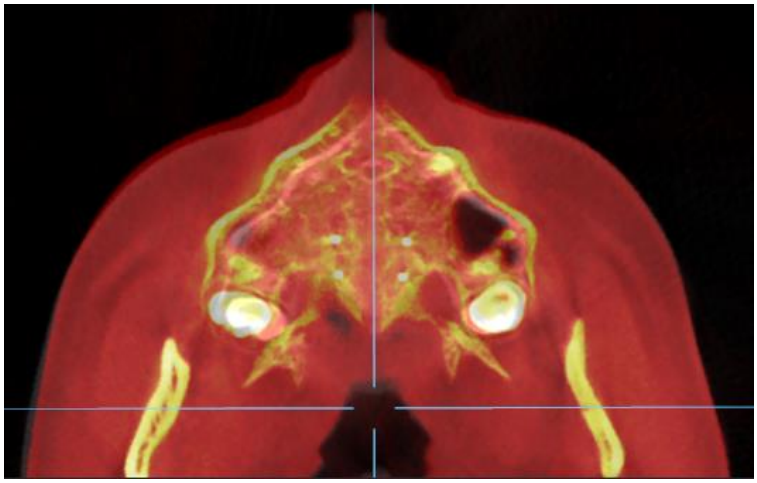

Fig. 2.34. Axial palatal section (APS): example of the superimposed image of a treated patient. The sagittal blue line is the MSP determined from the pre-expansion CBCT [36,44].

During maxillary expansion the midpalatal suture splits, and the anterior nasal spine (ANS) and the posterior nasal spine (PNS) are split in two halves producing Rt ANS, Lt ANS, Rt PNS and Lt PNS which can be identified in the post-expansion CBCT (Fig. 2.33). The distance from the maxillary sagittal plane (MSP) to Rt ANS, Lt ANS, Rt PNS and Lt PNS were measured as shown in Fig. 2.35.

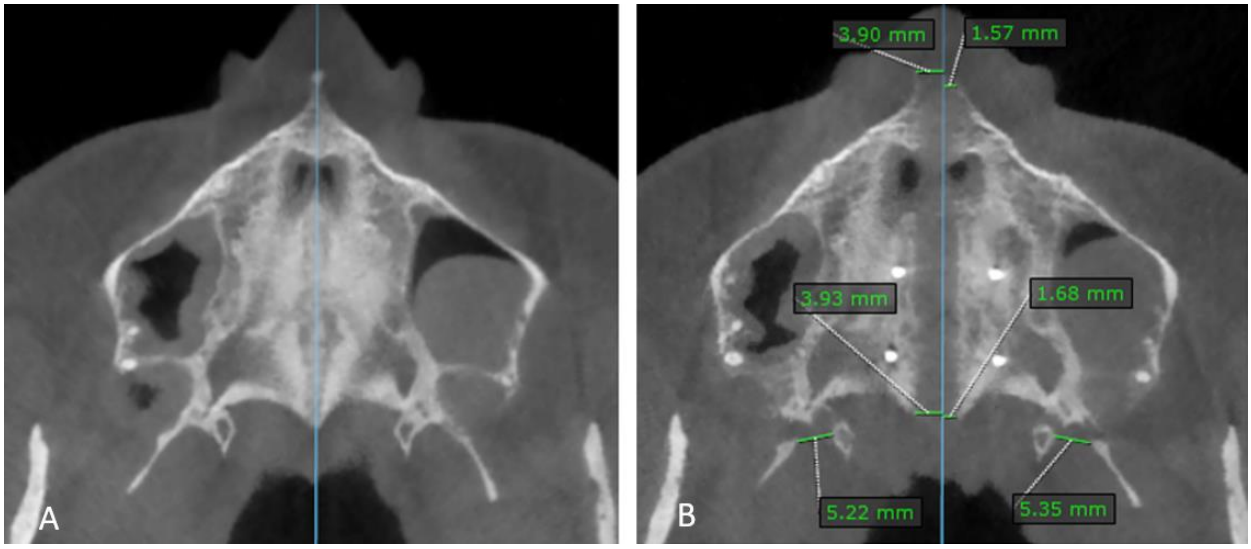

Fig. 2.35. Measurements on the axial palatal section (APS). A: pre-expansion. B: post-expansion. Blue line: maxillary sagittal plane (MSP). MSP passes through ANS and PNS in the pre-expansion CBCT and becomes a reference line for measuring the lateral movements of skeletal landmarks in the post-expansion CBCT [36,44].

Furthermore, in the present investigation, the skeletal effect at the anterior part of the palate was evaluated also utilizing the nasopalatine foramen as a reference, as shown in Fig. 2.36. In fact, the anterior nasal spine (ANS) may be cut by the piezoelectric blade during surgery, hence the most lateral point of the nasopalatine foramen may represent a more reliable skeletal landmark.

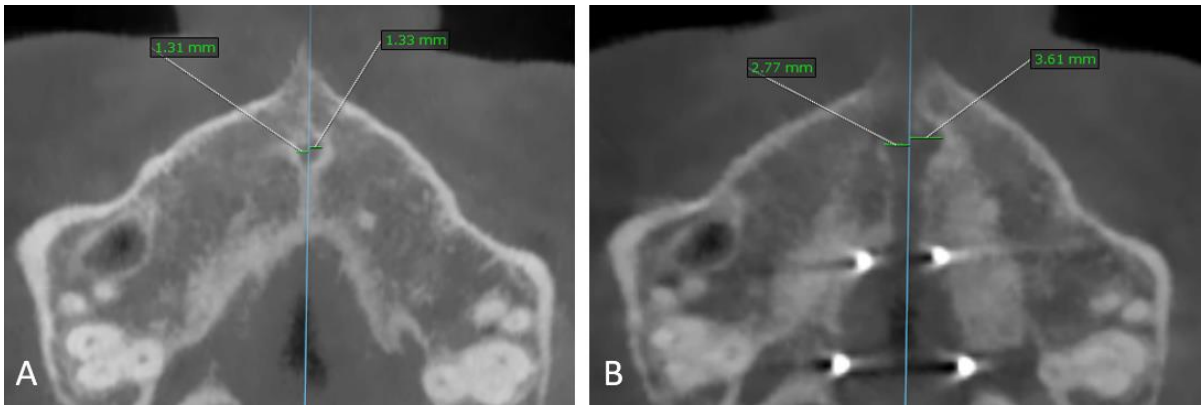

Fig. 2.36. Measurements on the axial palatal section (APS). A: pre-expansion. B: post-expansion. Blue line: maxillary sagittal plane (MSP). MSP passes through nasopalatine foramen (NPF) in the pre-expansion CBCT and becomes a reference line for measuring the lateral displacement of two halves of NPF in the post-expansion CBCT.

The **distance from the maxillary sagittal plane (MSP) to Rt ANS, Lt ANS, Rt PNS and Lt PNS** in the pre-expansion CBCT was given a value of zero. The distance of **Rt NPF and Lt NPF** from MSP in the pre-expansion CBCT was measured and averaged. In the post-expansion CBCT, the distance for each landmark from the maxillary sagittal plane was averaged, and then the Wilcoxon sign rank test was used to compare the pre-and post-expansion distances for statistical significance.

The **symmetry of the split** was also evaluated in the axial palatal section by comparing the lateral movement of right and left ANS and NPF. The adopted methodology is explained at the end of this chapter.

The **opening between the lateral and medial pterygoid plates** is due to the fact that the pyramidal process of the palatine bone is pulled away from the pterygoid plates during maxillary expansion [36,37,44]. The size of the opening is measured as the distance from the most medial point of the lateral pterygoid plate to the most lateral point of the medial pterygoid plate (Fig. 2.35 B).

When the opening was not visible in the axial palatal section (APS), the other axial slices slightly above the axial palatal section (APS) were checked because the openings sometimes appeared in the slices above APS (Fig. 2.37). If these openings were observed in several axial sections, the section with the largest opening was chosen for the measurement, as described in previous studies [36,44].

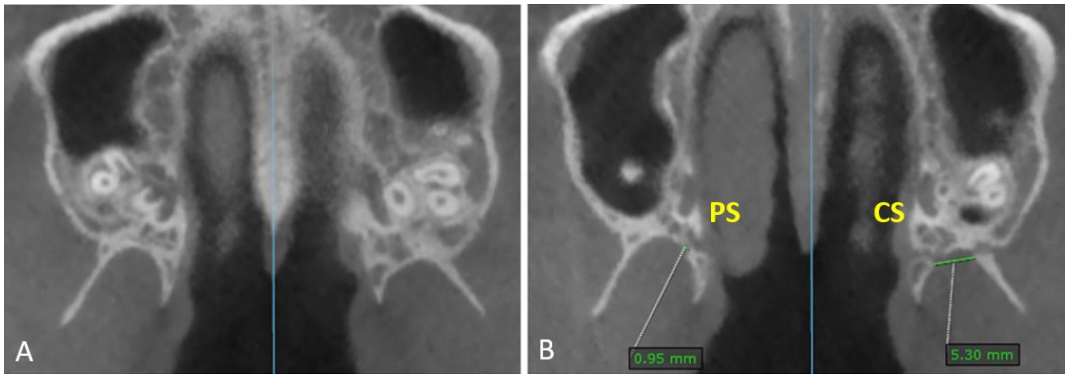

Fig. 2.37. CBCT of a treated patient. A: pre-expansion. B: post-expansion. Openings between the lateral and medial pterygoid plates detected on an axial slice situated slightly above the axial palatal section (APS) in the post-expansion CBCT. PS: partial split of the pterygopalatine suture; CS: complete split of the pterygopalatine suture [36,44].

In the case of a partial disengagement of the pyramidal process from the pterygoid notch ("PS" in Fig. 2.37 B), the width of the opening was measured from the pyramidal process to the pterygoid plate adjacent to the opening.

For each patient, on the right and left side of the skull, the type of split of the pterygopalatine suture, i.e. partial split (PS) or complete split (CS) (Fig. 2.37 B), was analyzed and assigned accordingly.

The **frequency of the openings** (i.e. the percentage of patients and sutures with openings) and the **average width of the opening** were calculated, and they were used as parameters for loosening of the pterygopalatine suture. In the pre-expansion CBCT, the frequency and

width of the openings were given a value of zero. The Fisher's exact test was used to evaluate the statistical significance of the changes for the frequency of openings. The non-parametric Wilcoxon sign rank test was used to compare the average width of the openings before and after expansion for statistical significance.

Furthermore, the **pterygoid plates width (PPW)** was measured as the distance between the most external point of right and left lateral pterygoid plates of sphenoid bone (Fig. 2.38).

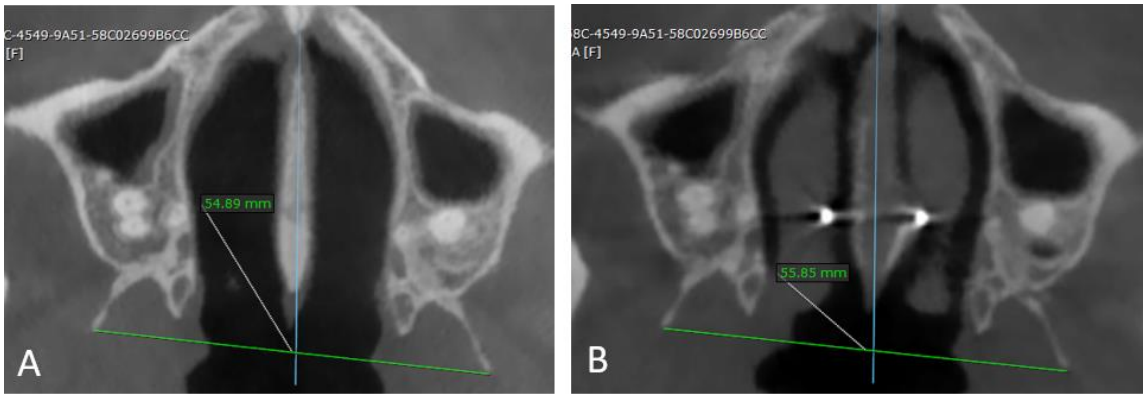

Fig. 2.38. CBCT of a treated patient. A: pre-expansion. B: post-expansion. Pterygoid plates width (PPW): defined as the distance between the most external point of right and left lateral pterygoid plates of sphenoid.

The measurements before treatment were subtracted from those after treatment to assess the treatment changes. The treatment change is equivalent to the lateral movement of the lateral pterygoid plates. The distance measurements were averaged, and a paired T-test was used for statistical significance.

To calculate the **average amount of activation of the expansion jackscrew** received by the patients, the distance between the two halves of the expansion screw was measured on the post-expansion CBCT (Fig. 2.39), and the pre-expansion distance, measured on 10

MSE appliances and averaged, was then subtracted. The values were averaged to determine the mean and the standard deviation.

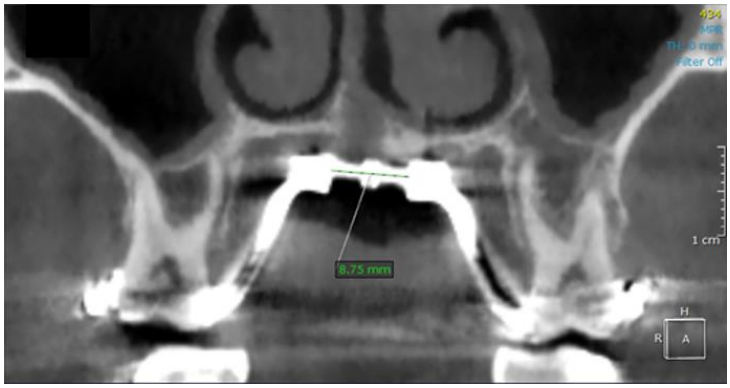

Fig. 2.39. Post-expansion CBCT of a treated patient. Measurement of the distance between the two halves of MSE expansion jackscrew [36,44].

Measurements in the upper nasal section (UNS)

The upper nasal section was also used to evaluate the changes in the maxilla. The landmarks analyzed were the most anterior point of the right and left maxilla (Rt Up Ant Mx and Lt Up Ant Mx), the posterior-medial point of the right and left maxilla (Rt Post-med Mx and Lt Post-med Mx) [36,44], as shown in Fig 2.40.

Fig 2.40. Landmarks identified in the upper nasal section (UNS). 1: Most anterior point of the right maxilla (Rt Up Ant Mx); 2: Most anterior point of the left maxilla (Lt Up Ant Mx); 3: Upper posterior-medial point of the right maxilla (Rt Up Post-med Mx); 4: Upper posterior-medial point of the left maxilla (Lt Up Post-med Mx) [36,44].

The parameters evaluated in the upper nasal section (UNS) are summarized in table 2.

Table 2. Parameters evaluated in the upper nasal section (UNS)

Transverse distances	
1	Distance of Rt Up Ant Mx from maxillary sagittal plane
2	Distance of Lt Up Ant Mx from maxillary sagittal plane
3	Distance of Rt Up Post-med Mx from maxillary sagittal plane
4	Distance of Lt Up Post-med Mx from maxillary sagittal plane

The post-expansion CBCT of the patient was superimposed on the pre-expansion CBCT, the MSP and APP were traced in the pre-expansion CBCT, and the upper nasal section was selected (Fig. 2.41).

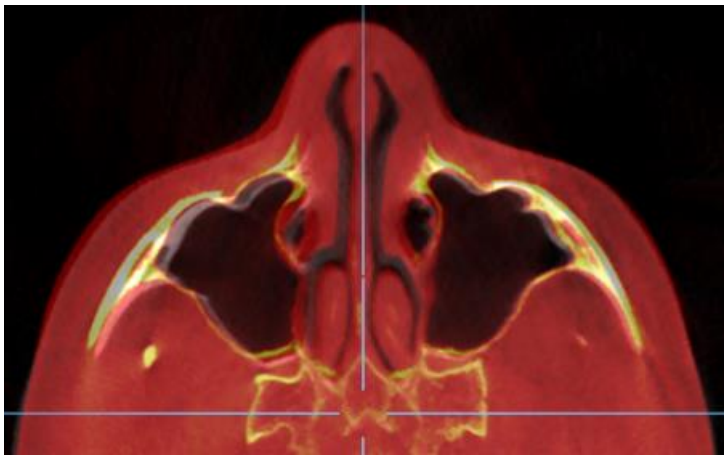

Fig 2.41. Upper nasal section (UNS): example of superimposed image of a treated patient. The sagittal blue line is MSP determined from the pre-expansion CBCT.

The distance from the maxillary sagittal plane to the landmarks were measured in the pre- and post-expansion CBCTs as shown in Fig 2.42.

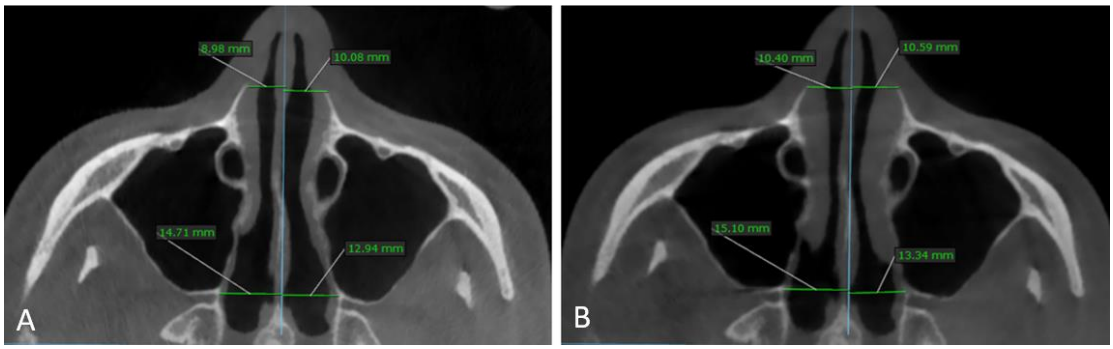

Fig 2.42. Transverse measurements on the upper nasal section (UNS) in a treated patient. A: pre-expansion. B: post-expansion.

The distances from the maxillary sagittal plane (MSP) to these landmarks were measured in the pre- and post-expansion CBCTs. The distance measurements before treatment were subtracted from those after treatment to assess the treatment changes. The treatment change is equivalent to the lateral movement of these landmarks. The distance measurements were averaged, and a paired T-test was used for statistical significance.

Measurements on the coronal zygomatic section (CZS)

To analyze the skeletal changes of the frontal bone, zygomatic bone and maxilla in the coronal plane, a slice was selected on the CBCT.

The **coronal zygomatic section (CZS)** passes through the uppermost point of the right and left frontozygomatic suture, through the lowest point of the right and left zygomaticomaxillary suture [43,44] (Fig 2.43).

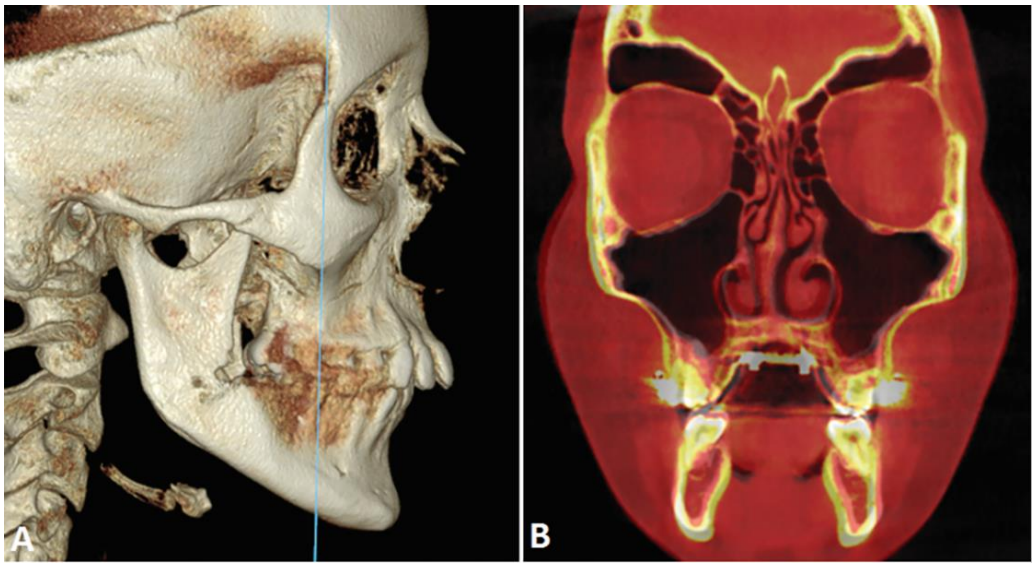

Fig 2.43. Coronal zygomatic section (CZS). A: lateral view of 3D rendering, showing the coronal zygomatic section in blue. B: pretreatment and posttreatment superimposed image of a treated patient [43,44].

The post-expansion CBCT was superimposed on the pre-expansion CBCT, the coronal zygomatic section (CZS) was selected (Fig. 2.43), and then skeletal linear, skeletal angular, and dentoalveolar measurements were taken from the pre- and post-expansion CBCTs, as reported in previous publications [43,44].

Parameters evaluated in the coronal zygomatic section (CZS) are listed in table 3.

Table 3. Parameters evaluated in the coronal zygomatic section (CZS)

ZR: most lateral point of the zygomatic process of right maxilla; ZL: most lateral point of the zygomatic process of left maxilla; MSP: maxillary sagittal plane

Skeletal linear measurements	
1	Upper inter-zygomatic distance
2	Nasal width
3	Distance of ZR from MSP
4	Distance of ZL from MSP
5	Sum of distance of ZR from MSP and distance of ZL from MSP (lower inter-zygomatic distance)
Skeletal angular measurements	
6	Right frontozygomatic angle (Rt FZA)
7	Left frontozygomatic angle (Lt FZA)
8	Right zygomaticomaxillary angle (Rt ZMA)
9	Left zygomaticomaxillary angle (Lt ZMA)
10	Right maxillary inclination (Rt Mx incl)
11	Left maxillary inclination (Lt Mx Incl)
Dentoalveolar measurements	
12	Inter-molar distance
13	Right molar basal bone angle (Rt MBBA)
14	Left molar basal bone angle (Lt MBBA)

Skeletal linear measurements in the CZS

Linear distances were as follows.

The upper inter-zygomatic distance (UID) extends from the most external point of the right frontozygomatic suture to the most external point of the left frontozygomatic suture (Fig. 2.44).

The nasal width (NW) extends from the right to the left side of the nasal cavity at the level of its most lateral point (Fig. 2.44)

The ZR-MSP distance extends from the most lateral point of zygomatic process of right maxilla to maxillary sagittal plane (MSP) (Fig. 2.44).

The ZL-MSP distance extends from the most lateral point of zygomatic process of left maxilla to maxillary sagittal plane (MSP) (Fig. 2.44).

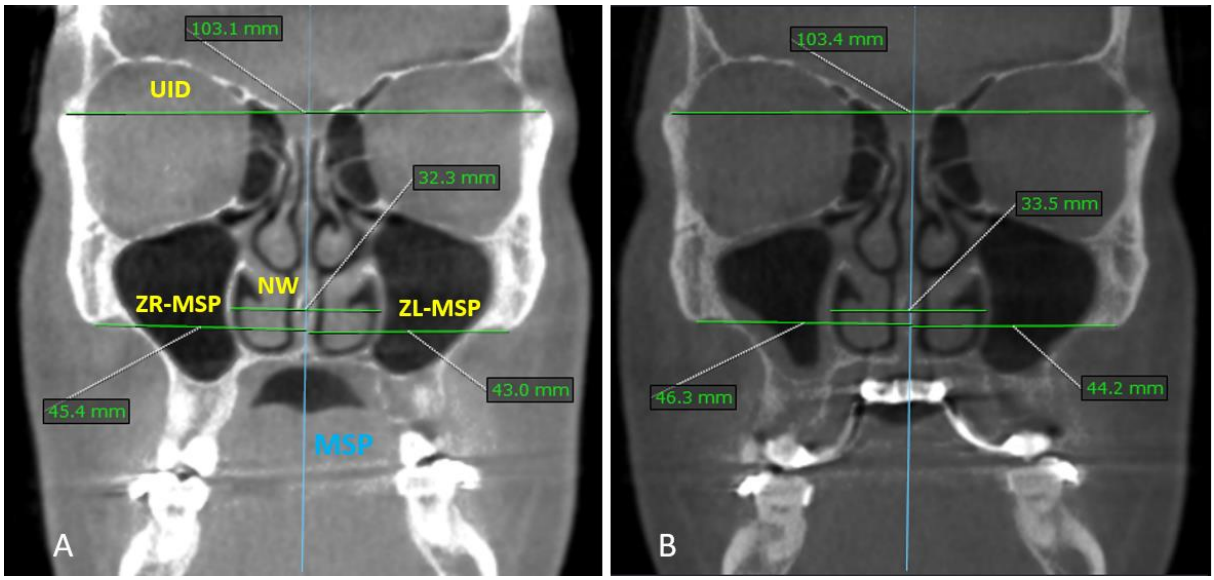

Fig 2.44. Coronal zygomatic section (CZS) in a treated patient. A: pre-expansion. B: post-expansion. Linear measurements: upper inter-zygomatic distance (UID), nasal width (NW), ZR-MSP distance, ZL-MSP distance. ZR: most lateral point of zygomatic process of right maxilla; ZL: most lateral point of zygomatic process of left maxilla; MSP: maxillary sagittal plane.

For the upper inter-zygomatic distance, the pre-expansion value was subtracted from the post-expansion value to calculate the treatment change. The distance measurements were averaged, and a paired T-test was used for statistical significance.

The same procedure was done to compare the pre- and post-expansion distance of ZR and ZL from MSP, and nasal width.

Skeletal angular measurements in the CZS

To analyze the rotation of the zygomaticomaxillary complex in the coronal plane, the following angles were evaluated: frontozygomatic angle, zygomaticomaxillary angle, maxillary inclination angle.

The frontozygomatic angle (FZA) is formed by the most external point of the zygomaticomaxillary suture, the most external point of frontozygomatic suture on the same side of the skull and the most external point of the contralateral frontozygomatic suture as shown in Fig. 2.45 and 2.46.

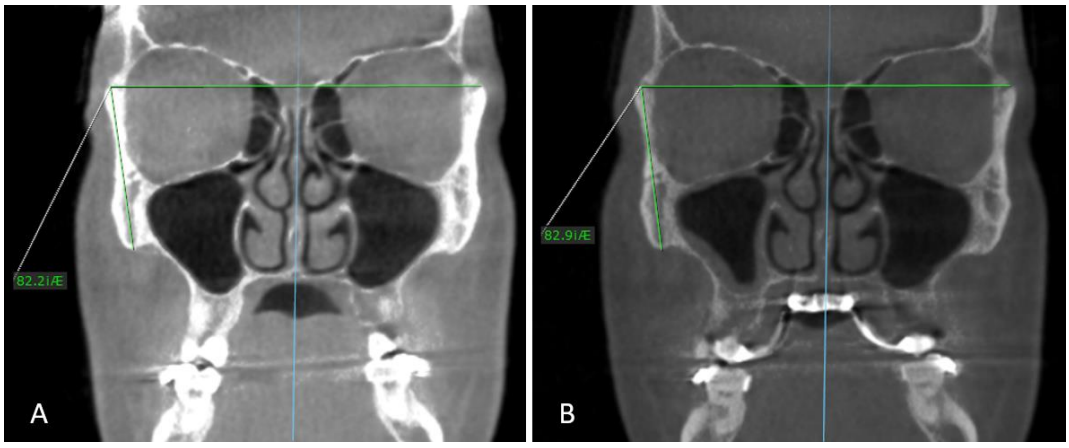

Fig. 2.45. Coronal zygomatic section (CZS) in a treated patient. A: pre-expansion. B: post-expansion. Angular measurements: right frontozygomatic angle (Rt FZA).

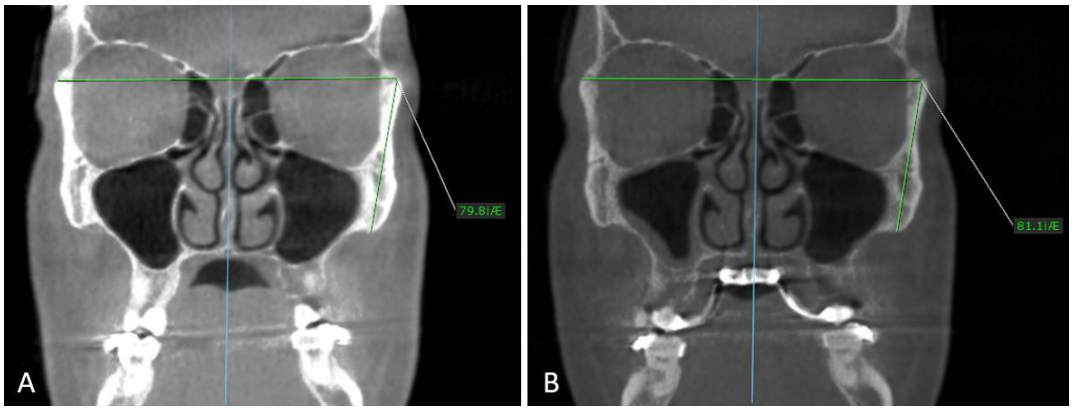

Fig. 2.46. Coronal zygomatic section (CZS) in a treated patient. A: pre-expansion. B: post-expansion. Angular measurements: left frontozygomatic angle (Lt FZA).

The pre-expansion value of the FZA was subtracted from the post-expansion value to assess the treatment change. These values were averaged, and a paired T-test was used for statistical significance.

The zygomaticomaxillary angle (ZMA) is formed by the most external point of the frontozygomatic suture, the most external point of the zygomaticomaxillary suture, and the point tangent to the floor of nasal cavity, as shown in Fig. 2.47 and 2.48.

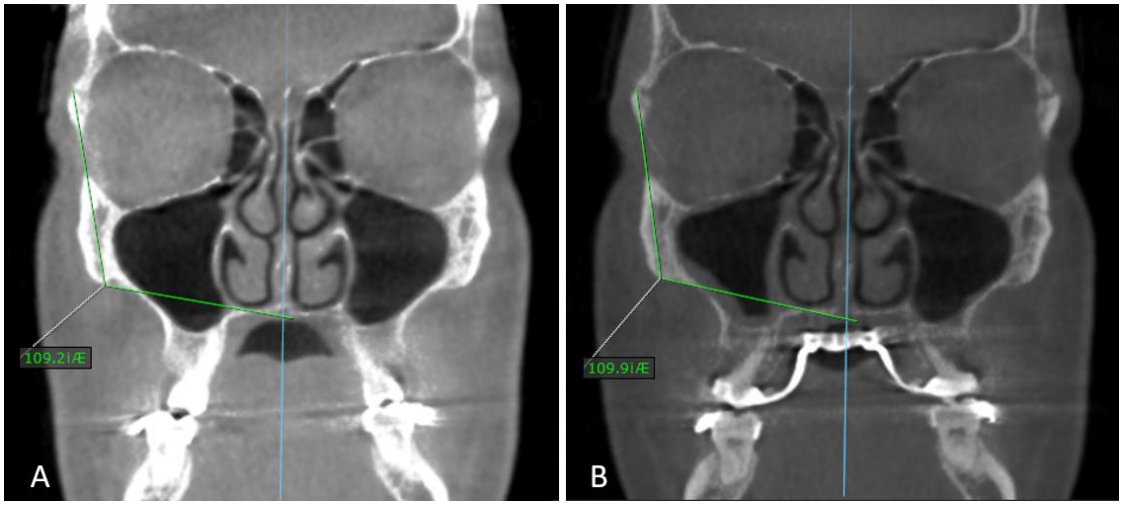

Fig. 2.47. Coronal zygomatic section (CZS) in a treated patient. A: pre-expansion. B: post-expansion. Angular measurements: right zygomaticomaxillary angle (Rt ZMA).

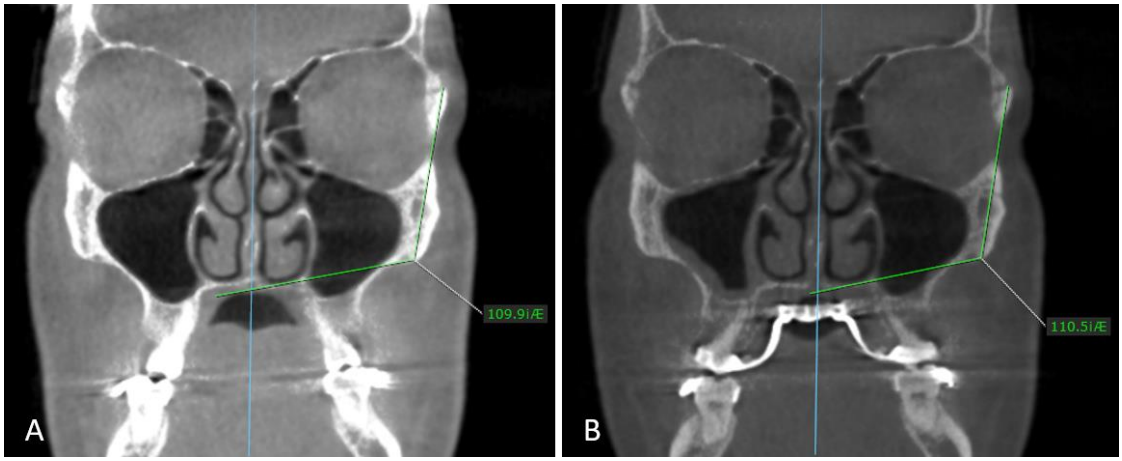

Fig. 2.48. Coronal zygomatic section (CZS) in a treated patient. A: pre-expansion. B: post-expansion. Angular measurements: left zygomaticomaxillary angle (Lt ZMA).

The pre-expansion value of the zygomaticomaxillary angle (ZMA) was subtracted from the post-expansion value to calculate the treatment change. These values were averaged, and a paired T-test was used for statistical significance.

The maxillary inclination (Mx Incl) was measured as follows. A line was drawn to connect the most lateral point of the maxilla to the point tangent to the nasal floor as shown in Fig. 2.49 and 2.50. The angulation of this line relative to the maxillary sagittal plane (MSP) was named “maxillary inclination” (Mx Incl).

The pre-expansion value of the maxillary inclination (Mx Incl) was subtracted from the post-expansion value to calculate the treatment change. The values were averaged, and a paired T-test was used for statistical significance.

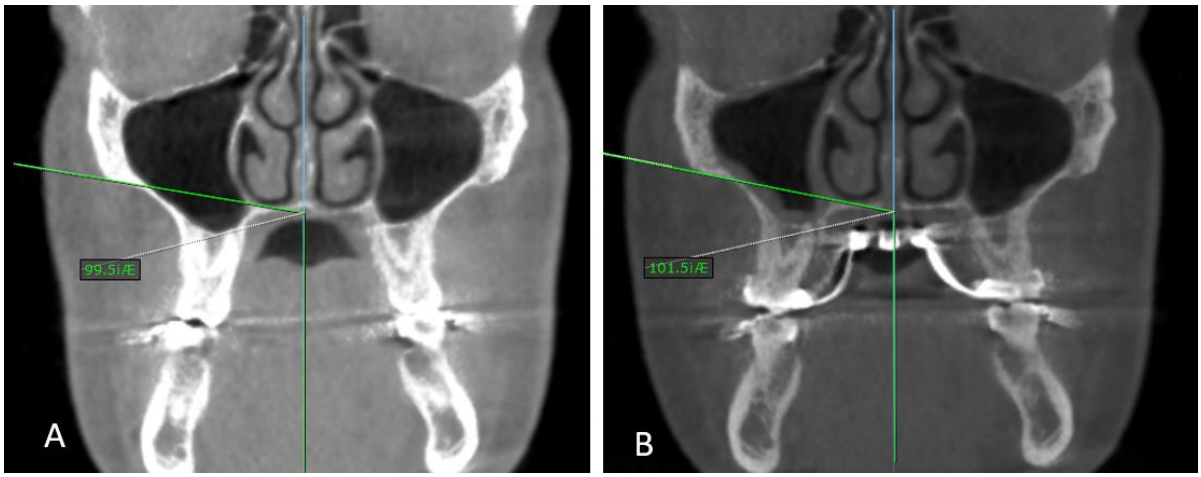

Fig. 2.49. Coronal zygomatic section (CZS) in a treated patient. A: pre-expansion. B: post-expansion. Angular measurements: right maxillary inclination (Rt Mx Incl). Vertical blue line is the maxillary sagittal plane (MSP).

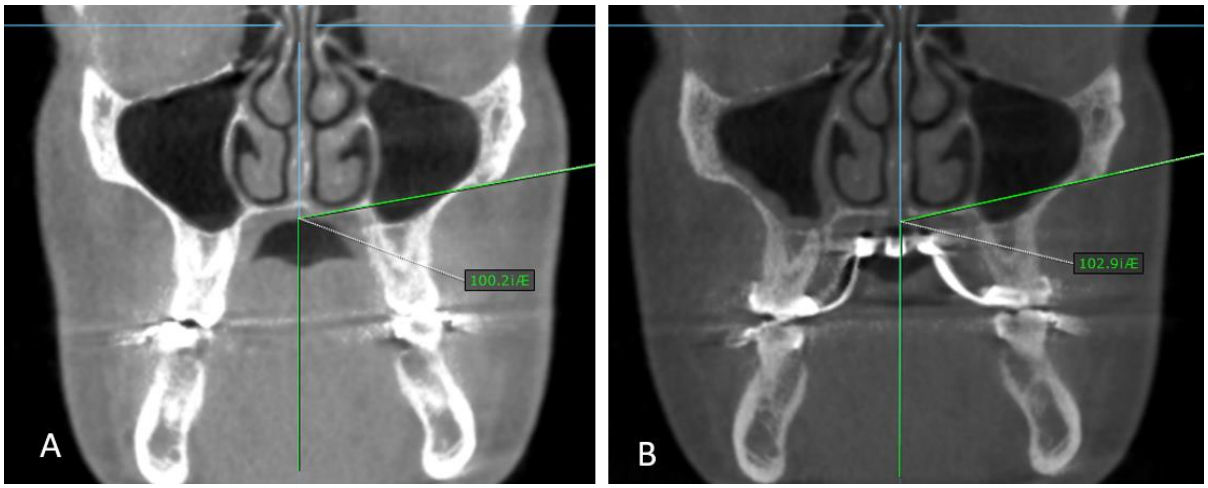

Fig. 2.50. Coronal zygomatic section (CZS) in a treated patient. A: pre-expansion. B: post-expansion. Angular measurements: left maxillary inclination (Lt Mx Incl). Vertical blue line is the maxillary sagittal plane (MSP).

Dentoalveolar measurements

Dentoalveolar measurements include the inter-molar distance (IMD) and the right and left molar basal bone angle (Rt MMBA and Lt MBBA).

The inter-molar distance extends from the most occlusal point of the palatal cusp of right upper first molar to the most occlusal point of the palatal cusp of the left upper first molar (Fig. 2.51).

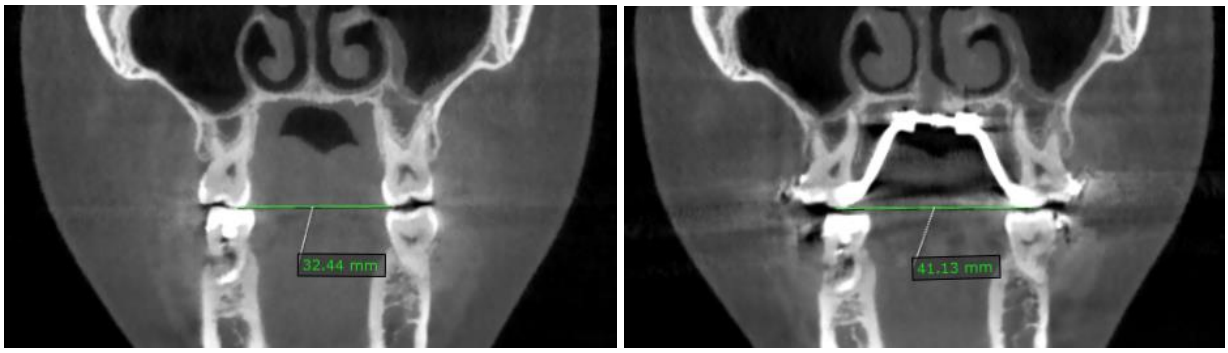

Fig 2.51. Coronal zygomatic section (CZS) in a treated patient. A: pre-expansion. B: post-expansion. Linear measurements: inter-molar distance.

The molar basal bone angle (MBBA) was calculated as follows. A line was drawn to connect the most lateral point of the maxilla to the point tangent to the nasal floor. A second line was drawn to connect the central pit of the molar crown to the furcation of the root. The angle formed between the two lines (Fig. 2.52 and 2.53) is named molar basal bone angle (MBBA).

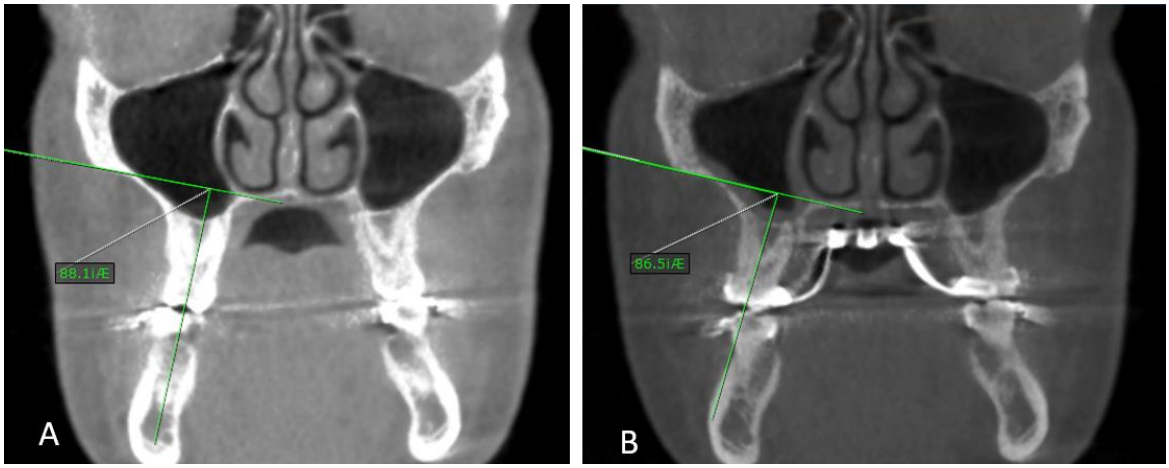

Fig. 2.52. Coronal zygomatic section (CZS) in a treated patient. A: pre-expansion. B: post-expansion. Angular measurements: right molar basal bone angle (Rt MBBA).

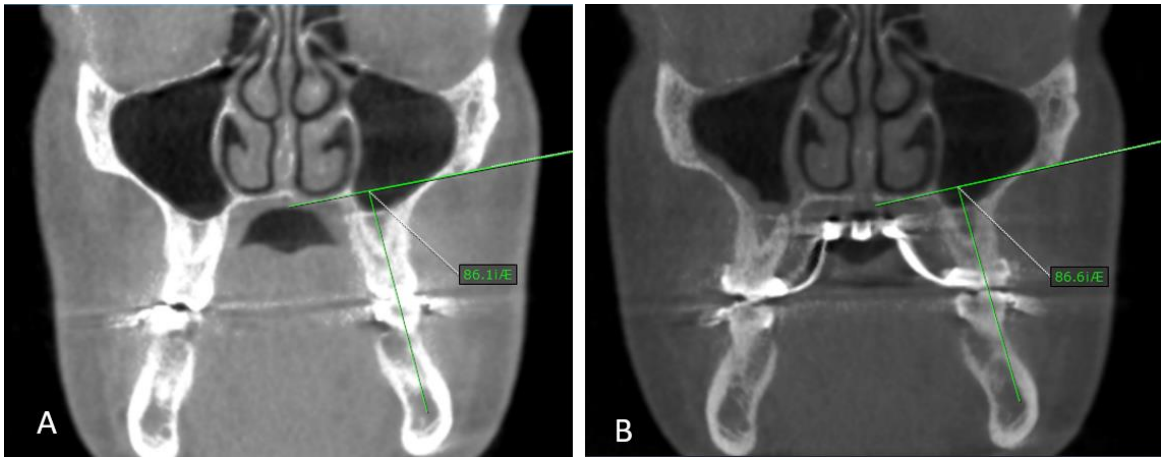

Fig. 2.53. Coronal zygomatic section (CZS) in a treated patient. A: pre-expansion. B: post-expansion. Angular measurements: left molar basal bone angle (Lt MBBA).

The pre-expansion MBBA value was subtracted from the post-expansion value for the treatment change. The values were averaged, and a paired T-test was used for statistical significance.

Measurements on the axial zygomatic section (AZS)

To analyze the skeletal changes of the temporal bone, zygomatic bone and maxilla in the horizontal plane, a slice was selected on the CBCT.

The **axial zygomatic section (AZS)** passes through the vertical midpoint of the zygomaticotemporal sutures and the vertical midpoint of the articular tubercle of the temporal bones (TBATs) [34,44] as shown in Fig. 2.54.

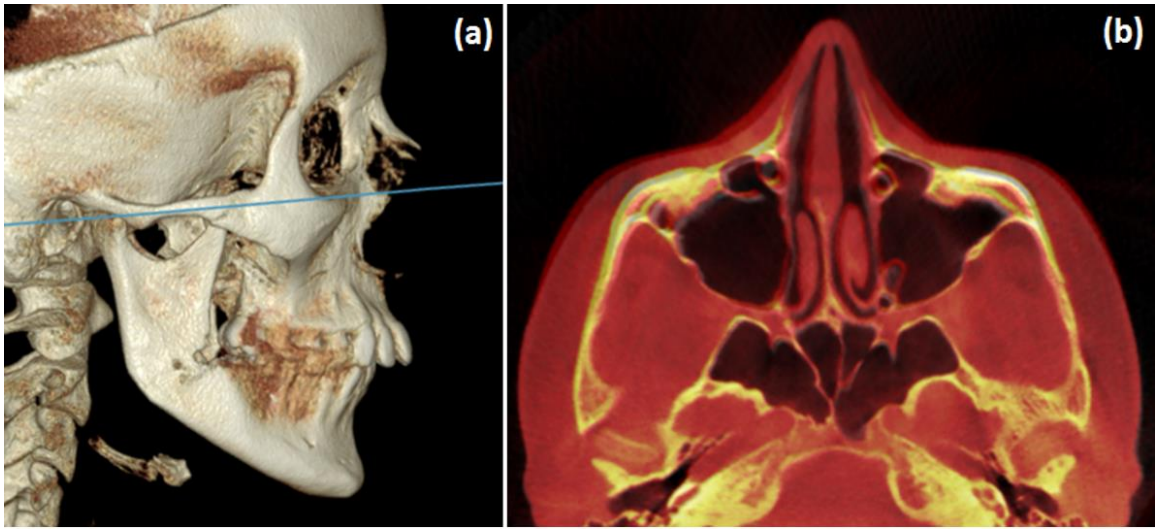

Fig. 2.54. Axial zygomatic section (AZS). A: Lateral view of 3D rendering, showing the axial zygomatic section traced in blue. B: Pre- and post-treatment superimposed image of a treated patient [34,44].

The post-expansion CBCT was superimposed on the pre-expansion CBCT, the axial zygomatic section (AZS) was produced (Fig. 2.54), and then the linear and angular

measurements were taken from the pre-expansion and post-expansion CBCT, as reported in previous publications [34,44].

Table 4 lists the parameters evaluated in the axial zygomatic section (AZS).

Table 4. Parameters evaluated in the axial zygomatic section (AZS)

Linear measurements	
1	Anterior inter-maxillary distance
2	Posterior inter-zygomatic distance
3	Posterior inter-temporal distance
Angular measurements	
4	Right zygomaticotemporal angle (Rt ZTA)
5	Left zygomaticotemporal angle (Lt ZTA)
6	Right angle of the zygomatic process of the temporal bone (Rt ZPA)
7	Left angle of the zygomatic process of the temporal bone (Lt ZPA)

Linear measurements on the axial zygomatic section (AZS)

The anterior inter-maxillary distance was measured from the most anterior point of the right maxilla to the most anterior point of the left maxilla as shown in Fig. 2.55.

The posterior inter-zygomatic distance was measured from the most external point of the right zygomaticomaxillary suture to the most external point of the left zygomaticomaxillary suture as shown in Fig. 2.55.

The posterior inter-temporal distance was measured from the most posterior point on the left and right articular tubercle of temporal bone as shown in Fig. 2.55.

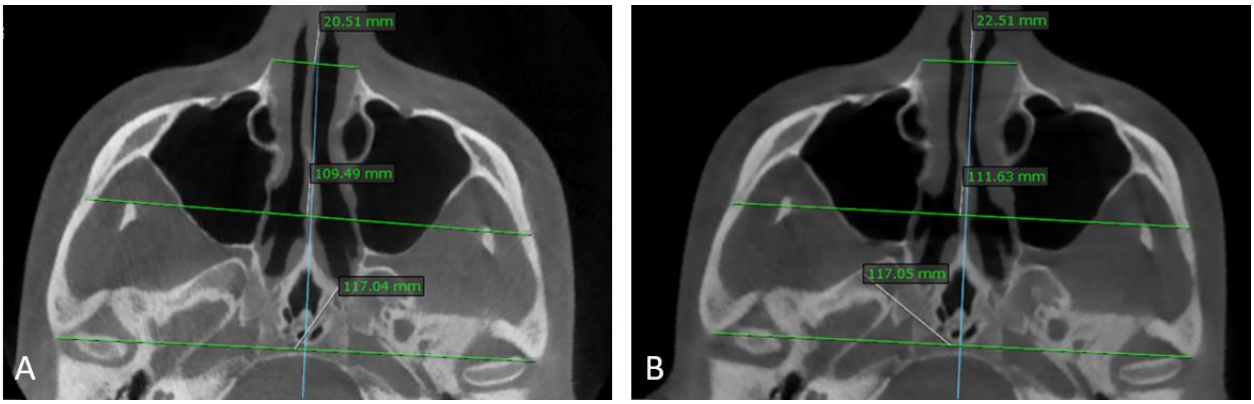

Fig. 2.55. Axial zygomatic section (AZS) in a treated patient. A: pre-expansion. B: post-expansion. Linear measurements: anterior inter-maxillary distance, posterior inter-zygomatic distance, posterior inter-temporal distance.

For the anterior inter-maxillary distance, the pre-expansion value was subtracted from the post-expansion value to calculate the treatment change. The values were averaged, and a paired T-test was used for statistical significance.

The same procedure was done for the pre- and post-expansion posterior inter-zygomatic and posterior inter-temporal distances.

Angular measurements

To further analyze the rotation of the zygomaticomaxillary complex in the horizontal plane, the zygomaticotemporal angle (ZTA) and the zygomatic process angle (ZPA) were evaluated.

The zygomaticotemporal angle (ZTA) is formed by the most anterior point of the maxilla, the most external point of the zygomaticotemporal suture and the most posterior-lateral point of the eminence of the glenoid fossa as shown in Fig. 2.56.

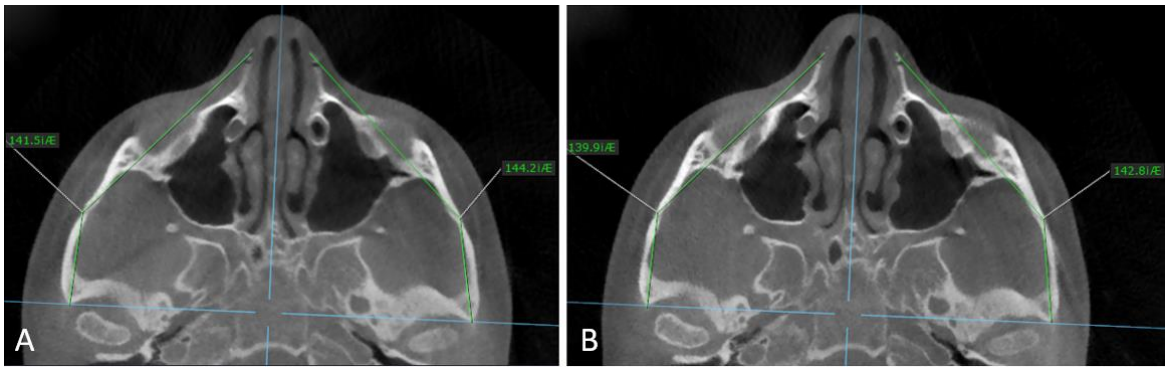

Fig. 2.56. Axial zygomatic section (AZS) in a treated patient. A: pre-expansion. B: post-expansion. Angular measurements: right and left zygomaticotemporal angle (ZTA).

The pre-expansion value of the zygomaticotemporal angle (ZTA) was subtracted from the post-expansion value to calculate the treatment change. The values were averaged, and a paired T-test was used for statistical significance.

Finally, to evaluate a possible bone bending of the zygomatic process of the temporal bone, the angle of the zygomatic process of the temporal bone (zygomatic process angle or ZPA) was measured as follows.

A line was drawn to connect the most posterior-lateral point of the eminence of the glenoid fossa on the right and left the temporo-mandibular joint. Then a line was drawn to connect the most posterior-lateral point of the eminence of the glenoid fossa of the temporo-mandibular joint to the most external point of the zygomaticotemporal suture. The angle formed between the two lines is the zygomatic process angle (ZPA) of the temporal bone as shown in Fig. 2.57.

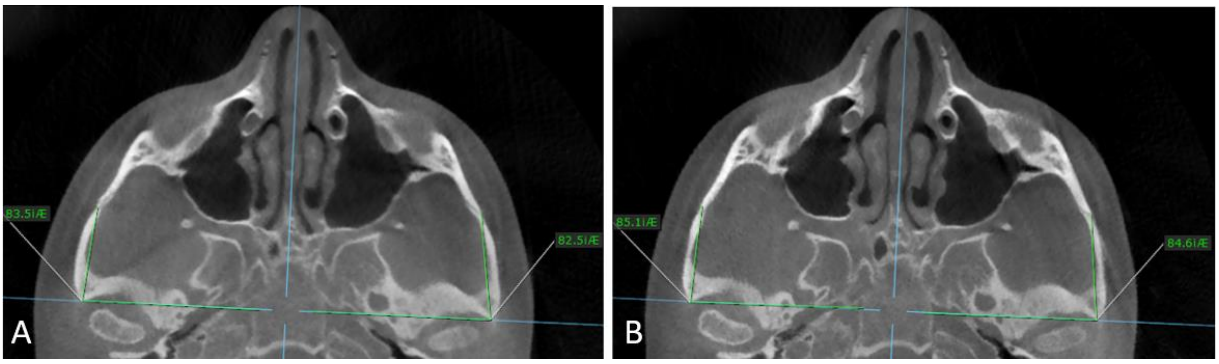

Fig. 2.57. Axial zygomatic section (AZS) in a treated patient. A: pre-expansion. B: post-expansion. Angular measurements: right and left angle of the zygomatic process of the temporal bone (Zygomatic Process Angle or ZPA)

The pre-expansion zygomatic process angle of the temporal bone (ZPA) was subtracted from the post-expansion value for the treatment change calculation. The values were averaged, and a paired T-test was used for statistical significance.

Statistical Analysis

Assessments of variables

Variables were compared from pre- to post-treatment parametrically using the paired T-test or non-parametrically using the Wilcoxon sign rank test as appropriate. Before applying the t-test, the normality of the data distribution was verified using the D'Agostino and Pearson omnibus normality test. The level of significance was set at P=0.05.

The frequency of openings in the lower part of the pterygopalatine suture were compared from pre- to post-treatment using the Fisher's exact test.

Reliability assessments

The method reliability was reported in previous publications [34,36-39,43].

In the published studies, reliability was evaluated in two ways: 1) by computing the coefficient of variation (CV) and 2) by computing the intra-class correlation coefficient (ICC).

The coefficient of variation (CV) - The variation across and/or within raters within patients is called the error SD (SD_{error}) or measurement error SD. For a given measure, the CV is defined as the ratio of the error SD to the overall mean. Therefore, the CV is the variability due to measurement error as a percent of the overall mean. If the measurements are the same between raters and within raters, then CV = 0 (perfect reliability) and error SD = 0. If reliability is high, the CV should be small (ideally not more than 2%).

The intraclass correlation coefficient (ICC) – In general, the variation in a given measure is due to 1) differences between patients (between patient SD) and 2) differences between

and/or within raters within patients (error SD). The ICC is the proportion of the total variation due to patient variation. When the error SD is zero, all of the variation is due to patient (perfect reliability). For excellent reliability, the ICC should be near 100%.

Reliability of skull orientation

Reliability of skull orientation was evaluated by re-orienting 30% of randomly selected CBCT scans (n = 5 patients), and calculating the intraclass correlation coefficient, using the posterior clinoid process and basion as landmarks for comparison, similarly to the method adopted by Woller et al. [69].

Skull orientation was highly reliable, as the obtained Cronbach's Alpha value was 0.987, as reported in a previous study [36].

Reliability of parameters in the axial palatal sections (APS)

Reliability of parameters in this axial section was reported in a previous publication [36].

Reliability of measured parameters was obtained on 10 different patients by 2 raters. Each parameter was measured twice by each rater. Reliability was evaluated by computing the intra-class correlation coefficient (ICC) ρ.

For the considered parameters, the intra-class correlation coefficient (ICC) ρ was at least 0.973 or more, showing that measurements were very reliable.

Reliability of parameters in the coronal zygomatic sections (CZS)

Reliability of parameters in the CZS was reported in a previous publication [43].

For the assessment of method reliability, measurements were obtained for all variables on 8 randomly selected patients by 2 raters. Measurements were then repeated for the second

time after 2 weeks by the same operators, after re-orienting the skull according to the reference planes, in order to compute reliability parameters that are the combination of error in identification of reference planes (CZS, MSP) and error in landmark localization. The calculated parameters were the following: rater standard deviation, rater coefficient of variation, error standard deviation, error coefficient of variation, intra-class correlation coefficient (ICC).

For the considered parameters, the rater coefficient of variation was 1.36% or less, and the error coefficient of variation was 1.75% or less, showing that measurements were highly reliable.

Reliability of parameters in the axial zygomatic sections (AZS)

Reliability of parameters in the AZS was reported in a previous study [34].

Method reliability was assessed by obtaining measurements for all variables on 8 randomly selected patients by 2 raters. Measurements were repeated after 2 weeks by the same operators after re-orientation of the skull on the reference plane (AZS). Indeed, reliability parameters are the combination of errors in reference plane identification and landmark location. Rater standard deviation and coefficient of variance; error standard deviation and coefficient of variation; and intra-class correlation coefficient (ICC) were calculated.

For the considered parameters, the rater coefficient of variation was 1.22 or less, and the error coefficient of variation was 1.97% or less, showing that the reliability of the measurement method was very high.

CHAPTER 3: RESULTS

Analysis of variables in the axial palatal section (APS)

The results of variables analyzed in the axial palatal section are shown in table 5 and 6.

Table 5. Results for axial palatal section (APS)

		Before Expansion		After Expansion		Treatment Change		significance	
		mean	sd	mean	sd	mean	sd	p-value	*/**
1	Rt ANS to maxillary sagittal plane	0.00	0.00	1,78	0,83	1,78	0,83	0.023	*
2	Lt ANS to maxillary sagittal plane	0.00	0.00	1,62	0,47	1,62	0,47	0.006	**
3	Rt NPF to maxillary sagittal plane	1,63	0,51	3,24	0,81	1,62	0,30	0.028	*
4	Lt NPF to maxillary sagittal plane	1,78	0,77	3,20	0,89	1,42	0,13	0.049	*
5	Rt PNS to maxillary sagittal plane	0.00	0.00	1,91	0,71	1,91	0,71	0.013	*
6	Lt PNS to maxillary sagittal plane	0.00	0.00	1,66	0,81	1,66	0,81	0.026	*
7	Lateral displacement of Rt ANS + Lt ANS	0.00	0.00	3,40	1,06	3,40	1,06	0.008	**
8	Lateral displacement of Rt NPF + Lt NPF	3,41	1,28	6,45	0,39	3,04	0,89	0.0006	**
9	Lateral displacement of Rt PNS + Lt PNS	0.00	0.00	3,58	0,79	3,58	0,79	0.003	**
10	Width of opening in Rt pterygoid process	0.00	0.00	1,50	1,32	1,50	1,32	0.108	
11	Width of opening in Lt pterygoid process	0.00	0.00	1,59	1,44	1,59	1,44	0.114	
12	Pterygoid plates width (PPW)	54,67	1,72	56,36	1,21	1,69	0,51	0.068	
13	Distance between the two halves of MSE appliance	3,70	3,70	9,67	2,24	5,97	1,46	0.013	*

** p<0.01 * p<0.05

Table 6. Statistical analysis of the frequency of openings in the lower part of the pterygopalatine suture: Fisher's exact test

	Before Expansion	After Expansion	P Value
Sutures with openings	0	6	0.0035**
Sutures without openings	8	2	

** p<0.01 * p<0.05

On average, **ANS moved laterally** by 1.8 mm (p<0.05) and 1.6 mm (p p<0.01) (Rt and Lt side), and **PNS moved laterally** by 1.9 (p<0.05) and 1.7 mm (p<0.05) (Rt and Lt side).

On average, **NPF moved laterally** by 1.6 mm (p<0.05) and 1.4 mm (p<0.05) (Rt and Lt side).

The **total split at ANS, NPF and PNS** was 3.4 mm (p<0.01), 3.0 mm (p<0.01), 3.6 mm (p<0.01), respectively (table 5 and Fig. 3.1).

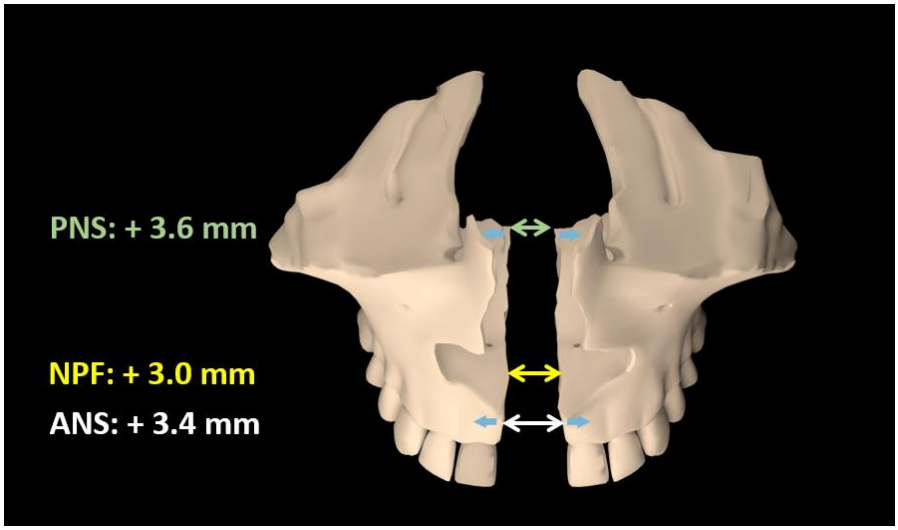

Fig. 3.1. Illustration showing the average increase of midpalatal suture width at various landmarks analyzed in the study. ANS: anterior nasal spine. NPF: nasopalatine foramen. PNS: posterior nasal spine.

Openings between the lateral and medial plates of the pterygoid process (Fig. 2.35 – 2.36) were detectable in all 4 patients: 2 patients with openings in both pterygopalatine sutures, 1 patient with opening only in the right suture (patient 3) and 1 patient with opening only in the left suture (patient 4).

If we count the **number of opened sutures** (Table 6), a sum of 6 sutures (3 right and 3 left) from 4 patients exhibited visible opening out of 8 sutures evaluated ($p<0.01$). That means 75% of all suture disarticulation was radiographically visible. The mean size of the visible opening was 1.5 mm for the right pterygopalatine suture and 1.6 mm for the left pterygopalatine suture (Table 5).

The **split in the pterygopalatine sutures** was partial in 5 sutures and complete in 1 suture. A partial split (PS) means that the pyramidal process separates from the medial pterygoid plate only, while a complete split (CS) means that the pyramidal process separates from both the medial and the lateral pterygoid plates of the sphenoid (Fig. 2.36 B).

The **pterygoid plates width (PPW)** increased by 1.7 mm with treatment (Table 5). This indicates that the pterygoid processes of the sphenoid bone were bent in a lateral direction with treatment.

The **average amount of MSE activation** was 6.0 mm ($p<0.05$) (Table 5).

Analysis of variables in the upper nasal section (UNS)

The results of variables analyzed in the upper nasal section are shown in table 7.

Table 7. Results for upper nasal section (UNS)

		Before Expansion		After Expansion		Treatment Change		significance	
		mean	sd	mean	sd	mean	sd	p-value	*/**
1	Rt Up Ant Mx to maxillary sagittal plane	8,57	0,88	9,98	1,26	1,41	0,38	0.111	
2	Lt Up Ant Mx to maxillary sagittal plane	9,07	2,07	10,05	1,76	0,98	0,31	0,347	
3	Rt Up Po-med Mx to maxillary sagittal plane	14,15	1,02	14,65	1,27	0,50	0,25	0.489	
4	Lt Up Po-med Mx to maxillary sagittal plane	12,91	1,61	13,29	1,48	0,38	0,13	0.643	

** p<0.01 * p<0.05

The most anterior point of the maxilla moved laterally by 1.4 mm and 1.0 mm (Rt and Lt side) in treated patients.

The posterior-medial point of the maxilla moved laterally by 0.5 mm and 0.4 mm (Rt and Lt side) in treated patients.

Pattern of lateral movement of the maxilla in the horizontal plane

If we consider the axial palatal section (APS), the lateral dislocation of Rt ANS and Lt ANS together was 3.4 mm, and the lateral dislocation of Rt PNS and Lt PNS together was 3.6 mm. The magnitude of expansion at PNS was 105% (3.4 / 3.6) of the expansion at ANS, indicating that the right and left borders of the midpalatal suture were nearly parallel to each other at the end of the expansion.

If we consider the upper nasal section (UNS), the average movement of the most anterior point of the maxilla (Rt side + Lt side) was 2.4 mm while the average movement of the most posterior point of the maxilla (Rt side + Lt side) was 0.9 mm. The average lateral movement of the posterior maxilla was 37% (0.9 / 2.4) of the expansion at the anterior maxilla, illustrating more “V-shaped” expansion than at the UNS level, with more movement anteriorly than posteriorly.

Analysis of variables in the coronal zygomatic section (CZS)

The results of variables analyzed in the coronal zygomatic section (CZS) are shown in table 8.

Table 8. Results for coronal zygomatic section (CZS)

		Before Expansion		After Expansion		Treatment Change		significance	
		mean	sd	mean	sd	mean	sd	p-value	*/**
Skeletal linear measurements									
1	Upper inter-zygomatic distance	97,67	3,96	97,90	3,98	0,23	0,02	0.915	
2	Nasal width	31,31	1,73	34,21	0,84	2,90	0,90	0.006	**
3	Distance of ZR from MSP	41,94	2,66	42,96	2,83	1,02	0,17	0.523	
4	Distance of ZL from MSP	40,48	2,16	42,37	2,59	1,89	0,44	0.241	
5	Sum of ZR-MSP and ZL-MSP (lower inter-zygomatic distance)	82,42	4,76	85,32	4,79	2,90	0,03	0.313	
Skeletal angular measurements									
6	Right frontozygomatic angle (Rt FZA)	81,48	2,34	82,95	1,13	1,48	1,21	0.08	
7	Left frontozygomatic angle (Lt FZA)	80,45	2,21	82,83	3,92	2,38	1,71	0.311	
8	Right zygomaticomaxillary angle (Rt ZMA)	109,50	4,16	109,48	4,01	-0,03	0,16	0.993	
9	Left zygomaticomaxillary angle (Lt ZMA)	110,65	5,83	110,43	6,08	-0,23	0,25	0.947	
10	Right maxillary inclination (Rt Mx Incl)	99,83	3,07	101,38	2,82	1,55	0,25	0.352	
11	Left maxillary inclination (Lt Mx Incl)	102,08	4,64	104,00	3,92	1,92	0,72	0.399	
Dentoalveolar measurements									
12	Inter-molar distance	37,59	6,17	45,00	7,92	7,41	1,75	0.158	
13	Right molar basal bone angle (Rt MBBA)	90,63	11,53	89,55	12,51	-1,07	0,98	0.874	
14	Left molar basal bone angle (Lt MBBA)	93,10	7,35	91,88	7,64	-1,22	0,29	0.77	

** p<0.01 * p<0.05

The upper inter-zygomatic distance increased by 0.2 mm.

The nasal width increased by 2.9 mm ($p<0.01$).

The most lateral points of maxilla moved laterally: ZR by 1.0 mm and ZL by 1.9 mm.

The lower inter-zygomatic distance, calculated as the sum of ZR-MSP distance and ZL-MSP distance, increased by 2.9 mm.

The frontozygomatic angle (FZA) increased by 1.5° and 2.4° (Rt and Lt side).

The zygomaticomaxillary angle (ZMA) changed by - 0.03° and - 0.2° (Rt and Lt side).

The maxillary inclination (Mx Incl) increased by 1.6° and 1.9° (Rt and Lt side).

The inter-molar distance increased by 7.3 mm.

The molar basal bone angle (MBBA) changes show that molars tipped buccally by 1.0° and 1.2° (Rt and Lt side).

The **average treatment changes** in the coronal zygomatic section are illustrated in Fig. 3.2, 3.3 and 3.4.

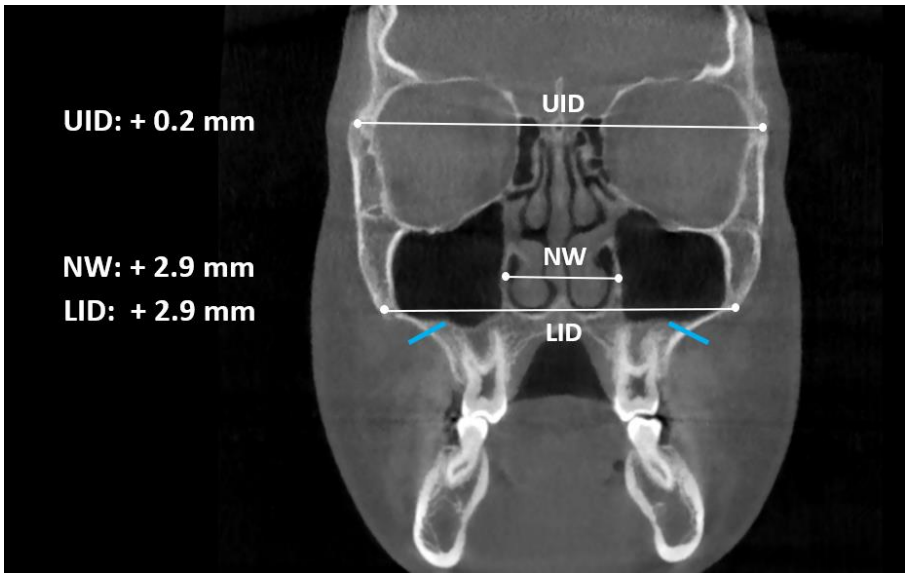

Fig. 3.2. Illustration showing average treatment changes for skeletal linear measurements in the coronal zygomatic section. UID: upper inter-zygomatic distance; NW: nasal width; LID: lower inter-zygomatic distance. Marks in light blue represent the location of lateral maxillary osteotomies (LMOs).

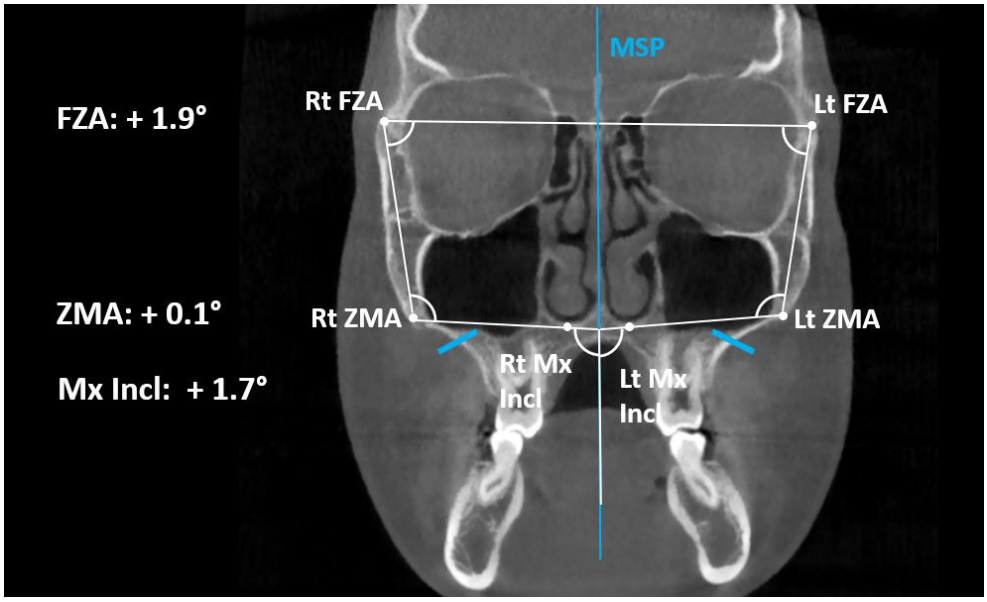

Fig. 3.3. Illustration showing average treatment changes for skeletal angular parameters (average of right and left) in the coronal zygomatic section. FZA: frontozygomatic angle; ZMA: zygomaticomaxillary angle; Mx Incl: maxillary inclination; MSP: maxillary sagittal plane. Marks in light blue represent the location of lateral maxillary osteotomies (LMOs).

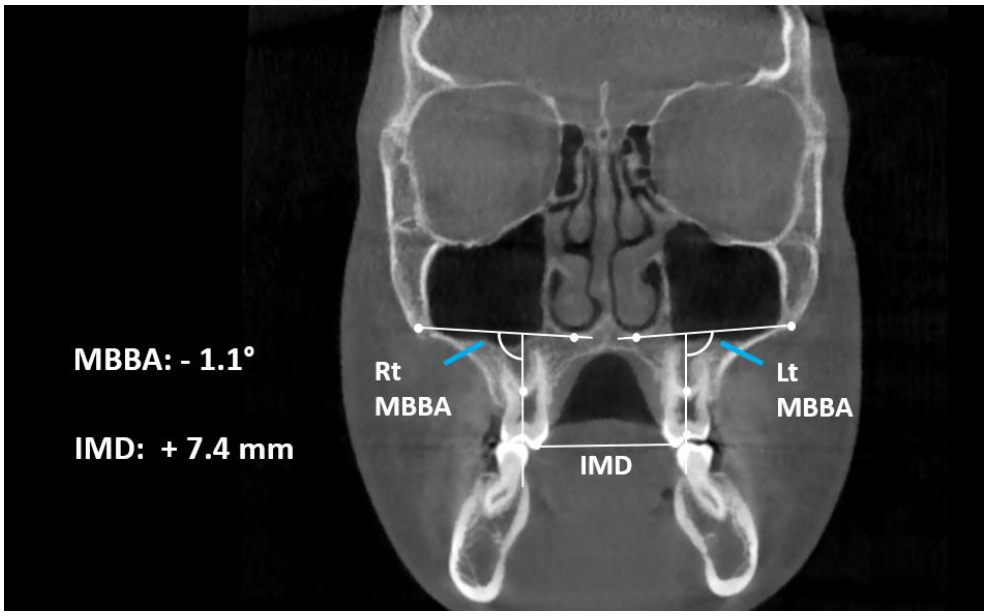

Fig. 3.4. Illustration showing average treatment changes for dentoalveolar parameters in the coronal zygomatic section. MBBA: molar basal bone angle. IMD: inter-molar distance.

Pattern of lateral movement of the maxillary and zygomatic bones in the coronal plane

The pattern of lateral movement of the maxilla is described by the ratio between the increase of the maxillary inclination (average of right and left side) and the increase of the lower inter-zygomatic distance.

The parameter maxillary inclination (Mx incl) represents the inclination of the maxilla relatively to the maxillary sagittal plane (MSP). In treated patients, the maxillary inclination increased by 1.7° (average of right and left side) after the expansion (Fig. 3.5 and Table 8).

Maxillary inclination increased during the expansion because the lateral displacement of the maxilla is not a translational movement, but rather a rotatory movement displacing the zygomaticomaxillary point laterally and superiorly. The more the maxilla and zygomatic bone move laterally, the most lateral points of the maxilla will move laterally and superiorly while medial points will move laterally and inferiorly, causing the maxillary inclination measurements to increase.

The increase in the lower inter-zygomatic distance expresses the lateral displacement of the right and left zygomaticomaxillary complex at the level of the lowest point of the zygomaticomaxillary suture.

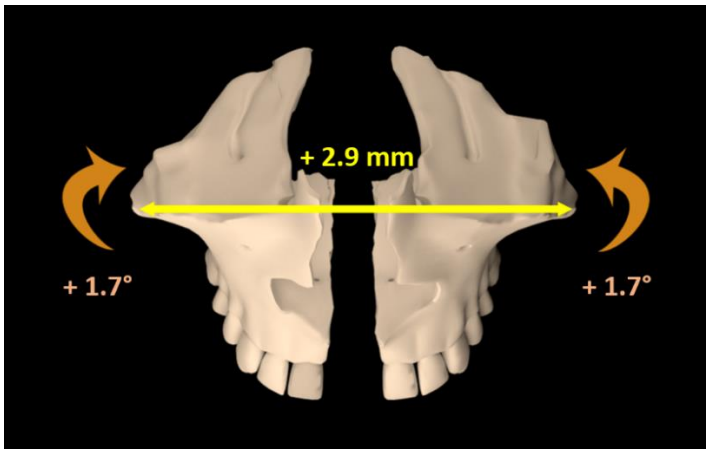

Fig. 3.5. Illustration showing the increase of 1.7° in the parameter maxillary inclination (Mx Incl) and of 2.9 mm in the parameter lower inter-zygomatic distance (LID), the average of right and left side, for the patients treated in the study.

The ratio between the increase in maxillary inclination and the increase in the lower inter-zygomatic distance was 0.6°/mm (1.74°/2.9mm). This indicates that for each mm of increase in the lower inter-zygomatic distance, the rotation of the maxilla was approximately 0.6° (Fig. 3.6).

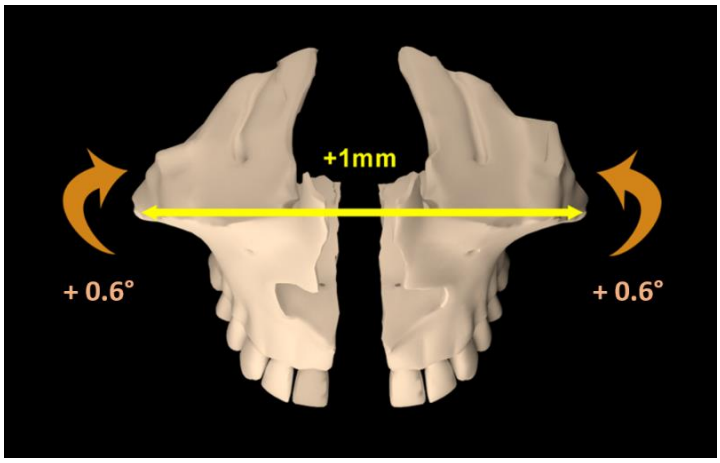

Fig. 3.6. Pattern of lateral movement of the maxilla in the coronal plane. For each mm of increase in the lower inter-zygomatic distance, the maxilla rotated 0.6°.

In a similar manner, the pattern of the lateral movement of the zygomatic bone can be evaluated. The frontozygomatic angle increased by an average of 1.9° in treated patients (average of right and left side), as shown in Fig. 3.7.

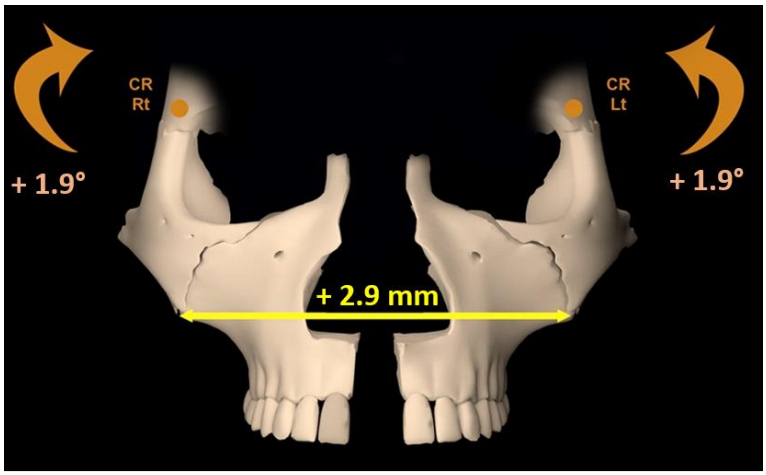

Fig. 3.7. Illustration showing the increase of 1.9° in the parameter frontozygomatic angle (FZA) and of 2.9 mm in the parameter lower inter-zygomatic distance (LID), the average of right and left side, for the patients treated in the study.

The ratio between the increase in frontozygomatic angle and the increase in the lower inter-zygomatic distance was 0.7°/mm (1.9°/2.9mm). This indicates that for each mm of increase in the lower inter-zygomatic distance, the rotation of the zygomatic bone was approximately 0.7° (Fig. 3.8).

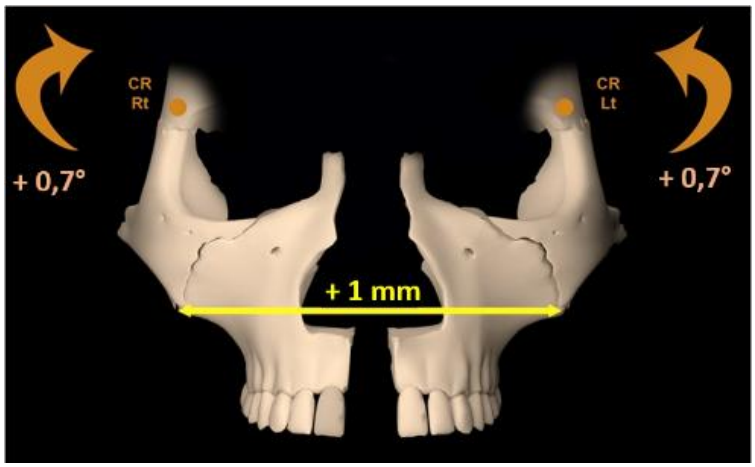

Fig. 3.8. Pattern of lateral movement of the zygomatic bone in the coronal plane. For each mm of increase in the lower inter-zygomatic distance, the zygomatic bone rotated 0.7°.

Analysis of variables in the axial zygomatic section (AZS)

The results of variables analyzed in the axial zygomatic section (AZS) are shown in table 9.

Table 9. Results for axial zygomatic section (AZS)

		Before Expansion		After Expansion		Treatment Change		significance	
		mean	sd	mean	sd	mean	sd	p-value	*/**
Skeletal linear measurements									
1	Anterior inter-maxillary distance	14,58	4,10	16,30	4,48	1,73	0,38	0.498	
2	Posterior inter-zygomatic distance	107,85	8,07	109,46	7,81	1,61	0,27	0.708	
3	Posterior inter-temporal distance	115,94	5,47	116,16	5,45	0,23	0,02	0.941	
Skeletal angular measurements									
4	Right zygomaticotemporal angle (Rt ZTA)	137,05	3,56	137,28	3,38	0,22	0,18	0.90	
5	Left zygomaticotemporal angle (Lt ZTA)	138,80	4,85	138,30	5,15	-0,50	0,30	0.858	
6	Right angle of the zygomatic process (Rt ZPA)	82,53	2,22	83,25	2,42	0,72	0,20	0.594	
7	Left angle of the zygomatic process (Lt ZPA)	82,28	3,45	83,78	3,49	1,50	0,04	0.453	

** p<0.01 * p<0.05

The anterior inter-maxillary distance increased by 1.7 mm.

The posterior inter-zygomatic distance increased by 1.6 mm.

The zygomaticotemporal angle (ZTA) underwent changes by +0.2° and -0.5° (Rt and Lt sides).

The angle of the zygomatic process of the temporal bone (ZPA) increased by 0.7° and 1.5° (Rt and Lt sides).

The **average treatment changes** in the axial zygomatic section are illustrated in Fig. 3.9 and 3.10.

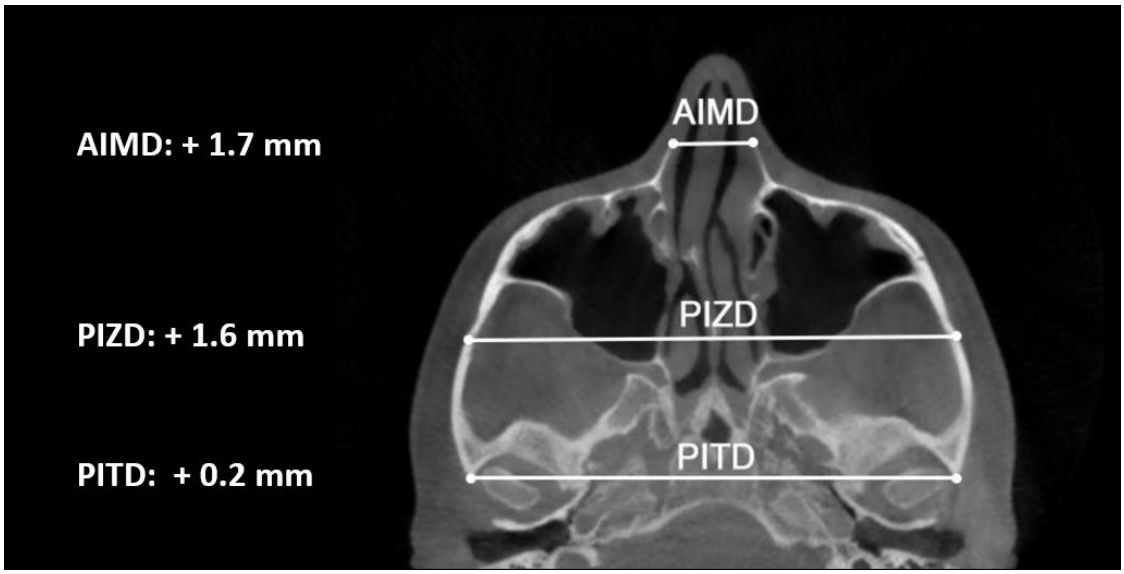

Fig. 3.9. Illustration showing average treatment changes for skeletal linear distances in the axial zygomatic section. AIMD: anterior inter-maxillary distance. PIZD: posterior inter-zygomatic distance. PITD: posterior inter-temporal distance.

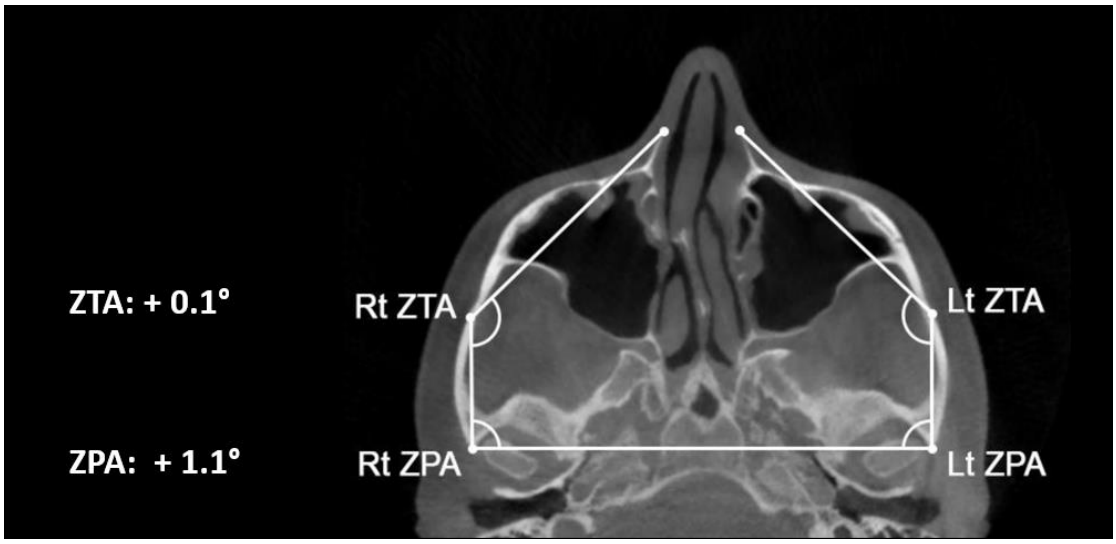

Fig. 3.10. Illustration showing average treatment changes for skeletal angular parameters (average of right and left) in the axial zygomatic section. ZTA: zygomaticotemporal angle; ZPA: angle of the zygomatic process of the temporal bone.

Analysis of symmetry of midface expansion

The symmetry of movement of midface bones was analyzed by the relative movement of **landmarks in the right and left halves of the skull** in two different CBCT sections (axial palatal section and coronal zygomatic section). The analyzed landmarks were anterior nasal spine (Rt ANS and Lt ANS) and nasopalatine foramen (Rt NPF and Lt NPF) in the axial palatal section, and the most lateral point of zygomatic process of maxilla (ZR and ZL) in the coronal zygomatic section (Table 10).

Regarding the **split of the midpalatal suture at the anterior nasal spine (ANS)**, in 3 patients the larger movement was at Rt ANS and in 1 patient at Lt ANS. On average, one side moved more than the contralateral half by 0.54 mm.

If we consider the **nasopalatine foramen (NPF)**, the movement was larger on the right side in 2 patients, and larger on the left half in the other 2 patients. On average, one side moved more than the contralateral half by 1.1 mm.

Finally, in the coronal zygomatic section, the **most lateral point of maxilla** moved more on the right side than the contralateral half in 3 patients and more on the left side in 1 patient. On average, one half moved more than the contralateral side by 1.3 mm.

Table 10. Results for analysis of midface expansion symmetry

ANS: anterior nasal spine; NPF: nasopalatine foramen; ZR: most lateral point of zygomatic process of right maxilla; ZL: most lateral point of zygomatic process of left maxilla.

Landmark analyzed	Larger movement	Average difference: larger movement – lesser movement
Anterior nasal spine (Rt ANS vs Lt ANS)	▪ 3 patients Rt side ▪ 1 patient Lt side	0.54 mm
Nasopalatine foramen (Rt NPF vs Lt NPF)	▪ 2 patients Rt side ▪ 2 patient Lt side	1.1 mm
Most lateral point of maxilla (ZR vs ZL)	▪ 3 patients Rt side ▪ 1 patient Lt side	1.3 mm

Midface Expansion Efficiency Index (MEEI)

The changes in midfacial bones are due to the force produced by MSE appliance at various levels of the skull. The force is generated by the activation of the appliance and is delivered to the bony structures within the skull. The resultant movement in midfacial bones is the consequence of robustness of the appliance, stability of the miniscrews, midface resistance and position of the bony structures relative to rotation fulcrums.

If the appliance gets deformed, or the miniscrews bend (deform) and/or tip, only a partial expansion force is transmitted to skull bones.

Moreover, the rotational effects must be considered: the zygomaticomaxillary complex rotates with a fulcrum located near the frontozygomatic suture in the coronal plane, and near the proximal portion of the zygomatic process of temporal bone in the horizontal plane. Even with a pure skeletal rotation, the landmarks located further from the rotational fulcrum undergo a larger lateral displacement.

Some of the most important parameters of midface modifications are summarized in Table 11, comparing the same parameters evaluated in the current study and the previous studies [34,36,43,44] conducted on non-surgical midface expansion with MSE.

In table 12, the average treatment changes in the discussed parameters have been divided by the average amount of MSE activation. The resultant ratio is a Midface Expansion Efficiency Index (MEEI) for each parameter considered. For example, in surgical expansion, the ratio between lower inter-zygomatic distance increase and MSE activation (MA) is 0.48, which means that for 1.00 mm of MSE activation, the lower inter-zygomatic distance increased by 0.48 mm. For non-surgical expansion, the ratio was 0.68, meaning that for 1.00 mm of MSE appliance activation, lower inter-zygomatic distance increased by 0.68 mm.

Table 11. Average treatment change in parameters evaluated in surgical and non-surgical midface expansion

(a): data from present study; (b): data from previous publications [34,36,43,44]; [1]: measured in axial palatal section; [2]: measured in upper nasal section; [3]: measured in coronal zygomatic section; [4]: measured in axial zygomatic section; ANS: anterior nasal spine; NPF: nasopalatine foramen; PNS: posterior nasal spine.

Parameter	**Surgical midface expansion with MSE (a)** **Average treatment change:**	**Non-surgical midface expansion with MSE (b)** **Average treatment change:**
Average patients age	27.6 years (range: 22.1 – 39.9)	17.2 years (range: 13.9 – 26.2)
Average MSE activation [1]	6.0 mm	6.8 mm
Total split at ANS [1]	3.4 mm	4.8 mm
Total split at NPF [1]	3.0 mm	Not measured
Total split at PNS [1]	3.6 mm	4.3 mm
Upper anterior maxilla width [2]	2.4 mm	3.4 mm
Upper posterior maxilla width [2]	0.9 mm	1.9 mm
Pterygoid plates width (PPW) [1]	1.7 mm	1.4 mm
Nasal width [3]	2.9 mm	Not measured
Lower inter-zygomatic distance [3]	2.9 mm	4.6 mm
Frontozygomatic angle [3]	1.9°	2.7°
Maxillary Inclination [3]	1.7°	2.3°
Anterior inter-maxillary distance [4]	1.7 mm	2.8 mm
Posterior inter-zygomatic distance [4]	1.6 mm	2.4 mm
Zygomatic process angle [4]	1.1°	1.9°
Frequency of pterygopalatine suture split (partial and complete) [1]	6/8 (75%)	16/30 (53%)
Frequency of pterygopalatine suture split (complete split only) [1]	1/8 (12.5%)	13/30 (43%)
Inter-molar distance [3]	7.4 mm	8.3 mm
Molar basal bone angle [3]	- 1.1°	-1.9°

Table 12. Ratio between average treatment change in parameters evaluated and MSE activation in surgical and non-surgical expansion patients(Midface Expansion Efficiency Index)

(a): data from present study; (b): data from previous publications [34,36,43,44]; [1]: measured in axial palatal section; [2]: measured in upper nasal section; [3]: measured in coronal zygomatic section; [4]: measured in axial zygomatic section; ANS: anterior nasal spine; NPF: nasopalatine foramen; PNS: posterior nasal spine; MA: MSE average activation.

Parameter	**Surgical midface expansion with MSE (a)**	**Non-surgical midface expansion with MSE (b)**
Total split at ANS [1] / MA	0.57 mm/mm	0.71 mm/mm
Total split at NPF [1] / MA	0.50 mm/mm	Not measured
Total split at PNS [1] / MA	0.60 mm/mm	0.63 mm/mm
Upper anterior maxilla width [2] / MA	0.40 mm/mm	0.50 mm/mm
Upper posterior maxilla width [2] / MA	0.15 mm/mm	0.28 mm/mm
Pterygoid plates width (PPW) [1] / MA	0.28 mm/mm	0.21 mm/mm
Nasal width [3] / MA	0.48 mm/mm	Not measured
Lower inter-zygomatic distance [3] / MA	0.48 mm/mm	0.68 mm/mm
Frontozygomatic angle [3] / MA	0.32 °/mm	0.40 °/mm
Maxillary Inclination [3] / MA	0.28 °/mm	0.39 °/mm
Anterior inter-maxillary distance [4] / MA	0.28 mm/mm	0.41 mm/mm
Posterior inter-zygomatic distance [4] / MA	0.27 mm/mm	0.35 mm/mm
Zygomatic process angle [4] / MA	0.18 °/mm	0.28 °/mm
Inter-molar distance [3] / MA	1.23 mm/mm	1.22 mm/mm
Molar basal bone angle [3] / MA	- 0.18 °/mm	- 0.28 °/mm

CHAPTER 4: DISCUSSION

Digital planning and manufacturing of MSE

MSE is a prefabricated appliance (Fig. 2.1 and 2.2), and its positioning is traditionally made based on dental arch stone models and 2D headfilms [11,34,36-44]. This approach presents some limitations, like the inability to identify MSE position relative to internal skeletal structures and the potential risk of damaging them.

To overcome the above limitations, a novel methodology has been developed to identify MSE position with the patient's CBCT, to optimize the biomechanical force distribution relative to midface skeletal structures, particularly the maxillary center of resistance and the midpalatal suture, and to avoid encroachment of miniscrews with critical anatomical areas like the nasal septum.

During digital planning, the position of MSE was chosen to maximize the bone thickness at the miniscrews insertion sites and to minimize the distance of MSE appliance from palatal mucosa in order to reduce the leverage effect on miniscrews during appliance activation (Fig. 2.9). Length of miniscrews was chosen to achieve a bicortical skeletal anchorage: miniscrews should penetrate the cortical bone layers (palatal vault and nasal floor) and 1 mm into the nasal cavity (Fig. 2.3). Furthermore, MSE was positioned as close as possible to the bi-zygomatic line (Fig. 2.6 D), which is considered to be the main maxillary resistance, and perpendicularly to the midpalatal suture (MS5 – MS7 line) to facilitate an expansion as symmetrical as possible in the horizontal plane (Fig. 2.6 and 4.1).

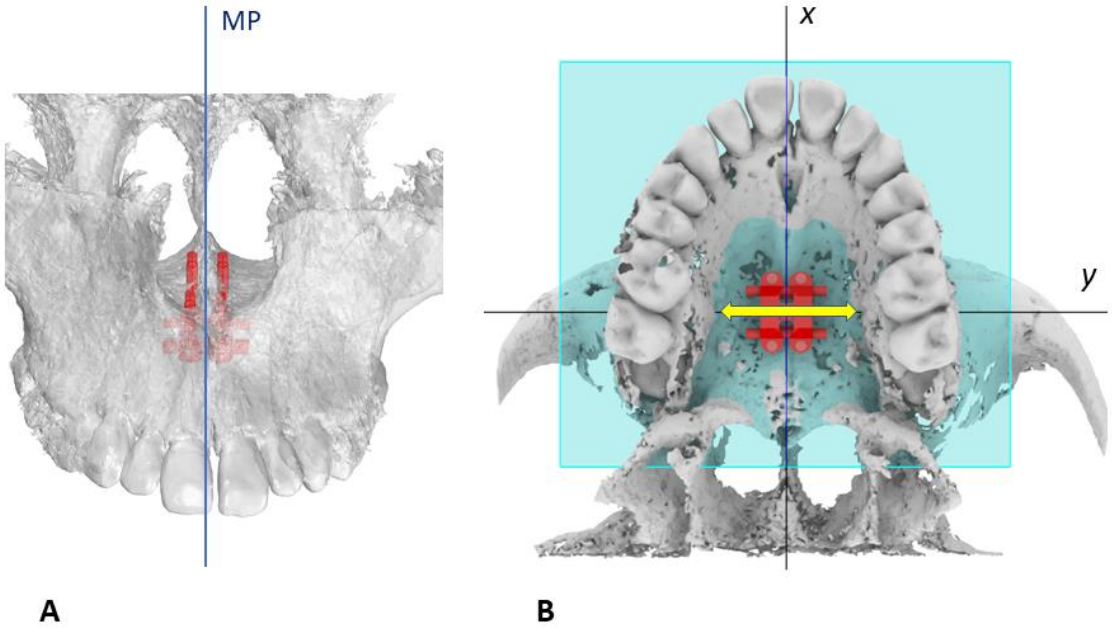

Fig. 4.1 Optimization of MSE position relative to midface skeletal structures: miniscrews do not encroach the nasal septum (A), and expansion force vector is perpendicular to midpalatal suture and close to the bi-zygomatic line (B) [64].

One particular feature of this digital workflow is that miniscrews are inserted after appliance cementation, the orthodontist doesn't need a surgical guide for the miniscrews since the appliance acts as a guide. The positioning guide is used only by the lab technician for bending and welding the MSE arms (Fig. 2.10).

This protocol allowed a safe and acurate insertion of miniscrews. In fact, the post expansion CBCTs showed that miniscrews did not encroach the nasal septum or other relevant anatomical structures.

However, after the first surgical intervention, a substantial bending/tipping of miniscrews was noticed in the post-expansion CBCT (Fig 4.2).

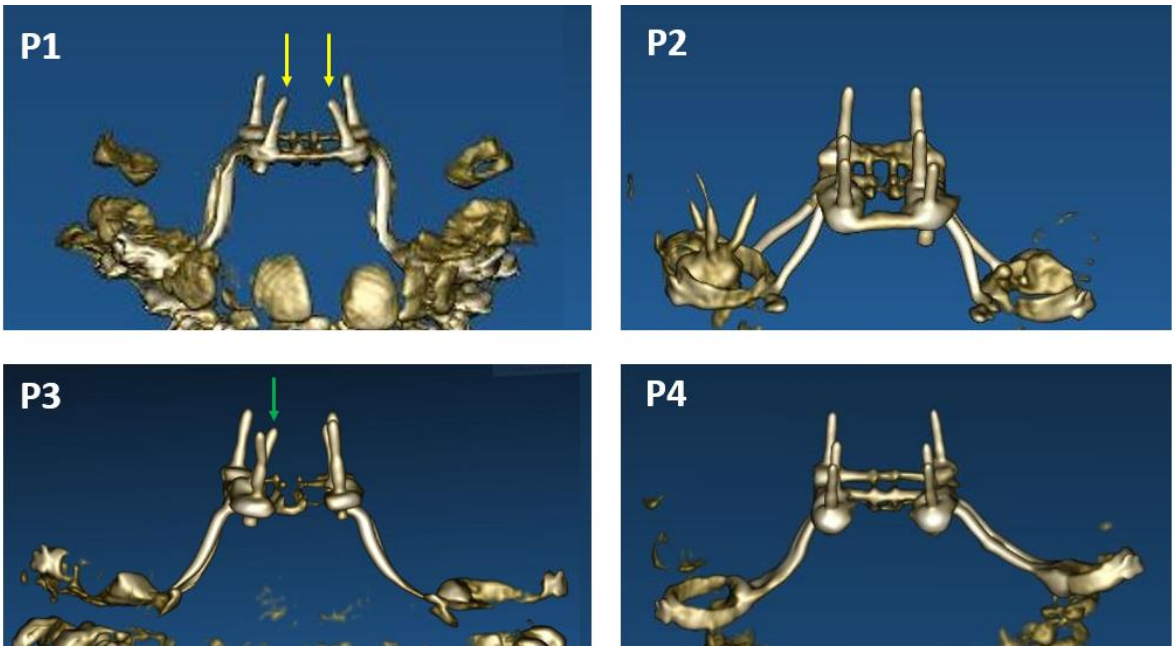

Fig. 4.2. 3D rendering of MSE appliance and miniscrews after maxillary expansion. In patient 1, both right and left anterior miniscrews tipped in a medial direction during maxillary expansion (yellow arrows). In patient 3, only middle right miniscrew tipped in a medial direction (green arrow). In patient 2 and 4, miniscrews were not deformed/tipped during maxillary expansion. Patient 1 had MSE with 4 miniscrews; patients 2, 3 and 4 had MSE with 6 miniscrews. P1: patient 1; P2: patient 2; P3: patient 3; P4: patient 4.

To limit miniscrews deformation and/or tipping, a few changes were made to the treatment protocol in patients after patient 1. In the modified protocol, two additional miniscrews were added to the original MSE design, MSE rigid arms instead of soft ones were utilized, horizontal arms running on the palatal surface of maxillary first molars, first and second premolars were added, and the appliance activation protocol was changed to a slower one, as shown in Table 13. The final design of MSE appliance of the modified protocol is shown in Fig. 2.16.

	ORIGINAL PROTOCOL (Patient 1)	MODIFIED PROTOCOL (Patients 2, 3, 4)
Number of miniscrews	**4**	**6**
Type of MSE arms	**Soft**	**Rigid**
MSE horizontal arms (palatal surface of first molars, first and second premolars)	**No**	**Yes**
MSE activation protocol	▪ **20 intra-operatory turns** (2.6 mm expansion) ▪ **7 days latency** ▪ **2 turns per day** (0.26 mm exp) until end of expansion	▪ **20 intra-operatory turns** (2.6 mm expansion) ▪ **7 days latency** ▪ **1 turn per day** (0.13 mm exp) until end of expansion

Table 13. Factors related to MSE appliance: original protocol adopted in patient 1, and modified protocol adopted in following patients 2, 3 and 4.

MSE rigid arms, connecting the MSE body with the molar bands, and horizontal arms running on the palatal surface of first molars, first and second premolars had the scope of increasing the rigidity of the appliance and the dental anchorage. In fact, the amount of intra-operatory activations (20 turns, 2.6 mm expansion) is very high, compared to the conventional non-surgical use of MSE. Our hypothesis is that such a high number of appliance activations in a short amount of time can bend (deform) and/or tip the miniscrews, since a high level of force is loaded on miniscrews before the sutures disarticulate. Given that the dental movement, consequence of biological mechanisms of bone resorption and apposition in the alveolar bone, starts on average 2 days after the application of a continuous force [70], it seems reasonable to exploit the dental anchorage during the intra-operatory activations, that last for a short time (few minutes). The increased dental anchorage reduces the load on miniscrews, and the risk of bending/tipping during the

aggressive intra-operatory activations, until the split of the midpalatal suture takes place and the inter-incisal diastema appears. In all patients, MSE appliance was activated intra-operatively until maxilla could be mobilized by an osteotome and an inter-incisal diastema appeared.

The addition of 2 miniscrews to the original MSE design was achieved through CAD-CAM technology. In the developed methodology, a virtual model of bushing and miniscrew was designed (Fig. 2.13) and imported in patient's CBCT. The bushings were produced with selective laser melting (SLM) technology and laser welded to the anterior portion of MSE body, using the 3D printed positioning guide that was designed on patient dental arch and CBCT composite model (Fig. 2.14 E). The rationale of adding two miniscrews to the original MSE design, which features 4 miniscrews, is to reduce the load on miniscrews and surrounding bone in order to limit their bending (deformation) and/or tipping during maxillary expansion. Additional miniscrews can be placed anteriorly to MSE body, shown in Fig. 2.14, or laterally on the palatal side of alveolar process between second premolar and first molar (Fig. 4.4 and 4.5).

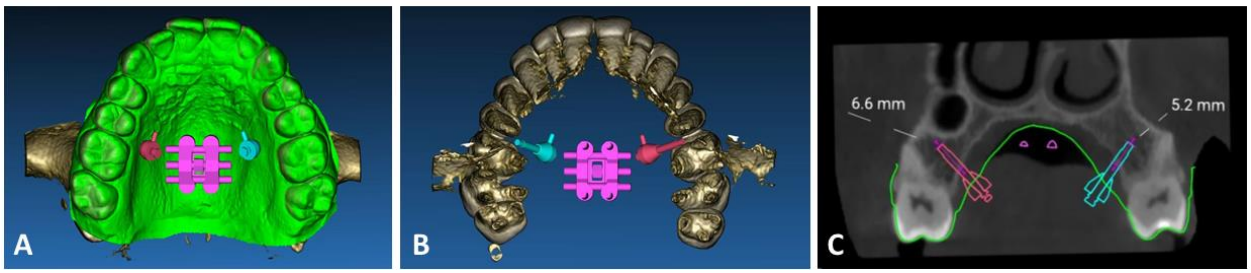

Fig. 4.3. Additional miniscrews positioned on the palatal side of the alveolar process between first molar and second premolar. A) Occlusal view; B) View from top after isolating dental crowns and roots; C) coronal view with measurement of bone thickness at miniscrew insertion sites [66].

Fig. 4.4. MSE with 2 additional miniscrews placed laterally, on the palatal side of alveolar process between second premolar and first molar. A) MSE cemented on first molars; B) insertion of miniscrews and steel tie between head of miniscrew and pin present on lateral bushings; B) covering of lateral miniscrews head with composite flow material [66].

The use of additional miniscrews positioned laterally, on the alveolar process between second premolar and first molar, has the advantage of being closer to the maxilla center of resistance (Fig. 4.6), a position more favorable for generating a parallel split of the midpalatal suture (Fig. 4.7).

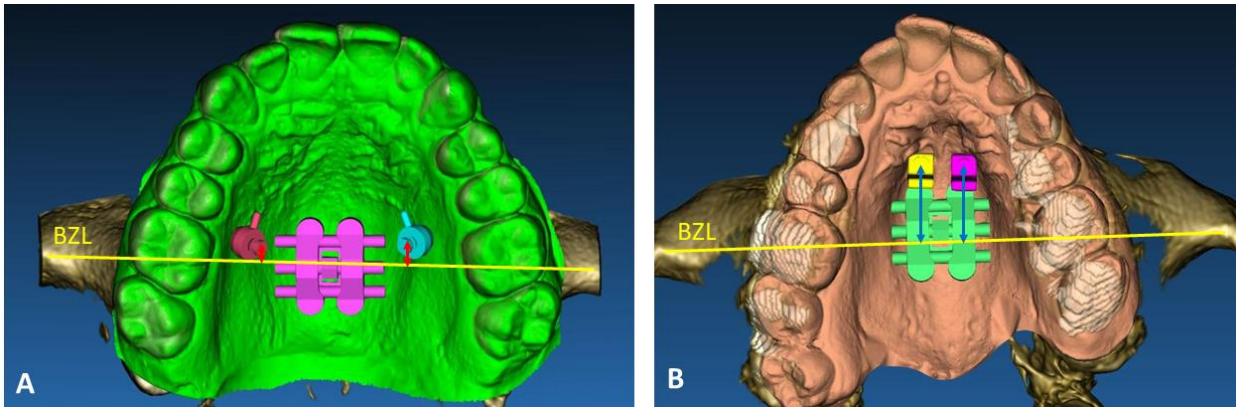

Fig. 4.5. Variation of distance from additional miniscrews to bizygomatic line (BZL), depending on location of miniscrews. Distance (red arrows) is much shorter for additional miniscrews placed laterally, between second premolar and first molar (A), than for miniscrews placed anteriorly to MSE body (distance represented by blue arrows) as shown in (B) [66].

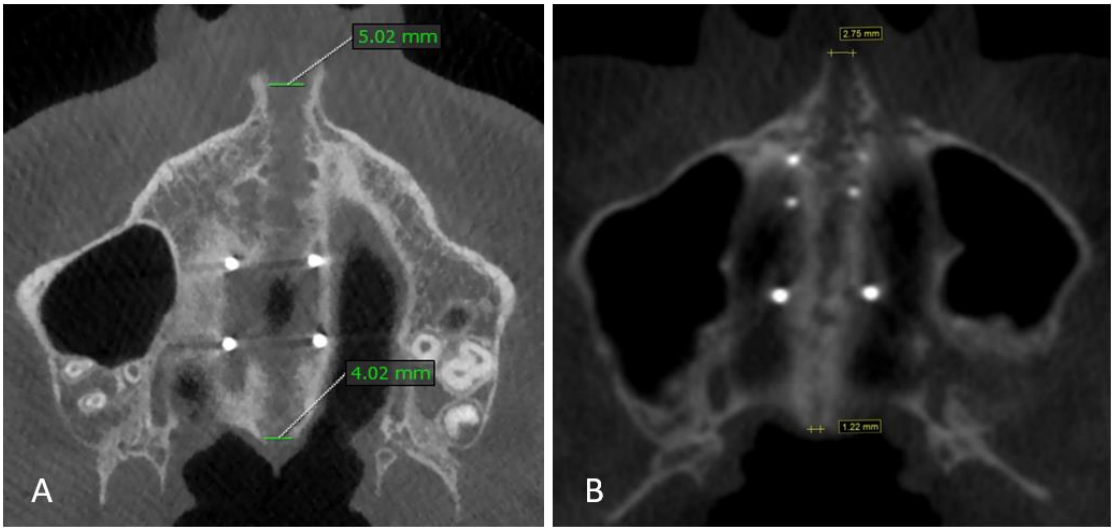

Fig. 4.6. Post-expansion CBCT showing the pattern of midpalatal suture split with non-surgical MSE with additional miniscrews placed laterally on the palatal side of alveolar process between second premolar and first molar (A) and anteriorly to MSE body (B). In (A) the midpalatal suture split is more parallel (ratio of split at PNS / split at ANS is 80%) than in (B) (ratio of split at PNS / split at ANS is 44%) [66].

However, additional miniscrews placed laterally have the disadvantage of limited space in the bone between dental roots, and complex appliance delivery because a steel tie must be placed between the head of the miniscrew and the bushing pin, and then the miniscrew head must be covered by composite material [66].

For the above reasons, in the current study, the additional miniscrews were positioned anteriorly to the MSE body, shown in Fig. 2.14 and 2.16.

Surgical intervention

Maxillary expansion is performed before or during puberty with tooth borne or tooth and tissue borne rapid palatal expansion (RPE) appliances such as the Hyrax or Haas expander [3-5]. However, during puberty a higher interdigitation takes place in midpalatal and

circummaxillary sutures [6-7], and the chances of obtaining a skeletal effect of midpalatal suture split in post-pubertal patients with tooth borne appliances is extremely low [6-9].

To overcome above limitations, miniscrews have been added to the original design of palatal expanders in the miniscrew assisted rapid palatal expansion (MARPE) protocol [10-26]. MSE is a particular type of MARPE appliance which utilizes 4 miniscrews with bicortical anchorage and is positioned in the posterior part of the palate to deliver the force close to the maxillary center of resistance to obtain a parallel split of the midpalatal suture and a larger midface skeletal effect [11,27-33].

MARPE appliances have shown to be effective in producing a maxillary skeletal expansion in adolescent and young adult patients [10-44]. However, this approach is not always successful in adult patients and the causes are not clear yet. Some Authors propose a classification of midpalatal suture maturation as a predictor factor for successful expansion [45], which however has not been confirmed by other Authors [46]. Age seems to be an important factor for MARPE case selection in adults, since successful maxillary expansion in patients with age above 25 years appears to be less likely [47]. A recent study found that above the age of 18 years, the risk of complications with miniscrew assisted palatal expansion (MAPE) increased by 10% per year, in a group of patients with age ranging from 18 years to 59 years [48]. Other considered influencing factors are individual patient bone density, patients' specific anatomy, the type of MARPE and activation protocol [47-48].

Surgically assisted rapid palatal expansion (SARPE) is the treatment of choice for adult patients where MARPE approach has failed or is considered inappropriate [49]. The surgery consists in osteotomies which have the aim to resect maxillary and peri-maxillary sutures and maxilla pillars, to mobilize the lower part of maxilla. Osteotomies involve mid-palatal suture, zygomatic buttress, piriform rim and pterygopalatine suture [51]. Rapid palatal

expander is activated intra-operatively until an inter-incisal diastema is generated and, after 7 days latency, the appliance is activated by the patient in the following days.

SARPE is potentially associated with complications such as bone fracture, nerve injury, carotid cavernous fistula, asymmetric maxillary expansion, post operative pain, discoloration, fracture or loss of central incisors due to the surgical mid-palatal suture split [54-59]. One of the most serious complications is bleeding, which manifests in the form of epistaxis, due to the interruption of terminal branches of internal maxillary artery during the surgical pterygopalatine suture disjunction [56].

To limit above problems associated with the conventional SARPE, Liu et al. propose the distraction osteogenesis maxillary expansion (DOME) technique where limited osteotomies are associated with MSE for maxillary expansion in adult patients [61-63]. The following osteotomies are performed: a lateral osteotomy, bilaterally, for addressing lateral resistance of the zygomatic buttresses with the involvement of the piriform rim of maxilla, and a vertical osteotomy at the anterior part of mid-palatal suture. No pterygopalatine suture disjunction is performed, to avoid the above-mentioned bleeding risks associated with this procedure. However, no midface skeletal effects of such procedure have been reported. Furthermore, because of the engagement of the piriform rim in the lateral osteotomies, there is a V-shaped pattern of midpalatal suture split (Fig. 4.7) and probably no modification in the upper part of the nasal cavity, located above the lateral osteotomies.

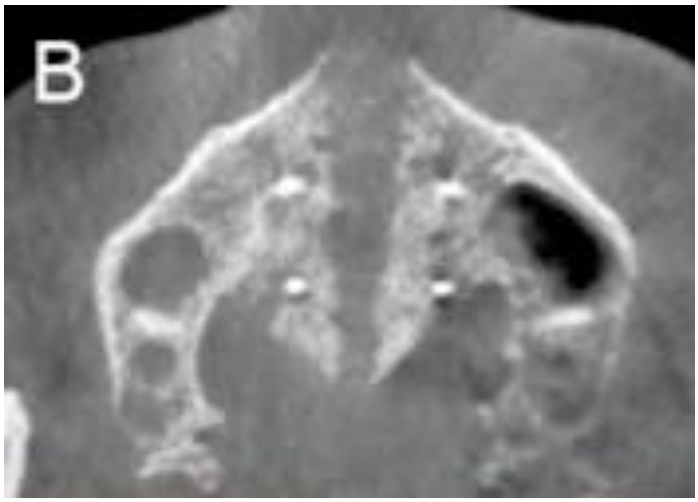

Fig. 4.7. V-shaped midpalatal suture split with the DOME technique. From: Yoon A at al. Distraction Osteogenesis Maxillary Expansion (DOME) for adult obstructive sleep apnea patients with narrow maxilla and nasal floor. Sleep Med. 2020 Jan;65:172-176 [63].

In the DOME technique, the lateral osteotomies at the basis of the zygomatic process of maxilla involve also the piriform rim, and after maxillary expansion a horizontal step is created between bony structures located above and below the lateral maxillary osteotomies (Fig. 4.8).

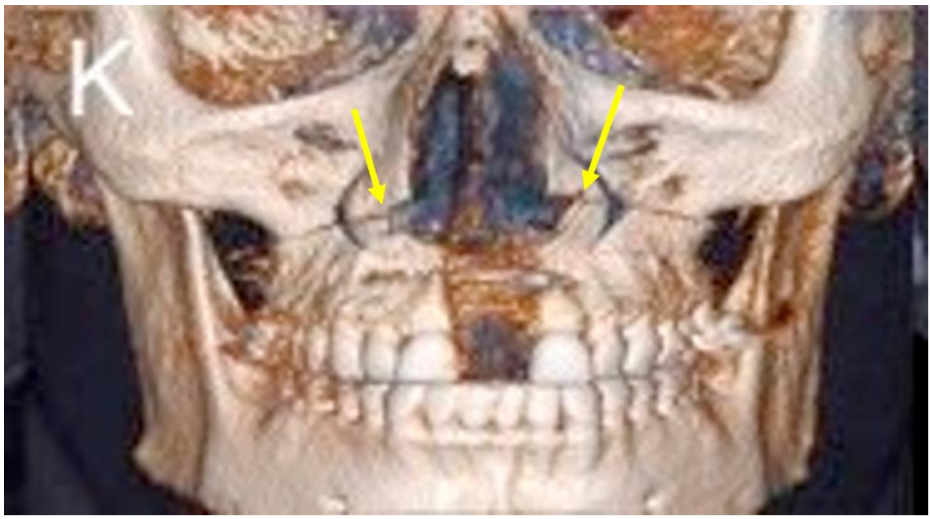

Fig. 4.8. In the DOME technique, lateral osteotomies at the basis of the zygomatic process of maxilla involve also the piriform rim; as a consequence, after maxillary expansion, a horizontal step (yellow arrows) is created between bony structures located above and below the lateral osteotomies. From: Yoon A at al. Distraction Osteogenesis Maxillary Expansion (DOME) for adult obstructive sleep apnea patients with narrow maxilla and nasal floor. Sleep Med. 2020 Jan;65:172-176 [63].

A very recent article, published in December 2021, describes a technique similar to DOME, the minimally invasive surgical and miniscrew-assisted rapid palatal expansion (MISMARPE) [71]. The technique consists in miniscrew-assisted rapid palatal expansion (MARPE) with a MARPE device positioned in the posterior part of the palate, with four miniscrews, without dental anchorage, associated with localized maxillary osteotomies performed with a piezoelectric instrument (Fig. 4.9). A less invasive surgery is adopted to reduce morbidity and post-operatory patient discomfort. The technique utilizes 4 osteotomies: a horizontal subspinal osteotomy to separate the anterior nasal spine, a vertical midline osteotomy at the anterior portion of the midpalatal suture extended into the nasal floor to the level of the middle thirds of the central incisors' roots, and two horizontal lateral osteotomies extending from the piriform aperture to the posterior maxilla (one per side).

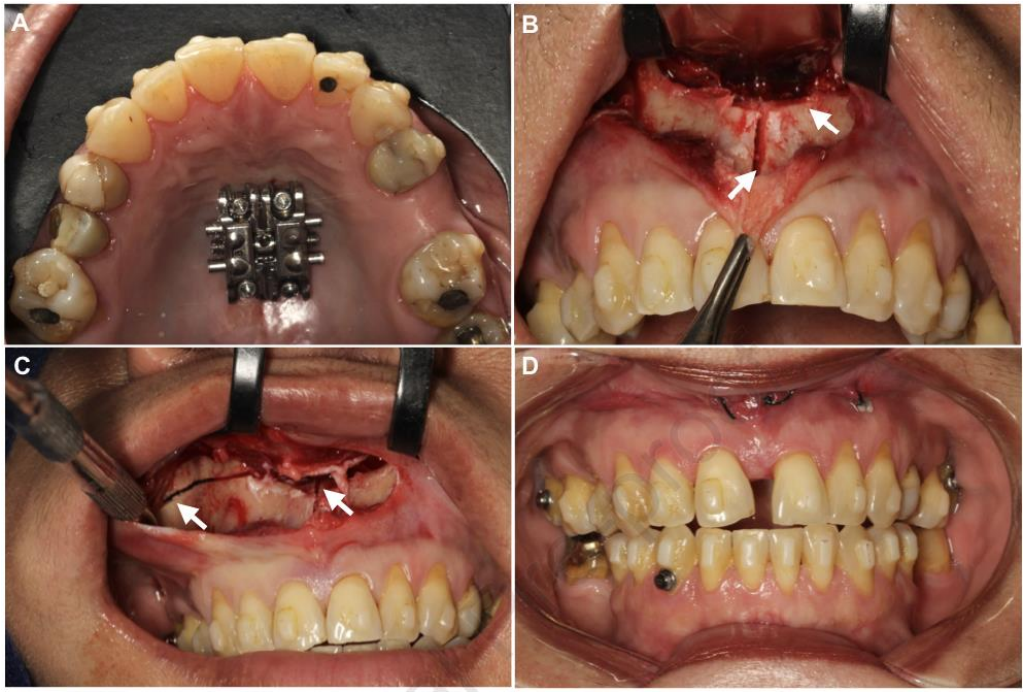

Fig. 4.9. Minimally invasive surgical and miniscrew-assisted rapid palatal expansion (MISMARPE) technique. A: MARPE appliance positioned in the posterior part of the palate; B: subspinal osteotomy and vertical osteotomy; C: horizontal osteotomy and intranasal osteotomy; D: MARPE activation and suture. From: Haas OL Jr et al. Minimally invasive surgical and miniscrew-assisted rapid palatal expansion (MISMARPE) in adult patients. Journal of Cranio-Maxillofacial Surgery (2022), available online December 27th 2021 [71].

MISMARPE technique was performed on patients with an average age of 38.9 years (range, 19.1 – 56 years): the Authors report a mean surgical operative time of 24 minutes, and a mild post-operative pain (overall mean visual analog score of 2.8). Reduced post-operative discomfort/pain was attributed by the Authors to avoidance of surgical pterygomaxillary disjunction, shortened operative time, less invasive soft tissue approach and use of piezoelectric instrument [71]. Authors propose different techniques based on patient age: conventional RPE for kids, MARPE for adolescents and young adults, MISMARPE for adults.

With MISMARPE, the midpalatal suture splits with a “V-shaped” pattern, and Authors conclude that the technique is useful mainly in cases where there is a discrepancy between the maxillary and mandibular arches, with a V-shaped maxillary arch and a U-shaped mandibular arch: the technique can correct the anterior maxillary constriction and coordinate the arches [71].

In the present study, maxillary expansion was performed with MSE associated with localized maxillary osteotomies executed with a piezoelectric instrument. The midpalatal osteotomy (MO) was performed at the anterior portion of midpalatal suture for a depth of 2 cm; the lateral maxillary osteotomies (LMOs) were performed at the basis of the zygomatic process of the maxilla, bilaterally, without involvement of the piriform rim (Fig. 2.19 – 2.21). The lack of surgical involvement of the piriform rim avoided the horizontal step between bony structures located above and below the lateral osteotomies found in the DOME technique, as shown in Fig. 4.10. This, in turn may facilitate the lateral movement of the lateral wall of the nasal cavity: in fact, one of the main scopes of the technique adopted in the present

study is to maximize the skeletal effect in the midface and to increase the width of the nasal cavity for a potential improvement of nasal breathing.

Even though the evaluation of post-operative discomfort was not the main objective of the present study, and no evaluation questionnaire was adopted, no complaint about post-operative pain was reported by the patients; also, they could regularly follow the appliance activation protocol that was given to them. Furthermore, no intra-operative hemorrhage nor post-operative bleeding was reported, probably because pterygomaxillary disjunction was not performed during surgery.

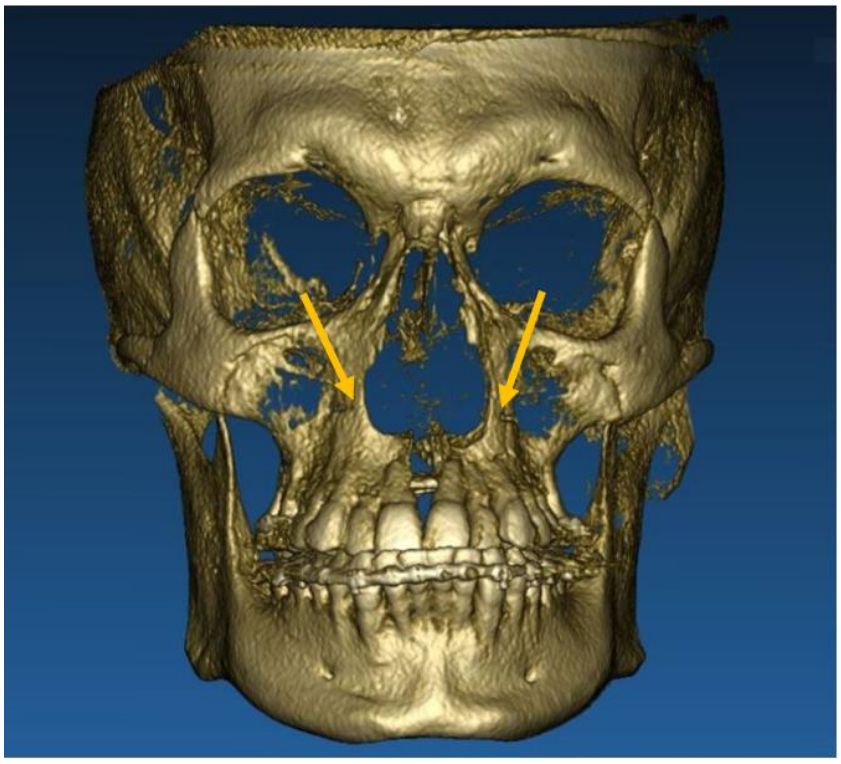

Fig. 4.10. 3D rendering of skull of a patient treated in the present study. Lateral maxillary osteotomies (LMOs) have a reduced extension and are interrupted about 5 - 8 mm distally to the piriform rim (orange arrows), so that the piriform rim is not cut. As a consequence of the surgical technique, no horizontal step is created between bony structures located above and below the LMOs.

Appliance activation protocol

In non-surgical midface skeletal expansion with MSE, the appliance is activated by 0.5 mm per day until an inter-incisal diastema appears, and then by 0.25 mm per day until completion of expansion [34-44]. The rationale of this activation protocol is that a high level of pressure is built into the appliance and midface bony structures which generates a disruption of midpalatal and circummaxillary sutures and facilitates maxillary movements.

In the DOME technique [61-63], one appliance activation (0.25 mm expansion) is performed intra-operatively, then no activation is done during the 7 days latency, finally the appliance is activated with a rate of 0.25 mm per day until the end of expansion. The total amount of appliance activation is 8 – 10 mm achieved in 4 – 5 weeks. During surgery, the appliance is activated by 1 turn only, to check the correct functioning of jackscrew, and then the suture is wedge opened with a straight osteotome and a hammer [61-63].

In the MISMARPE technique [71], the appliance is activated intra-operatively by 1.25 mm to check maxillary separation in the midline with the osteotome, no activation is then performed during the 7 days latency period, the appliance is then activated by 0.5 mm per day until an evident inter-incisal diastema appears, and then by 0.25 mm per day until end of expansion.

In the present study, MSE was activated intra-operatively by 20 turns (2.6 mm expansion), no activation was performed during the 7 days latency, then it was activated by 0.26 mm per day until end of expansion in the original protocol (patient 1), and by 0.13 mm per day in the modified protocol (patients 2, 3, 4).

Table 14 summarizes the activation protocols adopted in the present study, in DOME and MISMARPE techniques.

ORIGINAL PROTOCOL (Patient 1)	MODIFIED PROTOCOL (Patients 2, 3, 4)	DOME technique	MISMARPE technique
▪ **20 intra-operatory turns** (2.6 mm expansion) ▪ **7 days latency** ▪ **2 turns per day** (0.26 mm exp) until end of expansion	▪ **20 intra-operatory turns** (2.6 mm expansion) ▪ **7 days latency** ▪ **1 turn per day** (0.13 mm exp) until end of expansion	▪ **1 intra-operatory turn** (0.25 mm expansion) ▪ **7 days latency** ▪ **1 turn per day** (0.25 mm exp) until end of expansion	▪ **6 intra-operatory turns** (1.25 mm expansion) ▪ **7 days latency** ▪ **1 turn per day** (0.25 mm exp) until end of expansion

Table 14. Maxillary expander activation protocol in the present study (original and modified), in DOME [61-63] and MISMARPE [71] technique.

Our activation protocol included 20 intra-operatory turns (2.6 mm expansion). It was common experience that all 20 turns be performed before maxilla became mobile with the osteotome and that a clear inter-incisal diastema appeared visible. We preferred to make sure that midpalatal suture was open during surgery, differently from what is described in the DOME technique (1 intra-operative activation turn only), to avoid to be forced to repeat the surgical operation in case the midpalatal suture didn't split in following days.

However, the 20 intra-operative turns may generate too much force on the miniscrews that are 1.8 mm in diameter and surrounding bone which induce the miniscrews bending / tipping phenomenon described in the previous section in patient 1 (Fig. 4.2). To reduce the miniscrews bending / tipping, the protocol was modified by utilizing rigid arms, instead of soft ones, by fabricating horizontal arms running on palatal surface of first molars, first and second premolars, and by adding 2 more miniscrews to the anterior portion of MSE body, produced with Cad-Cam technology and laser welded, shown in Table 13. The final appliance was more rigid and more substantive dental anchorage was produced. Since the dental movement starts 2 days after application of a continuous force [70], dental anchorage can be a valid support during intra-operative activations.

Finally, after the 7 days latency period, the activation protocol was modified to a slower one (0.13 mm per day). The rationale is that during midface expansion with MSE, not only sutures, but several skeletal structures get involved and bone bending phenomena take place in the zygomatic process of the temporal bone, pterygoid processes of the sphenoid, perpendicular plates of palatine bone [34,44]. Bone bending is a phenomenon different from bone remodeling: it takes place in a shorter period of time, when a cyclical bending force is applied to a bone and is considered an adaptive mechanism to dissipate the energy in order to prevent an open fracture [72]. Lateral loads applied to a bone produce tensile forces at the bone surface facing the load and compressive forces at the opposite surface, generating microfractures in the trabeculae of the cancellous bone [72-73]. Microfractures subsequently activate self-repair mechanisms [74], leading to bone callus formation on the damaged trabeculae. Microfractures and self-repair through new bone formation progressively leads to a change in bone shape [72].

It has been reported that the bone resistance to a bending force depends on the density, calcium content, cortical to cancellous bone ratio, micro-architecture and geometry of the bone [75-76]. Regarding this last point, the resistance to bending is directly related to the third power of the bone diameter [77], and this can explain why thin and long bone are more prone to bone bending than thick and short ones.

Since bone bending take place in several regions of the skull during midface expansion, a slower expansion protocol may allow more time for these phenomena to take place, thus reducing the pressure on the MSE appliance and the chances of appliance deformation and/or miniscrews bending/tipping phenomena.

3D analysis

Cone beam computed tomography (CBCT) images allow the 3D visualization of skeletal structures and the evaluation of changes due to growth, aging, orthodontic treatment, orthognathic surgery or post-treatment relapse between exams taken at different time points [67-68,78]. Pre- and post-treatment CBCT data sets can be superimposed on desired regions of interest through a surface based, landmark-based or voxel-based method [78].

In the presented study the pre- and post-expansion CBCTs were superimposed on stable structures of anterior cranial base [67] through the “Automatic superimposition” tool present in the Fusion module of Ondemand3D software. The software automatic superimposition has the advantage of eliminating the error related to the operator, and it has been shown to have a sub-voxel accuracy (superimposition error lower than pixel size of 0.3 mm) [68]. The voxel-based superimposition exploits the grey scale difference in the volume of a selected volume of interest, such as the anterior cranial base.

After CBCTs superimposition, the main reference plane to orient the skull was the maxillary sagittal plane (MSP) as reported in previous publications (Fig. 2.23-2.25) [36,44]. MSP passes through anterior nasal spine (ANS), posterior nasal spine (PNS) and Nasion (N), it crosses the center of maxilla and midface, hence it makes it clearer to identify how selected skeletal or dental landmarks move away from MSP during maxillary expansion (Fig. 4.11). The difference of the distance between pre- and post-expansion CBCTs represents the lateral displacement of the landmark due to treatment. Several following publications were made adopting this methodology [34,37-39,43]; reliability of skull orientation and landmark identification has been reported to be high, with intra-class correlation coefficient of at least 0.973, rater coefficient of variation of 1.36% or less, error coefficient of variation of 1.97% or less for the selected parameters [34,36-39,43].

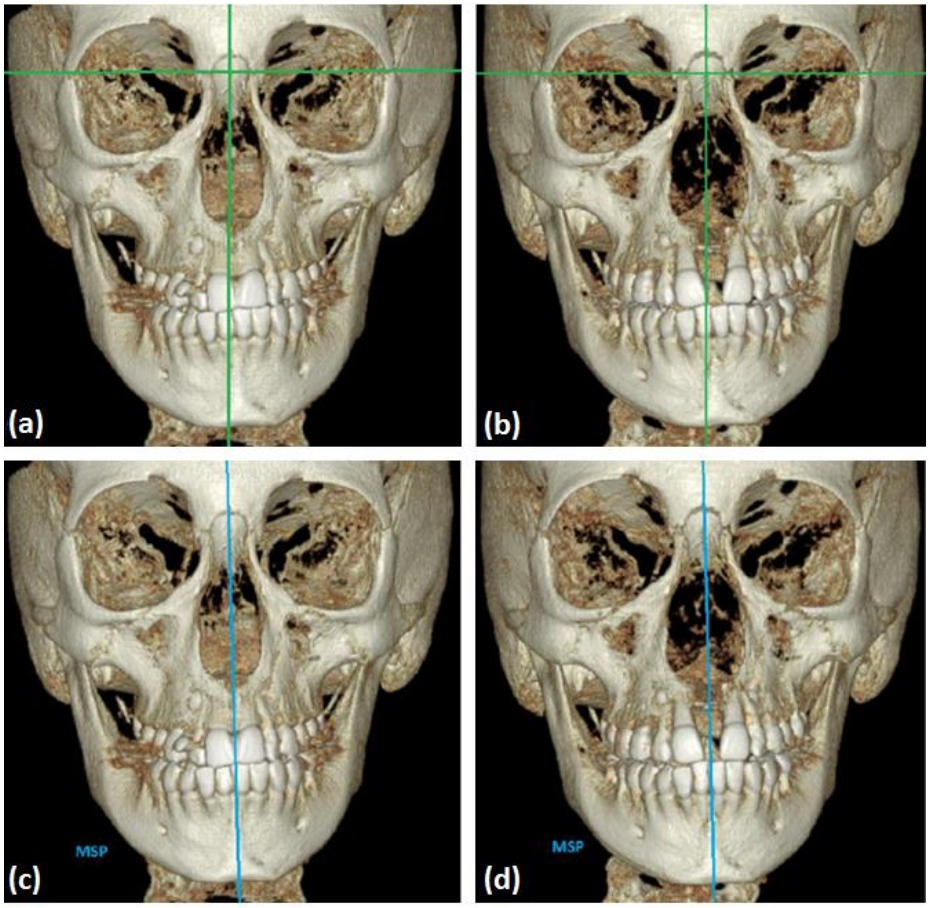

Fig. 4.11. Reference lines utilized in conventional 2D postero-anterior cephalometric analysis: a) pre-expansion and b) post-expansion do not necessarily cross the midpalatal suture. Maxillary sagittal plane (MSP), utilized in the study, crosses the midpalatal suture and the center of midface: c) pre-expansion and d) post expansion [36].

Since MSP crosses the center of midpalatal suture and midface, it is a clear reference plane to evaluate the level of asymmetry of midface expansion in the horizontal plane [36-43,44]. For a selected landmark, the lateral displacement on one side of the skull is compared (subtracted) from the lateral displacement of the same landmark on the contralateral side of the skull, and the difference represents the level of asymmetry of maxillary halves movement for the landmark (Fig 4.12).

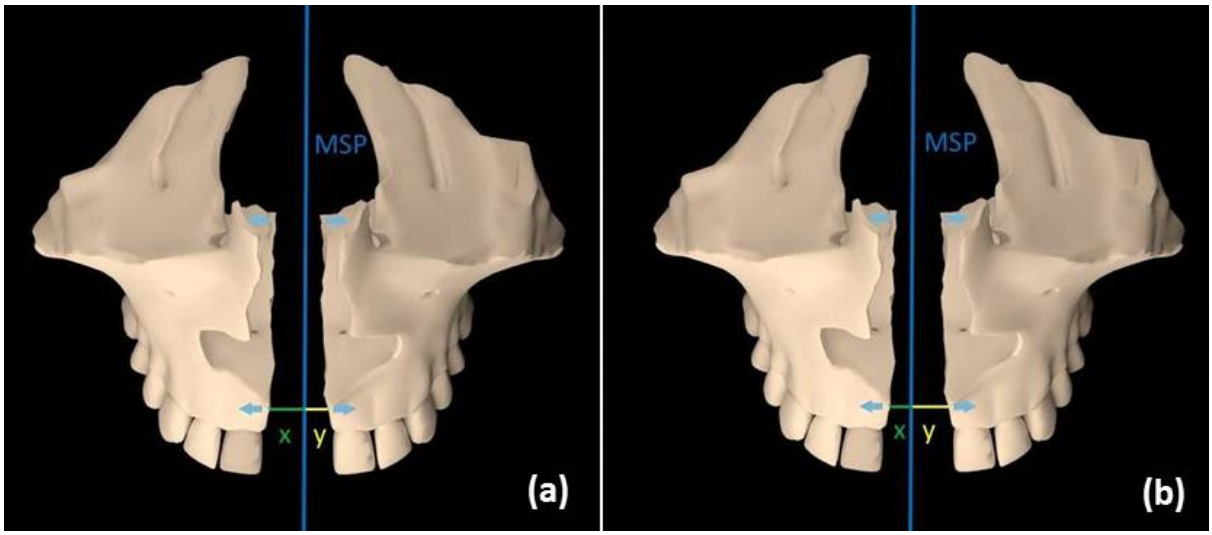

Fig. 4.12. Illustration showing maxillary sagittal plane (MSP) utilized as a reference plane to analyze the level of midface expansion asymmetry in the horizontal plane. a) example where the lateral movement of right maxilla (x) is larger than that of left maxilla (y). b) example where the lateral movement of right maxilla (x) is smaller than that of left maxilla (y). In this example, the halves of anterior nasal spine (ANS) are the landmark utilized for the analysis [36].

Midpalatal and pterygopalatine sutures modifications, maxillary movement

During maxillary expansion with tooth borne appliances, the pterygopalatine suture cannot be split [79-80] and it acts as a fulcrum for the movement of maxillary halves. As a consequence, the midpalatal suture is opened with a V-shaped pattern (Fig. 4.13), with a larger movement at the anterior nasal spine (ANS) and a smaller movement at posterior nasal spine (PNS) [3,4,5,44,80,81].

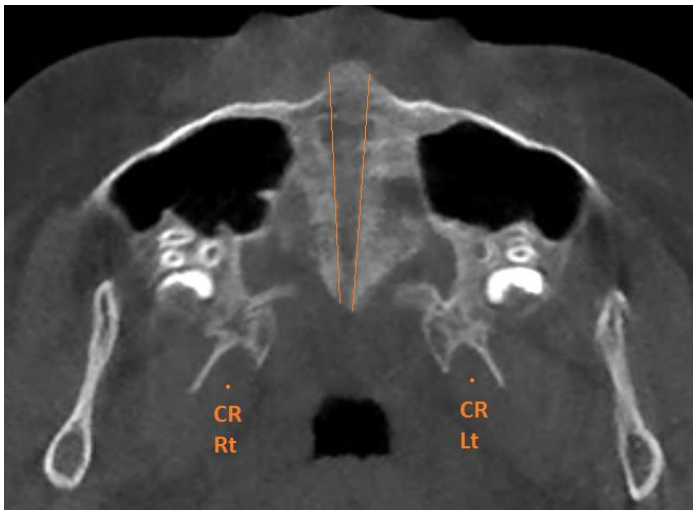

Fig. 4.13. With Hyrax appliance the pterygopalatine suture is not disarticulated during maxillary expansion, so it acts as a hinge for the maxillary halves movement; as a consequence, the midpalatal suture is opened with a V-shaped pattern, with a larger split anteriorly and a smaller split posteriorly [44]. CR: center of rotation.

Conversely, it has been shown that with non-surgical MSE the pterygopalatine suture can be split, as the pyramidal process of the palatine bone is pulled out of the pterygoid notch of the pterygoid process of the sphenoid bone [36,44] in 53% of the sutures in late adolescents and young adults. This finding has been confirmed by a following study [39], where the pterygopalatine suture disarticulation was visible in 84% of the examined sutures.

In non-surgical MSE [36,44], the pterygopalatine suture split was visible in 81% of the cases and partial in 19% of the cases [36,44]. A complete split (CS) happens when the pyramidal process of the palatine bone is completely pulled out of the pterygoid notch, whereas a partial split (PS) takes place when the pyramidal process is separated from the medial pterygoid plate but not from the lateral pterygoid plate (Fig. 2.37).

In the present study, the pterygopalatine suture split was visible with a high frequency, in 75% (6 out 8) of the examined sutures. The split was complete (CS) in 12.5% of the sutures and partial (PS) in 62% of the sutures. The frequency of complete split (12.5%) was lower

than in non-surgical MSE (43%) (Table 11), possibly due to the higher ossification of the suture. In fact non-surgical MSE was conducted in late adolescents and young adults (average age of 17.2 years) while surgical MSE of the present study was conducted mainly in adult patients (average age of 27.6 years). Another consideration is the sutural orientation. If the suture is oriented along the path of maxillary movement, the space would not be visible even with a disarticulation [36,44]. By the fact that both non-surgical and surgical MSE patients exhibited parallel split of the midpalatal sutures even in those without radiographically visible opening at the pterygopalatine sutures, the disarticulations of pterygoid palatine sutures in all MSE cases are probable.

The success rate of pterygopalatine suture disarticulation and the width of opening in the pterygoid process after the split can also be affected by anatomical factors. In fact, Lee and coworkers [79] describe 4 types of palatine bone pyramidal process, which are different in their shape and size (Fig. 4.14). Probably, pyramidal processes with a larger volume disarticulate with more difficulty than smaller ones.

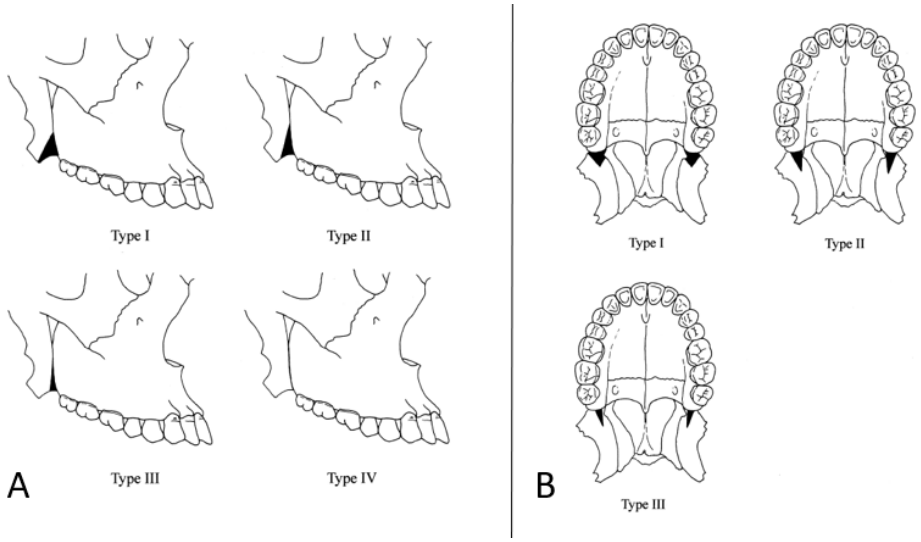

Fig. 4.14. 4 types of palatine bone pyramidal process. A) lateral view. B) occlusal view. From: Lee SP et al. Anatomical study of the pyramidal process of the palatine bone in relation to implant placement in the posterior maxilla. J Oral Rehabil. 2001;28:125-32.

It seems that the behavior of the pterygopalatine suture dictates the type of maxillary movement. The split of the pterygopalatine suture is associated with a parallel pattern of midpalatal sutures opening, whereas the lack of pterygopalatine split is associated with a V-shaped pattern of midpalatal suture opening [36-37,39,44,81,83]. Providing posterior force vector is an obvious requirement to achieve pterygopalatine disarticulation. However, the posterior palatal bone can be quite thin. With this regard, it is emphasized the importance of the miniscrews bicortical anchorage. In fact, the engagement of cortical bone layers of palatal vault and nasal floor significantly reduces the bending stress on miniscrews and the compressive forces on surrounding bone, as shown by a finite element method (FEM) study [35]. A higher miniscrews stability can be responsible for a better transmission of expansion force to skeletal structures and disarticulation of the pterygopalatine suture. Furthermore, a recent clinical study [84] found that, with non-surgical MSE, the presence of bicortical anchorage is associated with a higher frequency of pterygopalatine suture disarticulation and a larger split of the posterior nasal spine (PNS); and, in cases with lack of bicortical anchorage, the pterygoplatine suture disarticulation is less frequent and the opening at PNS is smaller. Another clinical study found that, overall, a bicortical anchorage is associated with a larger maxillary movement and a larger effect in the nasal cavity [85]. Clinically, the lack of bicortical anchorage generates a large deformation of miniscrews, so that most of appliance activation is not transmitted to the skeletal structures [86].

In the present study, posterior positioning of MSE and bicortical anchorage were ensured by the developed digital workflow. The miniscrews length and position were chosen based on patient's CBCT imaging to penetrate both cortical bone layers (oral cavity and nasal floor) and to penetrate 1 mm into the nasal cavity. Also, the 2 additional miniscrews in Cad-Cam

bushings were placed anteriorly to the MSE body, and bicortical engagements were planned by a digital workflow on patient's CBCT.

Similar to non-surgical expansion with MSE, the pattern of midpalatal suture split was parallel in the present study. the ratio of split at PNS (3.6 mm) divided by the split at ANS (3.4 mm) was 105%. For non-surgical MSE the ratio was 90% [36]. Given that the anterior portion of the midpalatal suture is cut by the piezoelectric instrument in the present study, the split at nasopalatine foramen (NPF) was utilized as a parameter to evaluate the movement in the anterior region of the maxilla, as proposed by a recent study [48]. If we analyze NPF split, the ratio between PNS split (3.6 mm) and NPF split (3.0 mm) was 120%. From above data, we can conclude that in surgical maxillary expansion with MSE, the pattern of midpalatal suture split was parallel, with slightly larger movement at PNS. The reasons can be that the miniscrews had a bicortical anchorage and the maxilla piriform rim, the anterior resisting structure, was not cut during surgery in the present study.

In the DOME and MISMARPE techniques, the piriform rim is cut by the piezoelectric instrument, and this reduces the maxilla resistance in its anterior region and generates a V-shaped movement of the maxilla [61-63,71]. The V-shaped maxillary movement is indicated in patients presenting a constriction only in the anterior part of the maxilla, with V-shaped maxillary and U-shaped mandibular dental arches [71]. However, in patients presenting a posterior cross-bite at the level of first molars, a parallel midpalatal suture split and a larger movement in the posterior part of the maxilla, as evidenced in the present study, can be more appropriate.

The pterygoid processes of the sphenoid bone undergo a bone bending phenomenon and are pulled laterally by the palatine bone which moves in a lateral direction, as shown in

Fig. 4.15. The portion of the pterygoid process further from the cranial base undergoes a larger movement than the portion closer to it. This has been found during maxillary expansion with the Hyrax appliance [81] as well as with non-surgical MSE [36,44].

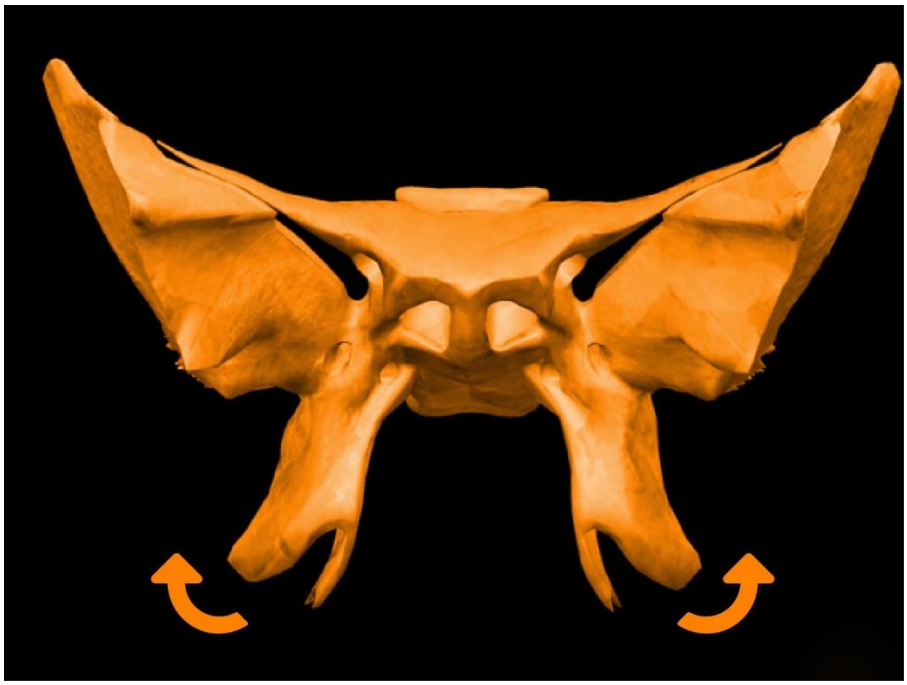

Fig. 4.15. Illustration showing the pterygoid processes of the sphenoid bone bending in a lateral direction during maxillary expansion [44].

As a consequence of bone bending in a lateral direction, the distance between the most lateral points of the lateral pterygoid plates increases [44,81]. Also in the present study, the pterygoid processes width (PPW) increased, by 1.7 mm. However, the results were without statistical significance, due to the small sample size.

Changes in the zygomaticomaxillary complex, nasal cavity and zygomatic arches

The lower interzygomatic distance (LID) is measured in the coronal zygomatic section (CZS) between the most lateral point of the right and left zygomaticomaxillary sutures and is an important parameter to analyze the amount of midface expansion. With tooth borne expanders, the lateral displacement of the zygomatic bone is of small entity: Baccetti et al. [87] found that the Haas appliance produces increases in bizygomatic width of 0.4 and 0.3 mm in early treated and late adolescent patients, respectively. Ong et al. [88] describe a transverse expansion of the zygomatic bones of 1.4 mm with a cast splint expander used in adolescents. The limited midface expansion with tooth borne expanders is due to the fact that part of the jackscrew activation is dissipated in dentoalveolar tipping, and only the residual activation generates orthopedic effects [5].

Conversely, with non-surgical MSE, the increase in lower interzygomatic distance has been of 4.8 mm [43] in late adolescents and young adults (mean age of 17.2 years). The use of 4 miniscrews with bicortical anchorage in the MSE is capable of transmitting most of the appliance activation to skull skeletal structures and to generate a larger midface expansion effect [43]. Since maxilla is located medially to the zygomatic bones, they are also affected by maxillary expansion and are laterally displaced; this is associated with an increase in the fromtozygomatic angle (FZA). It has been found that the whole zygomaticomaxillary complex rotates as a unit, with a fulcrum located at the frontozygomatic suture [43].

In the present study, the lower interzygomatic distance increased by 2.9 mm, the frontozygomatic angle by 1.5 ° and 2.4° (Rt and Lt), while the zygomaticomaxillary angle changed by a small entity (-0.03° on Rt side and -0.23° on left side). Although all changes were without statistical significance in the present study, probably due to the small sample size, a pattern of midface expansion similar to non-surgical MSE has been found. The

zygomaticomaxillary complex rotates outwards with a fulcrum located near the frontozygomatic suture.

The pattern of rotation has been calculated as the ratio between frontozygomatic angle increase (+ 1.9°, average of Rt and Lt side) and lower interzygomatic distance increase (+2.9 mm). The ratio is 0.7°/mm, indicating that for each 1.00 mm increase in lower interzygomatic distance, the rotation of the zygomaticomaxillary complex is approximately 0.7°.

Interestingly, the nasal width, measured in the CZS, as the distance between the most lateral point of right and left lateral nasal wall (Fig. 2.44), increased by 2.9 mm, with statistical significance ($p<0.01$). This result is the anatomical basis for an improvement in nasal breathing in patients suffering from increased nasal airway resistance, in agreement with studies that show that maxillary expansion is associated with increase in nasal cavity width [89-91] and improvement in nasal airflow [92].

With DOME technique [61-63], the Authors describe an improvement in Obstructive sleep apnea syndrome (OSAS) parameters, such us apnea-hypopnea index (AHI), nose obstruction symptom evaluation (NOSE) score, oxygen desaturation index (ODI), Epworth sleepiness scale (ESS) score, associated with an increase in the percentage of REM sleep. Improved breathing is attributed by the Authors to the following mechanisms: enlargement of nasal floor, internal nasal valve width and enlarged space for tongue position. The improved nasal airflow is associated to a reduction in the negative pressure during inspiratory acts and a reduced tendency of the pharynx to collapse. Regarding the appliance, the Authors emphasize the importance of miniscrews with bicortical anchorage in the posterior part of the palate to generate an expansion force that may be superior and posterior in the palatal vault to maximize the nasal floor expansion. However, the Authors

don’t report the amount of nasal cavity width increase. Also, in DOME, the lateral maxillary osteotomies (LMOs) are extended to the piriform rim, and a horizontal step is generated between skeletal structures located above and below the osteotomies after treatment (Fig. 4.9). This pattern of expansion limits superior and posterior widening of the nasal cavity. Conversely, in the present study, the LMOs didn’t involve the piriform rim and no horizontal step was found in the post expansion CBCTs at the level of the piriform rim. This, in turn, may be responsible for the large increase in nasal width (+2.9 mm) in treated patients.

Regarding dentoalveolar changes, the increase in inter-molar distance (IMD) was of 7.4 mm. The molars underwent a small dentoalveolar tipping of -1.1° and -1,2° (Rt and Lt side), as evidenced by the change in molar basal bone angle (MBBA).

The fact that the IMD increased more than the amount of MSE activation (6.0 mm) is probably due to the rotational type of movement of the zygomaticomaxillary complex [43] (Fig. 1.1). As the zygomaticomaxillary complex rotates around the fulcrum located at the frontozygomatic suture, for the same amount of angular rotation, points further from the rotational fulcrum (i.e. molar crowns) undergo larger linear displacements than points located near the fulcrum (i.e. the 2 halves of the expansion jackscrew) (Fig. 4.16).

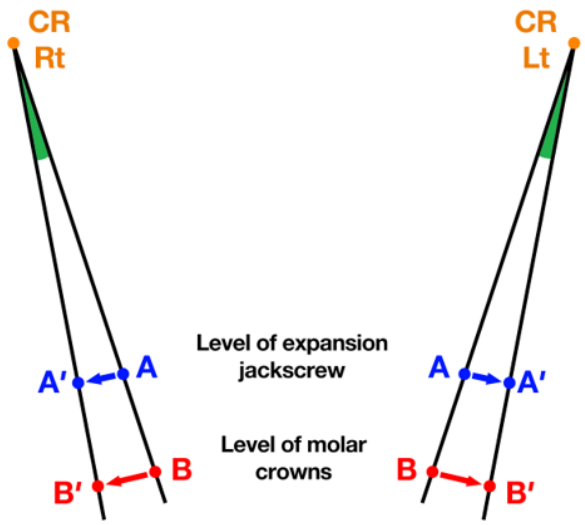

Fig. 4.16. Illustration showing that, for the same amount of angular rotation, points closer to the center of rotation (A point) undergo a shorter linear displacement than points farther from the center of rotation (B-point). CR Rt: center of rotation for the right zygomaticomaxillary complex; CR Lt: center of rotation for the left zygomaticomaxillary complex [43].

In the axial zygomatic section (AZS), with non-surgical MSE, the zygomaticomaxillary complex rotates with a fulcrum located at the proximal portion of the zygomatic process of the temporal bone [34] (Fig. 1.2). This is due to bone bending phenomena: the proximal portion of the zygomatic bone is the thinnest portion of the zygomatic arch, and hence the most prone to bending [72-77]. In fact, bone resistance to bending (rigidity) is directly proportional to bone diameter elevated at third power, and inversely proportional to bone length elevated at third power [77]. In the present study, the anterior intermaxillary distance increased by 1.7 mm, the posterior inter-zygomatic distance by 1.6 mm, while the largest change in angular parameters was at zygomatic process angle (ZPA) that increased by 0.7° and 1.5° (Rt and Lt). All changes in the AZS were without statistical significance, probably due to the small sample size. However, the pattern of movement with a fulcrum located in the proximal portion of zygomatic arch is similar to the results from the non-surgical MSE.

Interestingly, skeletal modifications were found in several parameters and regions of the skull located above the lateral maxillary osteotomies (LMOs), such us the upper nasal section, lower interzygomatic distance, nasal width, frontozygomatic angle, anterior inter-maxillary distance and posterior inter-zygomatic distance in the AZS (Fig. 3.2 and 3.3). This means that the MSE expansion force could be transmitted above the LMOs, probably due to the intact piriform rim during surgery.

Analysis of midface expansion symmetry

With non-surgical MSE, midface expansion has been found asymmetric in the transverse plane, with one half of anterior nasal spine (ANS) moving more than the contralateral one by an average of 1.1 mm, using maxillary sagittal plane (MSP) as reference for the analysis [34]. The asymmetry of maxillary movement with MSE was analyzed in a following study [37], where maxillary movement was judged symmetric if the difference between larger and lesser movement of ANS halves was 1.0 mm or less, and asymmetric if the difference was 1.1 mm or more. It was found that the movement was asymmetric in 16 out of 31 patients (52%). In the asymmetric group, on average the movement was 2.2 mm more on one side. The Authors found a possible correlation between the side of the lateral crossbite and direction of asymmetry.

In the present study, the maxillary sagittal plane (MSP) was used as reference for the analysis. The movement of three landmarks was utilized: anterior nasal spine (ANS) like in previous studies [34,37], and also nasopalatine foramen (NPF) and most lateral point of zygomatic process of maxilla (ZR and ZL). On average, the asymmetry of maxillary movement was of 0.54 mm at ANS, 1.1 mm at NPF, 1.3 mm at ZR/ZL points (Table 10). The amount of asymmetry varies at different landmarks and the difference can be due to the

rotational effect of maxillary halves movement, because linear displacement is larger for landmarks further for the fulcrum, or to measurement error due to the small sample size.

Possible reasons for asymmetric expansion can be a unilateral crossbite [37], or difference in suture interdigitation, bone density, skull morphology, bone geometric factors (length and diameter) between right and left side of the skull, especially in the zygomatic arches [34].

Midface Efficiency Expansion Index (MEEI)

During midfacial expansion with MSE, an expansion force is generated by the activation of the appliance and the resulting effect is the displacement of skeletal and dental landmarks in three planes of space. The relationship between appliance activation and landmarks displacement is summarized in Fig. 4.18.

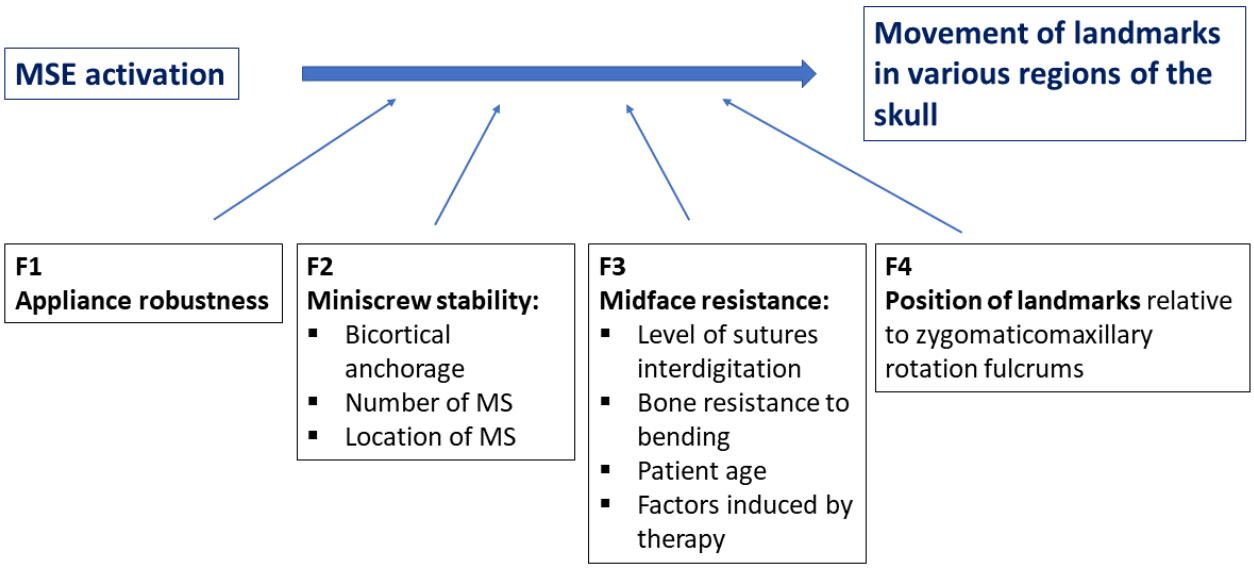

Fig. 4.18. Factors affecting the displacement of landmarks located in various regions of the skull after therapy with MSE. MS: miniscrew.

The first factor (F1) is appliance robustness. If the expansion appliance is robust, it doesn't get deformed during maxillary expansion and all activation can be transmitted to the minsicrews and skull bones.

The second factor (F2) is miniscrew (MS) stability. If miniscrews have a high primary stability, they don't bend (deform) or tip through bone. MS bicortical anchorage is of primary importance in this regard as demonstrated by FEM [35] and clinical studies [36,84,85]. Miniscrews stability depends also on their number, location, surrounding bone thickness and bone density. Also, the distance of MS from maxilla center of resistance (CR) is an important factor, in fact MS closer to CR generate a larger skeletal movement than MS positioned further from the CR.

The third factor (F3) is midface resistance, which depends on the level of midpalatal suture and circummaxillary sutures interdigitation. Also, since bone bending in various regions of the skull (zygomatic arches, pterygoid process of sphenoid, perpendicular plate of palatine bone) is a common finding with MSE, factors that affect bone rigidity such as bone density (calcification) and bone geometric factors (diameter and length) must be considered.

Patient age probably affects factor 3. In fact, most suture interdigitation takes place during puberty [7]: the reason why MARPE becomes less predictable after the age of 18-25 years [47-48] can be due to increased bone rigidity that reduces bone bending phenomena.

Finally, regarding factor 3, procedures induced by therapy can be considered the midpalatal suture corticopuncture [27] or maxillary osteotomies [61-63,71]. These procedures aim at reducing the midface resistance and also inducing the biological response (cortipuncture), in order to improve the efficacy of midface expansion. Extension and location of osteotomies may have an important role in determining the type of maxilla movement. In DOME and MISMARPE techniques, cutting the piriform rim leads to a V-shaped split of the midpalatal suture [61-63,71],

whereas preserving it in the present study led to a parallel pattern of midpalatal suture opening and more superior expansion.

Finally, factor 4 regards the rotational type of movement during midface expansion. The zygomaticomaxillary complex doesn't translate, but rather rotates around a rotation fulcrum located near the frontozygomatic suture in the coronal plane (Fig. 1.1) and at the proximal portion of the zygomatic process of temporal bone in the horizontal plane (Fig.1.2). As illustrated above, the landmarks further from the rotation fulcrum undergo a larger linear displacement than landmarks located near the fulcrum (Fig. 4.16). This factor must be taken into consideration when evaluating skeletal effects of the therapy.

All above factors influence the linear and angular displacement of landmarks in various region of the skull. Finally, amount of MSE activation must be considered, in fact, larger appliance activations should lead to larger landmark displacements. For this reason, the parameter treatment change can be divided by the amount of MSE activation, to generate the midface expansion efficiency index (MEEI) for each parameter. MEEI indicates the amount of angular or linear displacement of the landmark, for each mm of MSE activation, as reported in table 12.

Conclusions and future directions

- The developed methodology allowed digital planning of MSE and miniscrews positioning with the patient's CBCT, and incorporation of two additional miniscrews through Cad-Cam technology.
- Midpalatal suture was split in all patients, and the pattern of midpalatal suture split was parallel.
- In the coronal plane, the zygomaticomaxillary complex rotated with a fulcrum located near the frontozygomatic suture, as seen in non-surgical MSE treatments.
- The nasal width increased significantly, which is the anatomical basis for an improvement in nasal airway flow.
- Interestingly, skeletal modifications were found in the regions above the lateral maxillary osteotomies, such as the nasal cavity and zygomatic bones, probably due to the intact piriform rim during surgery.
- Regarding dentoalveolar changes, inter-molar width increased significantly (+7.4 mm), and molars underwent a small dentoalveolar tipping in a buccal direction by 1.1° (average of Rt and Lt side).
- No acute hemorrhage nor post-operative bleeding was reported in treated patients, probably as a consequence of avoidance of pterygopalatine suture surgical disjunction.
- Above results need confirmation by a larger number of patients, due to the small sample size of the present study (4 patients).

Acknowledgements

I want to thank all persons who in different ways collaborated to this research project.

First of all, my mentor, Prof. Massimo Del Fabbro, for his willing to undertake this new and exciting research project, for his knowledge and constant support.

Prof. Aldo Bruno Giannì and his equipe at the Maxillofacial Surgery Department, Dr. Diego Rossi, Dr. Michele Romano, Dr. Federico Cullati, Dr. Camilla Baserga, for sharing the knowledge and efforts to improve the technique, and for the great collaboration.

Dr. Ivan Mancini and colleagues at the Orthodontic Department, Dr. Francesca Nucci, Dr. Danilo Lucarelli, for the collaboration with the orthodontic phase, the enthusiasm on the project and the friendship.

Prof. Won Moon, for his longtime collaboration and friendship, his continuous support and challenging new ideas, and for his incitement to always set the bar at a higher level.

Eng. Gianpaolo Savio and the ICEA Department of the University of Padova, for the great support in the development of the digital workflow.

My PhD friend, Lorena Karanxha, for sharing many ideas and time and for her constant support in developing new perspectives and solving problems, and for her great enthusiasm.

Paolo Zanata, CDT, for his exceptional support in the technical part and digital applications, his constant presence and friendship.

Dr. Luca Guarda, Prof. Vincenzo Quinzi, Dr. Chiara Salvatorelli, for the collaboration in surgical operations and for sharing their knowledge.

Bibliography

1. McNamara JA. Maxillary transverse deficiency. Am J Orthod Dentofacial Orthop. 2000 117(5):567–70.
2. Angell, E.C. Treatment of irregularities of the permanent or adult teeth. *Dent. Cosmos*. 1860;1:540–544.
3. Hass AJ. The treatment of maxillary deficiency by opening the midpalatal suture. Angle Orthod. 1965;35(200):17
4. Haas AJ. Palatal expansion: just the beginning of dentofacial orthopedics. Am J Orthod. 1970 Mar;57(3):219-55. doi: 10.1016/0002-9416(70)90241-1. PMID: 5263785.
5. Weissheimer A, de Menezes LM, Mezomo M, Dias DM, de Lima EM, Rizzatto SM. Immediate effects of rapid maxillary expansion with Haas-type and hyrax- type expanders: a randomized clinical trial. Am J Orthod Dentofacial Orthop. 2011;140:366-376.
6. Baccetti T, Franchi L, Cameron CG, McNamara JA. Treatment Timing for Rapid Maxillary Expansion. Angle Orthod 2001;71(5):343–50.
7. Melsen B. Palatal growth studied on human autopsy material. A histologic microradiographic study. Am J Orthod. 1975;68(1):42–54
8. Baysal A, Uysal T, Veli I, Ozer T, Karadede I, Hekimoglu S. Evaluation of alveolar bone loss following rapid maxillary expansion using cone-beam computed tomography. Korean J Orthod. 2013;43(2):83–95.
9. Kiliç N, Kiki A, Oktay H. A comparison of dentoalveolar inclination treated by two palatal expanders. Eur J Orthod. 2008;30(1):67–72.
10. Lee KJ, Park YC, Park JY, Hwang WS. Miniscrew-assisted nonsurgical palatal expansion before orthognathic surgery for a patient with severe mandibular prognathism. Am J Orthod Dentofac Orthop [Internet]. 2010;137(6):830–9. Available from:

http://dx.doi.org/10.1016/j.ajodo.2007.10.065

11. Carlson C, Sung J, McComb RW, Machado AW, Moon W. Microimplant-assisted rapid palatal expansion appliance to orthopedically correct transverse maxillary deficiency in an adult. Am J Orthod Dentofacial Orthop. 2016;149:716-28.

12. Li N, Sun W, Li Q, Dong W, Martin D, Guo J. Skeletal effects of monocortical and bicortical mini-implant anchorage on maxillary expansion using cone-beam computed tomography in young adults. Am J Orthod Dentofac Orthop. 2020;157(5):651–61.

13. Ngan P, Nguyen UK, Nguyen T, Tremont T, Martin C. Skeletal, dentoalveolar, and periodontal changes of skeletally mature patients with maxillary deficiency teated with microimplant-assisted rapid palatal expansion appliances: a pilot study. APOS Trends Orthod. 2018;8:71–85.

14. Oh H, Park J, Lagravere-Vich MO. Comparison of traditional RPE with two types of micro-implant assisted RPE: CBCT study. Semin Orthod [Internet]. 2019;25(1):60–8. Available from: https://doi.org/10.1053/j.sodo.2019.02.007

15. Zong C, Tang B, Hua F, He H, Ngan P. Skeletal and dentoalveolar changes in the transverse dimension using microimplant-assisted rapid palatal expansion (MARPE) appliances. Semin Orthod [Internet]. 2019;25(1):46–59. Available from: https://doi.org/10.1053/j.sodo.2019.02.006

16. Celenk-Koca T, Erdinc AE, Hazar S, Harris L, English JD, Akyalcin S. Evaluation of miniscrew-supported rapid maxillary expansion in adolescents: A prospective randomized clinical trial. Angle Orthod. 2018;88(6):702–9.

17. Calil RC, Marin Ramirez CM, Otazu A, Torres DM, Gurgel J de A, Oliveira RC, et al. Maxillary dental and skeletal effects after treatment with self-ligating appliance and miniscrew-assisted rapid maxillary expansion. Am J Orthod Dentofac Orthop.

2021;159(2):e93–101.

18. Gunyuz Toklu M, Germec-Cakan D, Tozlu M. Periodontal, dentoalveolar, and skeletal effects of tooth-borne and tooth-bone-borne expansion appliances. Am J Orthod Dentofac Orthop. 2015;148(1):97–109
19. Mosleh MI, Kaddah MA, Abd Elsayed FA, Elsayed HS. Comparison of transverse changes during maxillary expansion with 4-point bone-borne and tooth-borne maxillary expanders. Am J Orthod Dentofac Orthop [Internet]. 2015;148(4):599–607. Available from: http://dx.doi.org/10.1016/j.ajodo.2015.04.040
20. Wilmes B, Nienkemper M, Drescher D. Application and effectiveness of a mini-implant- and tooth-borne rapid palatal expansion device: the hybrid hyrax. World J Orthod. 2010;11(4):323–30.
21. Vassar JW, Karydis A, Trojan T, Fisher J. Dentoskeletal effects of a temporary skeletal anchorage device-supported rapid maxillary expansion appliance (TSADRME): A pilot study. Angle Orthod. 2016;86(2):241–9.
22. Park JJ, Park YC, Lee KJ, Cha JY, Tahk JH, Choi YJ. Skeletal and dentoalveolar changes after miniscrew-assisted rapid palatal expansion in young adults: A cone-beam computed tomography study. *Korean J Orthod* 2017;47(2):77-86
23. Lagravere MO, Carey J, Heo G, Toogood RW, Major PW. Transverse, vertical, and anteroposterior changes from bone-anchored maxillary expansion vs traditional rapid maxillary expansion: a randomized clinical trial. Am J Orthod Dentofacial Orthop. 2010;137(3):304 e1–12 discussion-5.
24. Seo YJ, Chung KR, Kim SH, Nelson G. Camouflage treatment of skeletal class III malocclusion with asymmetry using a bone-borne rapid maxillary expander. Angle Orthod. 2015;85(2):322–34.
25. Lombardo L, Carlucci A, Maino BG, Colonna A, Paoletto E, Siciliani G. Class III

malocclusion and bilateral cross-bite in an adult patient treated with miniscrew-assisted rapid palatal expander and aligners. Angle Orthod. 2018; 88(5):649–64.

26. Yilmaz A, Arman-Ozcirpici A, Erken S, Polat-Ozsoy O. Comparison of shortterm effects of mini-implant-supported maxillary expansion appliance with two conventional expansion protocols. Eur J Orthod. 2015;37(5):556–64.
27. Suzuki SS, Braga LFS, Fujii DN, Moon W, Suzuki H. Corticopuncture facilitated microimplant-assisted rapid palatal expansion. Case Rep Dent. 2018;2018:1392895
28. MacGinnis M, Chu H, Youssef G, Wu KW, Machado AW, Moon W. The effects of micro-implant assisted rapid palatal expansion (MARPE) on the nasomaxillary complex--a finite element method (FEM) analysis. Prog Orthod. 2014;15:52.
29. Abedini S, Elkenawy I, Kim E, Moon W. Three-dimensional soft tissue analysis of the face following micro-implant-supported maxillary skeletal expansion. Prog Orthod. 2018;19(1)
30. Garcez AS, Suzuki SS, Storto CJ, Cusmanich KG, Elkenawy I, Moon W. Effects of maxillary skeletal expansion on respiratory function and sport performance in a para-athlete - a case report. Phys Ther Sport. 2019;36:70–7.
31. Brunetto DP, Sant'Anna EF, Machado AW, Moon W. Non-surgical treatment of transverse deficiency in adults using microimplant-assisted rapid palatal expansion (MARPE). Dental Press J Orthod. 2017;22(1):110–25.
32. Storto CJ, Garcez AS, Suzuki H, Cusmanich KG, Elkenawy I, Moon W, et al. Assessment of respiratory muscle strength and airflow before and after microimplant-assisted rapid palatal expansion. Angle Orthod. 2019;89(5):713–20.
33. Won Moon, Class III treatment by combining facemask (FM) and maxillary skeletal expander (MSE), *Seminars in Orthodontics,* doi:10.1053/j.sodo.2018.01.009

34. Cantarella D, Dominguez-Mompell R, Moschik C, Sfogliano L, Elkenawy I, Pan HC, Mallya SM, Moon W. Zygomaticomaxillary modifications in the horizontal plane induced by micro-implant-supported skeletal expander, analyzed with CBCT images. Prog Orthod. 2018 Oct 22;19(1):41. doi: 10.1186/s40510-018-0240-2. PMID: 30345476; PMCID: PMC6196147.
35. Lee RJ, Moon W, Hong C. Effects on monocortical and bicortical mini-implant anchorage on bone-borne palatal expansion using finite element analysis. *Am J Orthod Dentofac Orthop* 2017;151(5):887-97
36. Cantarella D, Dominguez-Mompell R, Mallya SM, et al. Changes in the midpalatal and pterygopalatine sutures induced by micro-implant- supported skeletal expander, analyzed with a novel 3D method based on CBCT imaging. Prog Orthod. 2017;18(1):34.
37. Elkenawy, I., Fijany, L., Colak, O. *et al.* An assessment of the magnitude, parallelism, and asymmetry of micro-implant-assisted rapid maxillary expansion in non-growing patients. *Prog Orthod.* **21,** 42 (2020). https://doi.org/10.1186/s40510-020-00342-4
38. Paredes, Ney et al. “Differential assessment of skeletal, alveolar, and dental components induced by microimplant-supported midfacial skeletal expander (MSE), utilizing novel angular measurements from the fulcrum.” *Progress in orthodontics* vol. 21,1 18. 13 Jul. 2020, doi:10.1186/s40510-020-00320-w
39. Colak O, Paredes NA, Elkenawy I. Tomographic assessment of palatal suture opening pattern and pterygopalatine suture disarticulation in the axial plane after midfacial skeletal expansion. Prog Orthod. 2020;21:21.
40. Brunetto DP, Sant’Anna EF, Machado AW, Moon W. Non-surgical treatment of transverse deficiency in adults using Microimplant-assisted Rapid Palatal Expansion (MARPE). *Dental Press J Orthod* 2017;22(1):110-25

41. Suzuki H, Moon W, Previdente LH, Suzuki SS, Garcez AS, Consolaro A. Miniscrew-assisted rapid palatal expander (MARPE): the quest for pure orthopedic movement. *Dental Press J Orthod* 2016;21(4):17-23
42. MacGinnis M, Chu H, Youssef G, Wu KW, Machado AW, Moon W. The effects of micro-implant assisted rapid palatal expansion (MARPE) on the nasomaxillary complex-a finite element method (FEM) analysis. *Prog Orthod* 2014;15:52
43. Cantarella D, Dominguez-Mompell R, Moschik C, et al. Midfacial changes in the coronal plane induced by microimplant-supported skeletal expander, studied with cone-beam computed tomography images. Am J Orthod Dentofac Orthop. 2018;154(3):337–45
44. Cantarella D. "Skeletal effects induced by Maxillary Skeletal Expander (MSE) and Hyrax appliance in the midface." Thesis, Master of Science in Oral Biology, University of California, Los Angeles, 2017.
45. Angelieri F, Cevidanes LH, Franchi L, Gonçalves JR, Benavides E, McNamara JA Jr. Midpalatal suture maturation: classification method for individual assessment before rapid maxillary expansion. Am J Orthod Dentofacial Orthop. 2013 Nov;144(5):759-69. doi: 10.1016/j.ajodo.2013.04.022. PMID: 24182592; PMCID: PMC4185298.
46. Isfeld D, Flores-Mir C, Leon-Salazar V, Lagravere M. Evaluation of a novel palatal suture maturation classification as assessed by cone-beam computed tomography imaging of a pre- and post- expansion treatment cohort. The Angle Orthodontist, 2019 Mar; 89(2), 252-261, 040518-258.1–. doi:10.2319/040518-258.1
47. Haichao Jia, Li Zhuang, Nan Zhang, Yuanyuan Bian, Song Li. Age dependent effects of transverse maxillary deficiency treated by microimplant-assisted rapid palatal expansion: A prospective cone-beam computed tomography study, American Journal of Orthodontics and Dentofacial Orthopedics, 2021

48. Winsauer H, Walter A, Katsaros C, Ploder O. Success and complication rate of miniscrew assisted non-surgical palatal expansion in adults - a consecutive study using a novel force-controlled polycyclic activation protocol. Head Face Med. 2021 Dec 11;17(1):50. doi: 10.1186/s13005-021-00301-2. PMID: 34895287; PMCID: PMC8665552.
49. Silverstein K, Quinn PD. Surgically-assisted rapid palatal expansion for management of transverse maxillary deficiency. J Oral Maxillofac Surg. 1997 Jul;55(7):725-7. doi: 10.1016/s0278-2391(97)90587-5. PMID: 9216505.
50. Bell W, Epker B: Surgical-orthodontic expansion of the maxilla. American Journal of Orthodontics, Vol 70, 1976, Pages 517-528, https://doi.org/10.1016/0002-9416(76)90276-1.
51. Suri L, Taneja P. Surgically assisted rapid palatal expansion: a literature review. Am J Orthod Dentofacial Orthop. 2008 Feb;133(2):290-302. doi: 10.1016/j.ajodo.2007.01.021. PMID: 18249297.
52. Betts NJ. Surgically Assisted Maxillary Expansion. Atlas Oral Maxillofac Surg Clin North Am. 2016 Mar;24(1):67-77. doi: 10.1016/j.cxom.2015.10.003. Epub 2015 Nov 24. PMID: 26847514.
53. Lehman JA Jr, Haas AJ, Haas DG. Surgical orthodontic correction of transverse maxillary deficiency: a simplified approach. Plast Reconstr Surg. 1984 Jan;73(1):62-8. doi: 10.1097/00006534-198401000-00013. PMID: 6691076.
54. Carvalho PHA, Moura LB, Trento GS, Holzinger D, Gabrielli MAC, Gabrielli MFR, Pereira Filho VA. Surgically assisted rapid maxillary expansion: a systematic review of complications. Int. J. Oral Maxillofac. Surg. 2019
55. Williams BJ, Currimbhoy S, Silva A, O'Ryan FS. Complications following surgically assisted rapid palatal expansion: a retrospective cohort study. J Oral Maxillofac Surg.

2012 Oct;70(10):2394-402. doi: 10.1016/j.joms.2011.09.050. Epub 2012 Apr 18. PMID: 22516838.

56. Zandi, Mohammad, et al. The Necessity of Pterygomaxillary Disjunction in Surgically Assisted Rapid Maxillary Expansion: a Short-term, Double-blind, Historical Controlled Clinical Trial. Journal of Cranio-maxillo-facial Surgery : Official Publication of the European Association for Cranio-Maxillo-Facial Surgery, vol. 44, no. 9, 2016, pp. 1181-6.
57. Mehra P, Cottrell D, Caiazzo A, Lincoln R. Life-threatening, delayed epistaxis after surgically assisted rapid palatal expansion: a case report. Journal of Oral and Maxillofacial Surgery. 1999 Feb;57(2):201-4.
58. Lanigan DT, Mintz SM. Complications of surgically assisted rapid palatal expansion: review of the literature and report of a case. J Oral Maxillofac Surg. 2002 Jan;60(1):104-10. doi: 10.1053/joms.2002.29087. PMID: 11757020.ù
59. Carneiro Jr JT, Paschoal EHA, Carreira ASD, Real RPV: Carotid cavernous fistula after surgically assisted rapid maxillary expansion with a bone anchored appliance. Int. J. Oral Maxillofac. Surg. 2013; 42: 326–328.
60. Koudstaal MJ, Smeets JB, Kleinrensink GJ, Schulten AJ, Van der Wal KG. Relapse and stability of surgically assisted rapid maxillary expansion: an anatomic biomechanical study. J Oral Maxillofac Surg. 2009 Jan;67(1):10-4. doi: 10.1016/j.joms.2007.11.026. PMID: 19070742.
61. Liu SY, Guilleminault C, Huon LK, Yoon A. Distraction Osteogenesis Maxillary Expansion (DOME) for Adult Obstructive Sleep Apnea Patients with High Arched Palate. Otolaryngol Head Neck Surg. 2017 Aug;157(2):345-348. doi: 10.1177/0194599817707168. Epub 2017 Jul 4. PMID: 28675100.
62. Abdelwahab M, Yoon A, Okland T, Poomkonsarn S, Gouveia C, Liu SY. Impact of Distraction Osteogenesis Maxillary Expansion on the Internal Nasal Valve in Obstructive

Sleep Apnea. Otolaryngol Head Neck Surg. 2019 Aug;161(2):362-367. doi: 10.1177/0194599819842808. Epub 2019 May 14. PMID: 31084256.

63. Yoon A, Guilleminault C, Zaghi S, Liu SY. Distraction Osteogenesis Maxillary Expansion (DOME) for adult obstructive sleep apnea patients with narrow maxilla and nasal floor. Sleep Med. 2020 Jan;65:172-176. doi: 10.1016/j.sleep.2019.06.002. Epub 2019 Jun 13. PMID: 31606311.
64. Cantarella D, Savio G, Grigolato L, Zanata P, Berveglieri C, Lo Giudice A, Isola G, Del Fabbro M, Moon W. A new methodology for the digital planning of micro-implant-supported maxillary skeletal expansion. Med Devices Evid Res. 2020;13:93-106.
65. Arcoverde N, Duarte RM, Barreto RM et al. Enhanced real-time head pose estimation system for mobile device. Integr Computed Aided Eng. 2014;21(3):281-293.
66. Cantarella D, Karanxha L, Zanata P, Moschik C, Torres A, Savio G, Del Fabbro M, Moon W. Digital Planning and manufacturing of maxillary skeletal expander for patients with thin palatal bone. Med Devices Evid Res. 2021;14:1-13.
67. Cevidanes LHS, Bailey LTJ, Tucker GR Jr, Styner MA, Mol A, Phillips CL, Proffit WR, Turvey T. Superimposition of 3-dimensional cone-beam CT models of orthognatic surgery patients. Dentomaxillofac Radiol. 2005;34:369-75
68. Weissheimer A, Menezes LM, Koerich L, Pham J, Cevidanes LHS. Fast three-dimensional superimposition of cone beam computed tomography for orthopaedics and orthognatic surgery evaluation. Int J Oral Maxillofac Surg. 2015;44(9):1188-96.
69. Woller JL, Kim KB, Behrents RG, Bushang PH. An assessment of the maxilla after rapid maxillary expansion using cone beam computed tomography in growing children. Dental Press J Orthod. 2014;19(1):26-35.
70. Giannelly AA: Force-induced changes in the vascularity of the periodontal ligament. Am J Orthod 55:5-11, 1969.

71. Haas OL Jr, Matie PRB, Rosa BM, Rojo-Sanchis C, Guijarro-Martinez R, Valls-Ontanon, Menezes LM, Hernandez-Alfaro F, De Olivera RB. Minimally invasive surgical and miniscrew-assisted rapid palatal expansion (MISMARPE) in adult patients. Journal of Cranio-Maxillofacial Surgery (2022), available online December 27th 2021.
72. Burr DB. Why bones bend but don't break. J Musculoskelet Neuronal Interact 2011; 11(4):270-285
73. Turner CH, Burr DB. Basic biomechanical measurements of bone: A tutorial. Bone 1993; 14, 595-608
74. Frost HM. Presence of microscopic cracks in vivo in bone. Henry Ford Hosp Med Bull 1960; 8:25-35
75. Currey JD. What determines the bending strength of a compact bone? The Journal of Experimental Biology 1999; 202, 2495-2503
76. Choi K, Goldstein A. A comparison of the fatigue behavior of human trabecular and cortical bone tissue. J Biomechanics 1992; 25(12):1371-1381
77. Rauch F. Bone growth in length and width: The Yin and Yang of bone stability. J Musculoskeletal Neuronal Interact 2005; 5(3):194-201
78. Ghoneima A, Cho H, Farouk K, Kula K. Accuracy and reliability of landmark-based, surface-based and voxel-based 3D cone-beam computed tomography superimposition methods. Orthod Craniofac Res 2017 Nov;20(4):227-236. doi: 10.1111/ocr.12205
79. Melsen B, Melsen F. The postnatal development of the palatomaxillary region studied on human autopsy material. Am J Orthod. 1982;82:329-42.
80. Ghoneima A, Abdel-Fattah E, Hartsfield J, ElBedwei A, Kamel A, Kula K. Effects of rapid maxillary expansion on the cranial and circummaxillary sutures. Am J Orthod Dentofac Orthop. 2011;140:510-9.

81. Lione R, Ballanti F, Franchi L, Baccetti T, Cozza P. Treatment and post-treatment skeletal effects of rapid maxillary expansion studied with low-dose computed tomography in growing subjects. Am J Orthod Dentofac Orthop. 2008;134:389-92.
82. Lee SP, Paik KS, Kim MK. Anatomical study of the pyramidal process of the palatine bone in relation to implant placement in the posterior maxilla. J Oral Rehabil. 2001;28:125-32.
83. Verstrateen J, Kuijpers-Jagtman AM, Mommaerts MY, Bergé SJ, Nada RM, Schols JGJH. A systematic review of the effects of bone-borne surgical assisted rapid maxillary expansion. J Cranio-Maxillofacial Surg. 2010;38(3):166-74.
84. Lee DW, Park JH, Moon W, Seo HY, Chae JM. Effects of bicortical anchorage on pterygopalatine suture opening with micro-implant-assisted maxillary skeletal expansion. Am J Orthod Dentofac Orthop. 2021 Apr;159(4):502-511. doi: 10.1016/j.ajodo.2020.02.013
85. LI N, Sun W, LI Q, Dong W, Martin D, Guo J. Skeletal effects of monocortical and bicortical mini-implant anchorage on maxillary expansion using cone-beam computed tomography in young adults. 2020 May;157(5):651-661. doi: 10.1016/j.ajodo.2019.05.021
86. Nojima LI, Nojima MCG, Cunha AC, Guss NO, Sant'Anna EF. Mini-implant selection protocol applied to MARPE. Dental Press Journal of Orthodontics. 23;5;Sept 2018
87. Baccetti T, Franchi L, Cameron CG, McNamara Jr JA. Treatment timing for rapid maxillary expansion. Angle Orthod 2001;71:343-50
88. Ong SC, Khambay BS, McDonald JP, Cross DL, Brocklebank LM, Ju X. The novel use of three-dimensional surface models to quantify and visualize the immediate changes of the mid-facial skeleton following rapid maxillary expansion. Surgeon. 2015; 13:132-138

89. Cordasco G, Nucera R, Fastuca R, Matarese G, Lindauer SJ, Leone P, Manzo P, Martina R. Effects of orthopedic maxillary expansion on nasal cavity size in growing subjects: a low dose computer tomography clinical trial. Int J Pediatr Otorhinolaryngol. 2012;76:1547-51.
90. Palaisa J, Ngan P, Martin C, Razmus T. Use of conventional tomography to evaluate changes in the nasal cavity with rapid palatal expansion. Am J Orthod Dentofacial Orthop. 2007;132:458-66.
91. Garrett BJ, Caruso JM, Rungcharassaeng K, Farrage JR, Kim JS, Taylor GD. Skeletal effects to the maxilla after rapid maxillary expansion assessed with cone-beam computed tomography. Am J Orthod Dentofacial Orthop. 2008;134:8-9.
92. Bazargani F, Magnuson A, Ludwig B. Effects on nasal airflow and resistance using two different RME appliances: a randomized controlled trial. *European Journal of Orthodontics*, Volume 40, Issue 3, June 2018, Pages 281–284, https://doi.org/10.1093/ejo/cjx081